HAL
archives-ouvertes.fr

Magma Storage Conditions of Large Plinian Eruptions of Santorini Volcano (Greece)

Anita Cadoux, Bruno Scaillet, Timothy H. Druitt, Etienne Deloule

▶ **To cite this version:**

Anita Cadoux, Bruno Scaillet, Timothy H. Druitt, Etienne Deloule. Magma Storage Conditions of Large Plinian Eruptions of Santorini Volcano (Greece). Journal of Petrology, Oxford University Press (OUP), 2014, 55 (6), pp.1129-1171. <10.1093/petrology/egu021>. <insu-00998989>

HAL Id: insu-00998989

https://hal-insu.archives-ouvertes.fr/insu-00998989

Submitted on 1 Jul 2014

HAL is a multi-disciplinary open access archive for the deposit and dissemination of scientific research documents, whether they are published or not. The documents may come from teaching and research institutions in France or abroad, or from public or private research centers.

L'archive ouverte pluridisciplinaire **HAL**, est destinée au dépôt et à la diffusion de documents scientifiques de niveau recherche, publiés ou non, émanant des établissements d'enseignement et de recherche français ou étrangers, des laboratoires publics ou privés.

Magma storage conditions of large Plinian eruptions of Santorini Volcano (Greece)

ANITA CADOUX*[1,2,3,4,5,6], BRUNO SCAILLET[1,2,3], TIMOTHY H. DRUITT[4,5,6] AND ETIENNE DELOULE[7]

[1] UNIVERSITÉ D'ORLÉANS, ISTO, UMR 7327, 45071, ORLÉANS, FRANCE.

[2] CNRS, ISTO, UMR 7327, 45071 ORLÉANS, FRANCE.

[3] BRGM, ISTO, UMR 7327, BP 36009, 45060 ORLEANS, FRANCE.

[4] CLERMONT UNIVERSITE, UNIVERSITE BLAISE PASCAL, LABORATOIRE MAGMAS ET VOLCANS, BP 10448, F-63038 CLERMONT-FERRAND, FRANCE.

[5] CNRS, UMR 6524, LMV, F-63038 CLERMONT-FERRAND, FRANCE.

[6] IRD, R 163, LMV, F-63038 CLERMONT-FERRAND, FRANCE.

[7] CRPG-CNRS, BP20, 54501 VANDOEUVRE LES NANCY, FRANCE.

* Corresponding author: Anita Cadoux

Tel.: 00 33 +2 38 25 53 83

E-mail: acadoux@cnrs-orleans.fr

Revised manuscript for *Journal of Petrology*

ABSTRACT

The intensive variables in dacitic-rhyodacitic magmas prior to four large Plinian eruptions of Santorini Volcano over the last 200 ka (Minoan, Cape Riva, Lower Pumice 2 and Lower Pumice 1) were determined by combining crystallization experiments with study of the natural products, including the volatile contents of melt inclusions trapped in phenocrysts. Phase equilibria of the silicic magmas were determined at pressures of 1, 2 and 4 kbar, temperatures of 850-900°C, fluid (H_2O+CO_2)-saturation, XH_2O [= molar $H_2O/(H_2O+CO_2)$] between 0.6 and 1 (melt H_2O contents of 2 - 10 wt%), and redox conditions of FMQ or NNO+1. Experiments were generally successful in reproducing the phenocryst assemblage of the natural products. The phase relationships vary significantly among the investigated compositions, revealing a sensitivity to small variations in whole rock compositions. Our results show that pre-eruptive storage conditions of the four silicic magmas were all very similar. The magmas were stored at T = 850 – 900°C and P ≥ 2 kbar, under moderately reduced conditions (ΔNNO = - 0.9 to - 0.1), with melts poor in fluorine (~500-800 ppm) and sulphur (≤ 100 ppm), but rich in water and chlorine (5-6 wt%, ca. 2500-3500 ppm, respectively). In all cases, melts were slightly undersaturated with respect to H_2O, but most probably saturated with respect to H_2O+Cl ± CO_2 and a brine. The Santorini magma plumbing system appears to be dominated by a large, long-lived (≥ 200 ka) predominantly-silicic magma storage region situated at ≥ 8 km depth, from which crystal-poor melt batches were extracted during the largest caldera-forming eruptions of the volcanic system.

KEY WORDS

Magma storage; Melt inclusions; Phase equilibrium; Santorini; Volatiles

INTRODUCTION

It has been increasingly recognized that dramatic changes in magma storage conditions can occur over very short periods of time at a single volcano. This was shown at, for example, Mt. St Helens and Mt. Vesuvius, where magma storage depths vary over timescales of several hundreds of years (e.g., between the Pompeii and Pollena eruptions at Mt. Vesuvius; Scaillet *et al.*, 2008) to a few years (between the Wn and We events at Mt. St Helens; Gardner *et al.*, 1995; Blundy *et al.*, 2008; Rutherford & Devine, 2008). These variations of magma ponding level may be attributed to differences in the volatile content and buoyancy of ascending magmas. They might also be related to changes in stress imposed on the crustal plumbing system by the overlying edifice (e.g., Pinel & Jaupart, 2003; Pinel *et al.*, 2010), following either caldera formation (Ventura *et al.*, 1999) or volcano spreading (Borgia *et al.*, 2005). It is remarkable indeed that, for these two volcanic systems, the largest and fastest pressure drops recorded by the magmas coincide with the partial destruction of the edifice subsequent to a major explosive eruption. Strain relaxation in the upper crust resulting from a decrease of edifice load could allow accumulation of magmas at shallower depths (Ventura *et al.*, 1999). Variations of magma storage conditions have also been correlated with changes in eruptive dynamics at Mt. Pelée, Mt. Vesuvius and Tenerife (e.g., Martel *et al.*, 1998; Scaillet *et al.*, 2008; Andújar & Scaillet, 2012a; Andújar & Scaillet, 2012b). For instance, Andújar & Scaillet (2012b) showed that the explosive-effusive style of phonolitic magmas correlates with the amount of volatiles, the degree of water-undersaturation and the depth of magma storage, the explosive character generally increasing with pressure, depth and dissolved water content. Determining magma storage conditions over time is thus crucial to understanding volcano behaviour, and may significantly contribute to the evaluation of volcanic hazards during periods of unrest.

Santorini volcano (South Aegean Arc, Greece), which has recently shown signs of seismic and geodetic unrest (2011-2012; e.g., Newman *et al.*, 2012), is an ideal target for unraveling these potential relationships, as its history is marked by recurrent large-scale Plinian eruptions (ca. every 20-30 ka). Some of these eruptions triggered caldera collapses, alternating with edifice construction and minor interplinian eruptions (Fig. 1). This study focuses on the silicic products of the four major Plinian eruptions of Santorini that have occurred over the last 200 ka (Fig. 1): the Lower Pumice 1, Lower Pumice 2, Cape Riva and Minoan eruptions. Magmas of Lower Pumice 1, Lower Pumice 2 and Minoan were dominantly rhyodacitic, and that of Cape Riva was dacitic. In order to define precisely the P, T, fO_2 and volatile (H_2O, CO_2, Cl, F, S) pre-eruptive storage conditions of these magmas, we carried out phase equilibrium crystallization experiments coupled with a petrological and geochemical study of the natural products. We present the stability fields of the phases for each eruption over the T-P-fO_2-XH_2O conditions explored: T = 850-900°C, P = 1, 2 and 4 kbar, fO_2 = FMQ and NNO+1, and XH_2O [= moles of H_2O/ (H_2O+CO_2)] between 1 (i.e., H_2O-saturated) and 0.6 (H_2O-undersaturated). The phase assemblages, abundances and compositions of the experimental and natural products are compared, and their implications for pre-eruptive conditions and for our understanding of the Santorini plumbing system are discussed.

GEOLOGICAL BACKGROUND

Eruptive history

Volcanism at Santorini began ca. 650 ka and subsequently involved two major explosive cycles between ~360 and ~3.6 ka that formed the bulk of the volcanic deposits (Druitt *et al.*, 1999). Twelve major Plinian eruptions occurred during the two cycles, with ejected volumes ranging from a few km^3 to several tens of km^3. The first explosive cycle

(360-172 ka) included five major Plinian eruptions, while the second cycle (172-3.6 ka) included seven (Fig. 1). The average time interval between these main eruptions was about 20 to 30 ka. Interplinian activity between the main explosive eruptions involved extrusive edifice construction and minor (subplinian or less) explosive activity (Huijsmans & Barton, 1986; Druitt *et al.*, 1999; Vespa *et al.*, 2006). All Santorini magmas belong to the calc-alkaline series, and range compositionally from basalt to rhyodacite; no rhyolite has been documented onland at Santorini except in the oldest (Akrotiri) sequences. Deposits of the major Plinian eruptions are compositionally zoned, but can be subdivided into those that are dominantly andesitic and those that are dominantly silicic (Druitt *et al.*, 1999). The dominantly silicic eruptions occur at the end of each cycle (Fig. 1).

The second cycle terminated with the Bronze-Age Minoan eruption (3.6 ka). Since then, effusive activity has constructed a ~3 km^3 dacitic lava shield on the floor of the Minoan caldera (Kameni Islands, 197 BC to AD 1950; Pyle & Elliott, 2006; Fig. 1). Since 1950, and until recently, activity on the Kameni islands has been characterized by the emission of low-temperature (< 100°C) fumarolic gases. However, between January 2011 and March 2012, increases of seismic activity, water temperature and CO_2 levels (e.g., ISMOSAV website; Papazachos *et al.*, 2012)**,** were accompanied by inflation of the northern part of the caldera (Newman *et al.*, 2012; Parks *et al.*, 2012). This has been attributed to the intrusion of 10–20 million m^3 of magma at about 4.4 km depth during this period (Parks *et al.*, 2012).

The four dominantly-silicic Plinian eruptions studied in this paper

The Lower Pumice 1 (LP1) and Lower Pumice 2 (LP2) eruptions terminated the first explosive cycle of Santorini (Fig 1). They have been dated at 184 and 172 ka, respectively, by correlation with deep-sea ash layers (V-3 and V-1, respectively; Keller et al., 2000; Schwarz, 2000); for LP1 this is consistent with the previously published K-Ar age of 203 ± 24 ka

(Druitt et al., 1999). The LP1 eruption began with a Plinian phase, generating a pumice fall deposit up to 5 m thick. This was followed by discharge of pyroclastic flows, which laid down lithic lag breccia and ignimbrite up to 14 m thick. The products of LP1 are mainly rhyodacitic, but the eruption ended with the venting of a smaller quantity of andesite (Druitt *et al.*, 1999). LP2 directly overlies LP1, separated by a palaeosol. The LP2 eruption began with a Plinian phase that laid down a pumice fall deposit up to 25 m thick. This was followed by pyroclastic flows and caldera collapse ('caldera 1'; Fig. 1). The products of LP2 are uniformly rhyodacitic apart for the Plinian deposit, which also contains scoria of basaltic to andesitic composition (Druitt *et al.*, 1999; Gertisser *et al.*, 2009).

The second explosive cycle culminated with the Cape Riva (CR) and Minoan eruptions (Fig. 1). The dacitic CR eruption began with a Plinian phase, the pumice fall deposit of which is compositionally zoned, with subordinate andesitic and banded pumices in its upper half. At the end of the Plinian phase, the eruption column collapsed yielding a welded ignimbrite. The eruption then escalated violently; pyroclastic flows were discharged all over the islands and a caldera collapsed ('caldera 3', collapse of the Skaros-Therasia edifice; Druitt & Francaviglia, 1992). The eruption has been dated at 22 ka (Wulf *et al.*, 2002; Fabbro *et al.*, 2013). The Minoan eruption (3.6 ka) began with a Plinian phase (phase 1). The pumice fall deposit contains a predominant rhyodacitic component and two andesitic components, whose abundances increasing up sequence: (1) cauliform andesitic enclaves and (2) a microphenocryst-rich andesitic pumice (Druitt *et al.*, 1999; Druitt, 2014). Subsequent access of sea water to the vent initiated violent phreatomagmatic explosions and the emplacement of base surge deposits (phase 2) overlain by massive tuff (phase 3) which are interpreted as the products of low temperature ($\leq$ 300°C), three-phase (solid, liquid, gas) pyroclastic flows (Sparks & Wilson, 1990). During the last phase of the eruption (phase 4), hot (300-350°C) pyroclastic flows were discharged and a caldera collapsed ('caldera 4', Fig. 1).

PREVIOUS CONSTRAINTS ON THE PRE-ERUPTIVE CONDITIONS

Pre-eruptive magma storage conditions have been determined previously for the Minoan and the Lower Pumice 2 eruptions. Experimental constraints exist only for the Minoan eruption (Cottrell *et al.*, 1999). No such constraints exist so far for the Cape Riva and Lower Pumice 1 eruptions.

Minoan rhyodacite pre-eruptive constraints

Using coexisting ilmenite-magnetite pairs, Sigurdsson *et al.* (1990) estimated a pre-eruptive temperature for the Minoan rhyodacitic magma of 850°C and an oxygen fugacity (fO_2) of 10^{-13}, close to the Ni-NiO (NNO) buffer. More recent studies have confirmed this first estimate: Druitt *et al.* (2012) found a temperature of 853 ± 12°C (Stormer, 1983; Anderson & Lindsley, 1985) while Cottrell *et al.* (1999) report a slightly higher temperature, 885 ± 7°C at an fO_2 of $10^{-11.7 \pm 0.2}$ (i.e., ~ NNO+0.5; Stormer, 1983; Anderson & Lindsley, 1988).

Pre-eruptive Minoan volatiles contents were determined by analysis of melt inclusions (MI) in plagioclase phenocrysts (Devine *et al.*, 1984; Sigurdsson *et al.*, 1990; Gardner *et al.*, 1996; Cottrell *et al.*, 1999; Michaud *et al.*, 2000). These studies yield water contents ranging from 3.5 to 6.5 wt%. No data exist for CO_2 content. Chlorine is the most abundant volatile phase after water, with contents of 2800-3200 ppm (Devine *et al.*, 1984; Cottrell *et al.*, 1999; Michaud *et al.*, 2000) whilst sulphur contents do not exceed 100 ppm (Sigurdsson *et al.*, 1990; Cottrell *et al.*, 1999; Michaud *et al.*, 2000). Cottrell *et al.* (1999) reported fluorine and boron contents of 685-910 ppm and 16-25 ppm, respectively.

According to Sigurdsson *et al.* (1990), the water pressure of the rhyodacite magma prior to the Minoan eruption was 1.5–2.5 kbar. The magma was probably water-undersaturated with a total pressure in the range 2.5 to 5 kbar, indicating a reservoir at 8 to 15 km depth.

Cottrell *et al.* (1999) conducted exclusively water-saturated phase equilibria experiments on Minoan rhyodacite pumice at temperatures ranging from 800 to 975°C, pressure varying from 50 MPa to 250 MPa, and redox conditions near the NNO buffer. According to these authors, the Minoan rhyodacite was first stored at pressures of > 200 MPa and T~ 825°C, then, a few months prior to eruption, it moved to a shallower ~ 50 MPa storage region where it reached a higher temperature (885°C), owing to mafic magma input. On the basis of their hypothesis, the Minoan rhyodacite would have contained ~ 3 wt% H_2O in the shallow reservoir, and ~ 6 wt% H_2O in the deeper one.

Lower Pumice 2 pre-eruptive constraints

Based on a study of natural rocks, Gertisser at al. (2009) determined a pre-eruptive Fe-Ti temperature of LP2 rhyodacitic magma of 831 ± 12°C and an oxygen fugacity of $fO_2 = 10^{-13.7 \pm 0.2}$ (thermometer of Andersen *et al.*, 1993), which is slightly above the FMQ (Fayalite-Magnetite-Quartz) oxygen buffer. The H_2O content of some glass inclusions was determined by FTIR spectroscopy, yielding pre-eruptive melt water contents of ~ 4.5 wt. %. No CO_2 was detected in any of the analysed glass inclusions, suggesting that there is less than 50 ppm (FTIR detection limit) of dissolved CO_2. The average chlorine content of the inclusion and interstitial glasses are similar (2490 ± 530 ppm and 2630 ± 210 ppm, respectively), suggesting that chlorine had insufficient time to degas during eruption (Gertisser *et al.*, 2009). In contrast, part of the sulphur was degassed during eruption, since glass inclusion sulphur content (140 ± 50 ppm) is higher than that of the interstitial glass (80 ± 20 ppm). Finally, Gertisser at al. (2009) determined a pre-eruptive storage pressure of 4.3 kbar (i.e., ~ 16 km depth assuming a crustal density of 2.7 g/cm^3), based on the Al content of scarce amphibole phenocrysts in the rhyodacitic pumice (using the aluminium-in-hornblende geobarometer of Johnson & Rutherford, 1989).

SAMPLES SELECTION AND EXPERIMENTAL TECHNIQUES

Sampling strategy, starting material composition and preparation

For each eruption, we collected pumice clasts from the base of the Plinian fall deposit, which represents the first eruption phase. This strategy allowed us: 1/ to ensure that only the purest silicic component was sampled (avoiding mixed components generally located in the upper levels of the pumice fall) and, 2/ to ascertain the storage conditions at the top of the reservoir.

The selected natural silicic components of the four eruptions have broadly similar major elements compositions (Table 1): rhyodacites for the Minoan, LP2 and LP1 eruptions ('dry' SiO_2 = 68.7-70.6 wt%) and dacite for the Cape Riva ('dry' SiO_2 = 66.9 wt%). They share an identical mineral assemblage, in which plagioclase and orthopyroxene (the most abundant phases) are accompanied by clinopyroxene, ilmenite, magnetite, apatite and pyrrhotite (commonly as inclusions in pyroxenes). We did not observe any amphibole, although this phase has been reported to occur at trace levels in both the Minoan and the LP2 products (Cottrell *et al.*, 1999; Gertisser *et al.*, 2009). The LP1 and LP2 pumices are crystal-poor (1-3 wt% and 6-8 wt%, respectively), while the CR and Minoan pumices have crystallinities higher than 10 wt% (~ 20 and 10-15 wt%, respectively; Electronic Appendix 6).

The whole rocks were crushed in an agate mortar and about 10 g of the resulting powders were melted twice, to ensure homogenization, at 1400°C and 1 atm. for 3-4 hours in a Pt crucible opened to air, then quenched. The dry glass thus obtained was analysed by electron microprobe (Cameca SX 50, BRGM-ISTO, Orléans) with a sample current of 6 nA, an acceleration voltage of 15 kV and a defocused beam (5-6 μm). It was found to be similar to that of the whole-rock composition, except for a small depletion (< 0.8 wt%, Table 1) in Na_2O content. The glass was then reduced to powder and used as starting material for the experiments.

Choice of experimental conditions and general experimental strategy

The choice of experimental P, T, XH_2O, fO_2 conditions was guided both by our study of the natural samples and by the results of previous investigations (e.g., Cottrell *et al.*, 1999; Gertisser *et al.*, 2009). Our analyses of natural ilmenite-magnetite pairs indicate pre-eruptive temperatures ranging from ca. 850°C to 900°C (Table 2 & Fig. 2). The formulation of Ghiorso & Evans (2008) gives higher temperatures (+9 - 13°C) and lower fO_2 (up to 0.5 log fO_2) than those obtained using the calculation scheme of Stormer (1983) with the algorithm of Andersen & Lindsley (1985) (ILMAT software, Lepage, 2003). Hereafter, we will refer to the temperatures and oxygen fugacities calculated from Stormer (1983) and Andersen & Lindsley (1985) because their formulation gives the best agreement with data from phase equilibria experiments within the 850–900°C temperature range (Fig. 13 in Blundy & Cashman, 2008). Pre-eruptive temperatures are: 853 ± 7°C for the Minoan rhyodacite, 879 ± 15°C for the Cape Riva dacite, 856 ± 16°C for the Lower Pumice 2 rhyodacite and 869 ± 20°C for the Lower Pumice 1 rhyodacite. Redox conditions are close to FMQ (i.e., NNO-0.7) for CR, LP2 and LP1 (mean log fO_2 = -12.92 to -13.45), while the Minoan oxides record more oxidizing conditions, close to NNO. This fO_2 jump of almost one log unit from the pre-Minoan magmas to Minoan magma is a remarkable feature of Santorini's recent magmatic evolution (Fig. 2). Our T-fO_2 estimates are consistent with those of Sigurdsson *et al.* (1990) and Gertisser *et al.* (2009) for the Minoan and LP2, respectively (Fig. 2). We thus performed experiments at 850°C and 900°C with redox conditions close to FMQ (experiments #1 to 4) and close to NNO+1 (experiments #5 and 6; Table 3). We explored a wide range of H_2O and CO_2 contents, with XH_2O [= molar $H_2O/(H_2O+CO_2)$] ranging from 1 (i.e., H_2O-saturated) to 0.6 (i.e., H_2O-undersaturated). Our study thus complements previous similar work by Cottrell et al (1999), who investigated H_2O-saturated conditions only. The investigated pressures were 4, 2 and 1 kbar according to the previous literature constraints (see section above).

Because of their comparable chemical compositions (Table 1) and their similar pre-eruption magmatic temperatures (850-900°C) at any investigated P-T-fO_2, we systematically ran the four compositions together for each experiment, so as to minimize experimental errors in P, T, and fO_2, and to produce an internally consistent database. This approach ensured that any differences in phase relationships or in phase compositions between the different starting compositions observed at the same P-T-fO_2 conditions, are most probably related to bulk compositional effects (see below).

Charge preparation and experimental equipment

Known amounts of CO_2 (added as silver oxalate), distilled H_2O, and ~30 mg of silicate powder were loaded into Au capsules (15 mm length, 2.5 mm internal diameter and 0.2 mm wall thickness), as described elsewhere (e.g., Scaillet *et al.*, 1995; Martel *et al.*, 1998; Di Carlo *et al.*, 2010). All charges were H_2O+CO_2 fluid-saturated. The bulk volatile content (H_2O+CO_2) was maintained at 9-10 wt%, and the initial fluid/silicate weight ratio at ~ 0.1 (i.e., the H_2O+CO_2 mass was 3 mg for 30 mg of glass powder). Five different XH_2O values were explored for each composition (i.e., eruption), which led to five capsules per composition for each experiment (except for experiments #5 and #6; Table 3).

Crystallization experiments were performed at ISTO (Orléans) with an Internally-Heated Pressure Vessel (IHPV) oriented vertically and equipped with a molybdenum furnace. The pressurizing medium was a mixture of Ar and H_2, the Ar/H_2 ratio of which was fixed by sequential loading at room temperature, so as to reach the desired target fO_2 (Scaillet *et al.*, 1992, 1995). One or two redox sensors capsules were run with the experimental charges in order to determine *a posteriori* the fO_2 prevailing during each experiment. The sensor consisted of two pellets of hand-pressed Co-Pd-CoO (for FMQ buffered experiments) or Ni-Pd-NiO (NNO experiments) powder loaded with ~3 μl of distilled water into Au capsules and

lined with ZrO_2 powder to prevent contamination from the capsule (Taylor *et al.*, 1992; Pownceby & O'Neill, 1994).

Pressure was recorded by a transducer calibrated against a Heise–Bourdon tube gauge (uncertainty ± 20 bars), while temperature was recorded by two S-type thermocouples. The overall temperature uncertainty is ± 5 °C (Scaillet *et al.*, 1992; Schmidt *et al.*, 1995).

Runs were terminated by switching off the power supply, and subsequent drop quench. Upon quenching, the sample holder fell immediately into the coldest part of the vessel (~50°C), producing a total pressure increase of ~ 40 bars. Run durations varied between 5 to 7 days (Table 3). After each experiment, the capsules were first weighted to check for leaks and opened. For each charge about one half of the run product was mounted in epoxy resin and polished.

ANALYTICAL TECHNIQUES AND CONDITIONS

Run Products

A total of 91 charges were first analysed by scanning electron microscopy (JEOL WINSET JSM 6400, ISTO Orléans) for preliminary textural analysis and phase identification; BSE images were acquired with a current of 7 nA and an acceleration voltage of 20 kV. Experimental glasses, minerals and solid sensors were then analysed by electron microprobe (Cameca SX 50 BRGM-CNRS-University of Orléans shared facility, and Cameca SX100 of the 'Laboratoire Magmas et Volcans', Université Blaise Pascal, Clermont-Ferrand, France). Glasses and crystals were analysed with a sample current of 6 nA and an acceleration voltage of 15 kV, counting time of 10 s on peak and background for all elements; Na and K were analysed first and a ZAF correction was applied. The beam size was 5 to 10 μm for glass analyses, whereas it was focused for mineral analyses. Interstitial glasses were analysed together with dacitic and rhyolitic glass internal standards (Pinatubo 1991 eruption; Scaillet &

Evans, 1999) containing 0, 2, 4 and 6 wt% H_2O as determined by Karl Fischer titration. These standards were used in order to correct the electron microprobe analyses for Na migration under the beam and to estimate the amount of water dissolved in the interstitial glass using a modification of the by-difference method (Table 3; Devine *et al.*, 1995; Scaillet *et al.*, 1995). Owing to their small grain size, microprobe analyses of the experimental Fe-Ti oxides free from contamination from interstitial glass were difficult to obtain; most of them were recalculated assuming a SiO_2 content (wt%) near zero. Yet, in several charges, Fe-Ti oxides could not be analysed because they were smaller than the electron microprobe beam size (< 2 μm), and the glass contamination was too high to allow approximate correction using SiO_2 content.

Analytical conditions for Co-Pd-CoO and Ni-Pd-NiO sensors analyses were 20 kV – 20 nA, 10 s on each peak and 5 s on the background, the standards used during acquisition were Co or Ni-Pd-FeS-Au.

The intrinsic fH_2 prevailing during each experiment was calculated from the dissociation reaction of water using the fO_2 retrieved from the sensor, as given by the composition of the metallic alloys (Taylor *et al.*, 1992), the fugacity of pure water ($fH_2O°$) as given by Burnham *et al.* (1969), and the water dissociation constant of Robie *et al.* (1978). The fO_2-fH_2 values calculated in this way correspond to those of water-saturated charges. Then, the fO_2 of each water under-saturated charge was determined using the method of Scaillet & Evans (1999), in which the XH_2O of the charge is taken as a proxy for the prevailing fH_2O (the term $fH_2O°$ is replaced by XH_2O*$fH_2O°$) (see also Di Carlo *et al.*, 2010; Andújar & Scaillet, 2012a; Table 3). Such an approach calculates maximum fO_2 for each corresponding charge. An fO_2 decrease of 0.4 log units occurs when XH_2O decreases from 1 to 0.6, that is, redox conditions become slightly more reduced in water-undersaturated capsules (Table 3). Altogether, we estimate that reported fO_2 are accurate within ± 0.3 log units.

Analysis of natural products

Natural phase compositions and proportions are given in Electronic Appendices 5 and 6 (available for downloading from http://www.petrology.oxfordjournals.org). Major element compositions for the Minoan phenocrysts and glasses come from T. Druitt (unpublished data); it was completed for volatile measurements of the melt inclusions in the present study. Crystal and glass compositions for CR, LP2 and LP1 eruptions are from this study.

Plagioclase and pyroxene crystals were extracted from pumice clasts of CR, LP2 and LP1 and embedded in epoxy resin so as to expose the (010) face of plagioclase crystals and the (100) or (010) faces of pyroxene crystals. Then, they were polished and coated with carbon for SEM imagery and electron microprobe analysis.

Major elements, chlorine, fluorine and sulphur were analysed in interstitial glasses and phencocryst-hosted melt inclusions using a Cameca SX 100 electron microprobe ("Laboratoire et Magmas et Volcans", Clermont-Ferrand, France) with a 15 kV accelerating voltage. Major elements analyses were performed using a defocused electron beam (5 - 20 μm diameter depending on melt inclusion size), a sample current of 2 - 8 nA and 10s counting time on-peak. Na, K and Si were analysed first.

Analyses of F, S, P and Cl were performed at 30 or 80 nA with a 5 to 20 μm defocused beam depending again on the melt inclusion size. Cl, S and P were analysed on a Large PET crystal, while F was analysed simultaneously on three TAP crystals allowing low detection limits. In order to minimize volatile loss, each analysis of a single point was divided into five iterative sequences separated by beam blanking with the Faraday cup (Moune *et al.*, 2007). Thus, the total on-peak acquisition time was 25s for P, 50s for Cl and S and 300s for F. Detection limits for Cl, F and S were respectively: ~80 ppm, 200 ppm and 50 ppm. Measured contents of

fluorine and in particular sulphur are generally close to, or lower than, the detection limit (Electronic Appendix 5a).

In order to obtain high-precision mineral analyses, measurements were performed using a 15 kV accelerating voltage, a focused beam and currents of 30 nA and 50 nA for plagioclase and pyroxenes, respectively. Despite relatively high current values, no sodium loss was observed. Fe-Ti oxides were analysed with a focused beam at 15 nA and 15 kV.

H_2O, CO_2, Cl, F and S concentrations of melt inclusions were determined by Secondary Ion Mass Spectrometry (Cameca IMS 1280, CRPG, Nancy, France) using a Cs^+ primary beam projected onto a 10 µm diameter spot in Köhler mode with a 4-5 nA intensity. The electron gun was used with a HV adjusted by limiting the H^- emission below 1000 cps. The positive secondary ions were measured at a mass resolution of 8000 in order to get a full separation of $^{16}OH^-$ and $^{17}O^-$ with a 30 ± 10 eV energy filtering and by peak switching in ion counting mode. The acquisition cycles included the mass 11.8 for the background, ^{12}C, ^{17}O, ^{16}OH, ^{19}F, ^{18}O and ^{29}Si, ^{30}Si, ^{32}S, ^{35}Cl. For each measurement, the sample was pre-sputtered for 1 minute, the beam position and the magnetic field checked automatically, and 12 cycles were acquired for 9 minutes. The CO_2, H_2O, F, S, and Cl concentrations were calculated using the C^-/Si^-, OH^-/Si^-, F^-/Si^-, $S^-/Si^-$and Cl^-/Si^- ratios, respectively, with the relative useful yield relative to Si being determined on MPI-DING, natural and experimental glasses: StHs6/80-G (andesite; Jochum *et al.*, 2006), Ke-12 (rhyolite from Kenya; Mosbah *et al.*, 1991) and BT2 628-5, -6 and -7 (Bishop Tuff rhyolites synthetized by B. Scaillet, H_2O and CO_2 FTIR measurements performed by A. Cadoux). In spite of careful cleaning and polishing of the crystals aiming at removing carbon coat, SIMS carbon signal pointed out contamination which made our C^-/Si^- data unworkable. H_2O, Cl, F and S contents from SIMS measurements are reported in Table 4. There is close agreement between the Cl, F and S contents measured by EMP (Electronic Appendix 5a) and those measured by SIMS.

EXPERIMENTAL PHASE EQUILIBRIA

General observations

Experimental conditions and phases proportions are reported in Table 3. Phase proportions were calculated for each charge by mass balance using major element compositions of experimental glasses and crystals (Electronic Appendices 1 to 4, available for downloading from http://www.petrology.oxfordjournals.org). Run products include glass, amphibole, clinopyroxene, plagioclase, orthopyroxene, ilmenite, magnetite and vesicles with sizes and proportions varying with XH_2O, or with melt water content which, as estimated with the by-difference method, ranges from 2.5 up to 9.8 wt%. The presence of vesicles in almost all charges is taken as evidence of fluid saturation. Crystals have euhedral to sub-euhedral shapes: in most charges their size is smaller than 20 μm, the larger crystals (up to 150 μm length) occurring generally in H_2O-saturated ($XH_2O = 1$) charges. Crystallinity varies from 0 to 58 wt%, depending on XH_2O. Plagioclase is the most abundant mineral phase at XH_2O = 0.7-0.6, with mass proportions varying from trace amounts up to 47 wt% at $XH_2O = 0.6$. Orthopyroxene is generally the second most abundant phase (up to 10 wt% at $XH_2O = 0.6$), being sometimes superseded by amphibole, the abundance of which reaches up to 14 wt% at $XH_2O = 0.9$. Glass, amphibole, clinopyroxene and Fe-Ti oxides are the dominant phases at H_2O-saturation ($XH_2O = 1$), whilst plagioclase and orthopyroxene occur at drier conditions, except at 1 kbar-NNO+1 where both minerals occur at H_2O-saturation (Table 3). At 900°C and H_2O-saturation, clinopyroxene is the liquidus phase at 2 and 4 kbar, except for the LP2 rhyodacite, the liquidus phase of which is orthopyroxene. In contrast, at 850°C and H_2O-saturation, amphibole is the dominant phase for Minoan, Cape Riva and LP2 compositions, at both 2 and 4 kbar and at FMQ and NNO+1, clinopyroxene being even absent in Cape Riva indicating that clinopyroxene and amphibole are in a reaction relationship as temperature

decreases in the water-rich part of the phase diagrams. For the LP1 rhyodacite clinopyroxene crystallized first in all the experiments, suggesting the amphibole stability field lies at temperatures lower than 850°C over the investigated pressure and fO_2 range. Above-liquidus charges were only produced in experiments at 900°C, and under water-rich conditions.

Fe-Ti oxides are mostly < 3 μm in size, which makes them very difficult to identify and analyze. Magnetite was not identified in any charge of the FMQ experiments (Table 3): although it cannot be ruled out that trace amounts may have been overlooked, we believe that the lack of magnetite more likely reflects the moderately reduced conditions imposed in our experiments. In contrast, magnetite was identified in the NNO+1 experiments, but no ilmenite was found, probably because of the relatively oxidizing conditions.

In the LP2 rhyodacite, clinopyroxene was not detected in any of the run products, whereas orthopyroxene was present in most of the LP2 charges. In contrast, clinopyroxene was an almost ubiquitous phase in the LP1 run products and orthopyroxene crystallized only at 2 kbar-850°C-FMQ and at $XH_2O \leq 0.7$ (Table 3). This is a remarkable feature considering the very similar bulk rock compositions of LP1 and LP2 (Table 1). It can be noticed that when both pyroxenes crystallize, their respective fields of stability generally overlap very little (e.g., Figs. 3b and 4). Orthopyroxene and plagioclase both crystallized at H_2O-saturation at 1 kbar-850°C and NNO+1. At this pressure, no clinopyroxene was detected except in the LP1 rhyodacite, which crystallized clinopyroxene at H_2O-saturation, as observed at 2 and 4 kbar (Table 3).

Phase relationships

Phase boundaries (Figs. 3-6) were first drawn on the basis of phase assemblages of run products and subsequently refined using phase proportions (Table 3). For each composition, phase equilibrium diagrams are shown at constant pressure (2 and 4 kbar) and fO_2 (FMQ) as a

function of XH_2O and of temperature (°C). For the Minoan, a phase diagram of pressure versus XH_2O at 850°C and fO_2 = NNO+1 is also presented (Fig. 3c). For the four compositions, the effect of increasing pressure from 2 to 4 kbar is to displace each mineral-in curve towards lower temperature and lower XH_2O. Similarly, the main effect of an increase of fO_2 from FMQ to NNO+1 is the replacement of ilmenite by magnetite (Table 3).

Minoan rhyodacite

At 2 and 4 kbar (Fig. 3), clinopyroxene is the liquidus phase crystallizing near 900°C at XH_2O = 1 (i.e., H_2O_{melt} > 6 wt%). Clinopyroxene reacts out at temperatures below 850°C at H2O-saturation, and at slightly higher temperatures as H_2O_{melt} decreases (Fig. 3a). It is accompanied by amphibole at temperatures lower than ca. 875°C and H_2O_{melt} > 5 wt%. At 2 kbar, the stability field of amphibole is restricted to XH_2O = 0.9-1, while at 4 kbar it extends towards lower XH_2O (= 0.7). At 850°C and 4 kbar, the abundance of amphibole is higher at XH_2O = 0.9 (6.6 wt%) than at H_2O-saturation (2.2 wt%). Orthopyroxene occupies essentially the dry portion of the phase diagram: the back bending of its stability curve at low temperatures, at both 2 and 4 kbar, is inferred from previous detailed experimental work on similar intermediate to silicic magmas (Scaillet & Evans, 1999; Dall'Agnol *et al.*, 1999; Klimm *et al.*, 2003; Costa *et al.*, 2004). At 2 kbar, both clinopyroxene and orthopyroxene coexist in several charges at 850°C and 900°C (Fig. 3). We did not observe these minerals together at 4 kbar (orthopyroxene is absent in the experiments at 900°C), yet, based on the 2 kbar observations, a narrow co-existence domain is suggested on the corresponding phase diagram between 875 and 850 °C and XH_2O = 0.7-0.8. At 2 and 4 kbar, plagioclase requires less than 4.5 wt% H_2O_{melt} to crystallize at 900°C, and about 5.2-6.3 wt% H_2O_{melt} at 850°C (including at NNO+1, Fig. 3c).

Ilmenite is only stable at temperatures lower than 900°C at both 2 and 4 kbar in the FMQ experiments (Table 3). Magnetite is present in all the run products of 850°C-NNO+1 experiments, both at 2 and 1 kbar, in the XH_2O range explored (= 0.8 to 1).

At 850°C, 2 kbar and XH_2O = 0.8-1, the main effect of a higher fO_2 (NNO+1) on phase equilibria of the Minoan rhyodacite is to expand the stability field of amphibole to $XH_2O \leq$ 0.8, in addition to the replacement of ilmenite by magnetite (see experiments #2 and #5; Table 3).

A partial isothermal(850°C)-polybaric section shows that at 1 kbar - 850°C - NNO+1, plagioclase and orthopyroxene occur at water-saturated conditions along with amphibole (~ 3 wt% H_2O_{melt}) (Fig. 3c), clinopyroxene being absent. At this temperature, clinopyroxene is not stable below 1.5 kbar at H_2O-saturation.

Cape Riva dacite

The phase equilibria of the Cape Riva (Fig. 4) broadly resemble those of the Minoan, except that the T-XH_2O coordinates of any liquidus curve are different. At H_2O-saturation (XH_2O = 1), clinopyroxene is the liquidus phase, crystallizing slightly above 900°C. In contrast, at 850°C and H_2O-saturation, only amphibole (± ilmenite) is found at either 2 or 4 kbar. As stated previously, this indicates that clinopyroxene and amphibole are in a reaction relationship as temperature decreases. At 2 kbar, the clinopyroxene stability field is restricted to temperatures of > 850°C, as well as to higher H_2O_{melt} (> ~6 wt%), being replaced by both orthopyroxene and plagioclase as H_2O_{melt} decreases. At 4 kbar, the clinopyroxene stability field extends towards lower H_2O_{melt}, but is not stable at 850°C. The field of amphibole extends towards lower XH_2O (= 0.6) at 4 kbar than at 2 kbar (= 0.8), though these XH_2O correspond to essentially the same H_2O_{melt} values (6 wt%). As observed for the Minoan at 4 kbar-850°C, amphibole abundance reaches its maximum (up to 14 wt% at 850°C - 2 kbar) at

XH_2O = 0.9, and not at H_2O-saturation. Whatever the pressure and temperature, plagioclase in Cape Riva magma appears before orthopyroxene. Plagioclase is the most abundant phase, with mass proportions increasing with decreasing XH_2O up to 47 wt% at 850°C - 2 kbar and XH_2O = 0.6. Ilmenite is almost ubiquitous over the P-T-XH_2O conditions explored, appearing after clinopyroxene or amphibole, depending on XH_2O.

Lower Pumice 2 rhyodacite

Except for the location of the plagioclase stability curve, which remains broadly the same (plagioclase being the dominant phase in the water–poor part of the diagrams), the phase equilibria of the Lower Pumice 2 rhyodacite (Fig. 5) differ significantly from those of the Minoan and Cape Riva magmas, in particular in the lack of clinopyroxene.

At 2 kbar – 900°C, ilmenite is the liquidus phase, crystallizing slightly below H_2O-saturation, while it is replaced by amphibole at lower temperatures. In contrast to the Minoan and Cape Riva, orthopyroxene always crystallizes before plagioclase, whatever the pressure and temperature, and it is stable even at H_2O-saturation at 850°C (Fig. 5 and Table 3).

At 4 kbar, the ilmenite curve is significantly shifted toward lower temperatures as compared to the 2 kbar field. Orthopyroxene is the liquidus phase up to XH_2O = 0.9, but is replaced by amphibole at higher H_2O_{melt} values (> 5 wt%) and lower temperatures (< ca. 875°C). Amphibole is not stable at 900°C, as also observed at 2 kbar.

At 2 kbar-850°C and H_2O-saturation, increasing fO_2 from FMQ to NNO+1.8 makes orthopyroxene unstable (Table 3). At 1 kbar-850°C-NNO+1.7, both plagioclase and orthopyroxene occur at H_2O-saturation (i.e., H_2O_{melt} = 3.4 wt%, Table 3).

Lower Pumice 1 rhyodacite

At 2 and 4 kbar (Fig. 6), clinopyroxene is the liquidus phase stable almost all over the explored P-T-XH_2O conditions. At 4 kbar, its stability field is slightly smaller than at 2 kbar; the upper limit being displaced to $XH_2O < 1$ at 900°C, and the lower limit being moved to temperatures > 850°C at $XH_2O < 0.7$ (Fig. 6). The plagioclase stability field is similar to that of the Minoan, CR and LP2 phase diagrams. Amphibole was not detected in any of the run products but, by analogy with the other three compositions, is inferred to crystallize at T < 850°C. Ilmenite is ubiquitous at 2 kbar, while at 4 kbar it is stable only below 900°C. Low-Ca pyroxene (pigeonite) was identified at T = 850°C and $XH_2O \leq 0.8$, at 2 and 4 kbar in the FMQ experiments. At 1 kbar – 850°C –NNO+1.7, LP1 rhyodacite crystallizes plagioclase at H_2O-saturation (H_2O_{melt} = 3.2 wt%, Table 3) as in the three other compositions.

EXPERIMENTAL PHASE COMPOSITIONS

General observations

The following features are common to the four eruptions (Figs. 7 to 14):

(1) The experimental glasses show systematic compositional variations with increased crystallization: at fixed P-T-fO_2, decreasing XH_2O (i.e., H_2O_{melt}) produces an increase in SiO_2 and K_2O contents, and a decrease in Al_2O_3, FeO, MgO and CaO (Figs. 7 to 10).

(2) The melts produced at 900°C are less SiO_2- and K_2O-rich than those produced at 850°C. Similarly, at a fixed temperature, the melts produced at higher pressure are less SiO_2- and K_2O-rich than those produced at lower pressure, owing to the increasing water solubility with increasing pressure and lower crystallinity of the run products. At fixed P and T, the effect of increasing fO_2 from FMQ to NNO+1 is to produce melts richer in SiO_2 and K_2O (Figs. 7 to 10) and products richer in crystals (Figs. 11a, 12a, 13a, 14a).

(3) The melt H_2O content at saturation is similar for all compositions, varying between 3-4 wt% at 1 kbar, 6-8 wt% at 2 kbar, up to 9-10 wt% at 4 kbar, in agreement with solubility constraints of H_2O for silicic magmas (e.g., Newmann & Lowenstern, 2002)

(4) Crystallinity increases with decreasing XH_2O (Figs. 11a, 12a, 13a, 14a)

(5) Mineral compositions vary with intensive parameters (Figs. 11 to 14). The compositions of ferro-magnesian minerals (pyroxenes, amphiboles, Fe-Ti oxides) are strongly affected by fO_2 variations, while plagioclase composition is sensitive to temperature and H_2O_{melt}.

Minoan rhyodacite

Interstitial glass

In all analysed charges, the experimental Minoan glasses are homogeneous within analytical uncertainty (Electronic Appendix 1a). They have compositions ranging from rhyodacitic to rhyolitic (SiO_2 = 71.5-76.8 wt%), depending on the experimental parameters (T-P-fO_2-XH_2O; Fig. 7) as stated above. The glass water content (H_2O_{melt}) decreases with decreasing pressure: at H_2O-saturation (XH_2O = 1), it is estimated to be 7-8 wt% at 4 kbar-FMQ and 850-900°C (Table 3), close to 6 wt% at 2 kbar and 850-900°C (both at FMQ and NNO+1), and decreases to 3 wt% at 1 kbar – 850°C – NNO+1.7.

Plagioclase

The plagioclase compositions given in Electronic Appendix 1b are average analyses, selected on the basis of a total close to 100 wt% and on the correctness of the structural formula. The anorthite contents (An) range between An_{24} and An_{42}. At fixed P and fO_2, the anorthite content generally decreases with falling XH_2O (i.e., H_2O_{melt}) and increases with increasing temperature from 850°C to 900°C (Fig. 11b). The effect of temperature and H_2O_{melt} on

plagioclase composition is more important than that of the pressure, as also observed for the interstitial glass compositions (Fig. 7).

Orthopyroxene

Though corrected for glass contamination, a number of analyses of experimental Minoan orthopyroxenes (Electronic Appendix 1c) still contain some Al_2O_3 (up to 2.7 wt%), due to the very small size of the crystals (< 5 μm), particularly in charges with XH_2O < 0.8. The wollastonite component ranges from 3 to 12 %; it tends to increase with XH_2O (reaching pigeonite-like composition for XH_2O < 0.8), variations with other experimental parameters being less apparent (Fig. 5c). However, the FeO*/MgO ratio (where FeO* is total Fe as FeO) is lower for the orthopyroxenes produced at fO_2 = NNO+1 than for those crystallized under more reduced FMQ conditions (Fig. 11d).

Clinopyroxene

The wollastonite component of experimental Minoan clinopyroxenes (Electronic Appendix 1d) ranges from 29 to 47 %. At 900°C, the wollastonite contents are lower (29- 41%) than at 850°C (41-47%; Fig. 11e), being also positively correlated with H_2O_{melt}. Increasing fO_2 induces lower FeO*/MgO ratios (Fig. 11f), as also observed in orthopyroxene.

Amphibole

Amphibole crystallized in the Minoan charges (Electronic Appendix 1e) exclusively at 850°C, at 1, 2 and 4 kbar and fO_2 = FMQ and NNO+1, but was not found at XH_2O lower than 0.8. The Mg# [Mg/(Mg+Fe)*100] values reflect the effects both of H_2O_{melt} content and fO_2: they tend to decrease progressively with decreasing XH_2O and are higher at fO_2 = NNO+1 (Mg# =

65-72%) than at fO_2 = FMQ (Mg# = 64-54%; Fig. 11h). The effect of pressure on amphibole composition is moderate.

Fe-Ti oxides

Fe–Ti oxides were observed exclusively in experiments performed at 850°C. FMQ runs crystallized only ilmenite while NNO+1 runs crystallized only magnetite (Table 3). The mole fraction of ilmenite (X Ilm) calculated from Stormer (1983) is 0.95-0.96 and the mole fraction of ulvöspinel (X Usp) for the magnetite is in the range 0.17-0.23 (Fig. 11g). X Ilm and X Usp both increase slightly with decreasing XH_2O.

Cape Riva dacite

Interstitial glass

Compositions of interstitial glasses in the Cape Riva run products (Electronic Appendix 2a) are rhyodacitic to rhyolitic (SiO_2 = 68-76 wt%; Fig. 8). The glass water content decreases with decreasing pressure: at H_2O-saturation, it is estimated to be in the range 8.7-9.6 wt% at 4 kbar-FMQ and 850-900°C, and close to 7 wt% at 2 kbar and 850-900°C (both at FMQ and NNO+1), decreasing to 3.6 wt % at 1 kbar – 850°C – NNO+1.7 (Table 3).

Plagioclase

The anorthite contents of the experimental Cape Riva plagioclases range between An_{22} and An_{39} (Electronic Appendix 2b). At fixed P- fO_2, the anorthite component generally decreases with falling XH_2O (i.e., H_2O_{melt}), and increases with increasing temperature from 850°C to 900°C (Fig. 12b).

Orthopyroxene

The wollastonite component of the experimental Cape Riva orthopyroxenes ranges between 3 to 22 % (Electronic Appendix 2c). From Figure 12c, no clear relationship can be established with XH_2O or any other experimental parameters. At fO_2 = FMQ, the FeO*/MgO ratio is higher for the orthopyroxenes produced at 850°C (1.7-3.0) than at 900°C (1.3-2.1) and, at fixed T, FeO*/MgO ratio is slightly higher at 2 kbar than at 4 kbar (Fig. 6d). Finally, the NNO+1 experiment produced the orthopyroxene with the lowest FeO*/MgO (= 0.65) and the lowest wollastonite content (Figs. 12c and 12d).

Clinopyroxene

With the Cape Riva dacitic magma, clinopyroxene (Electronic Appendix 2d) was produced exclusively in experiments performed at 900°C-FMQ in the pressure and XH_2O range explored (Table 3). For the same XH_2O (= 0.9-0.8), clinopyroxenes crystallized at 2 kbar have lower wollastonite contents (Wo_{38-41}) and higher FeO*/MgO ratios (1.05-1.12) than those crystallized at 4 kbar (Wo_{41-42} and FeO*/MgO =0.85-0.94; Figs. 12e and 12f). The wollastonite content increases with XH_2O up to 0.9 (Fig. 12e).

Amphibole

As in the Minoan rhyodacite, Cape Riva experimental amphibole (Electronic Appendix 2e) crystallized exclusively at 850°C, and is stable down to XH_2O = 0.7 (H_2O_{melt} = 5.8 wt%) at 4 kbar-FMQ (Table 3). The Mg# of the amphibole is affected by the H_2O_{melt} content and pressure, but more importantly by the fO_2: it tends to decrease progressively with decreasing XH_2O, whilst it displays slightly higher values at lower pressure and significantly higher values in oxidizing conditions (NNO+1: Mg# = 69-73%) compared to relatively reduced conditions (at FMQ: Mg# = 54-44%; Fig. 12h).

Fe-Ti oxides

Fe–Ti oxides were produced in the Cape Riva magma in all experiments (Electronic Appendix 2f). The X Ilm of ilmenite (FMQ runs) is 0.93-0.98 and the X Usp for the magnetite (NNO+1 runs) is 0.19-0.20 (Fig. 12g).

Lower Pumice 2 rhyodacite

Interstitial glass

The composition of interstitial glasses in the LP2 experiments (Electronic Appendix 3a) is rhyodacitic to rhyolitic (SiO_2 = 69-75 wt%), depending on T-P-fO_2-XH_2O conditions (Fig. 9). The glass water content decreases with decreasing pressure: at H_2O-saturation, it is in the range 8.4-9.6 wt% at 4 kbar-FMQ and 850-900°C, and about 5.6 to 8.0 wt % at 2 kbar and 850-900°C (both at FMQ and NNO+1), and it decreases to 3.4 wt% at 1 kbar – 850°C – NNO+1 (Table 3).

Plagioclase

The anorthite content of the experimental LP2 plagioclases ranges between An_{26} and An_{44} (Electronic Appendix 3b). At fixed P, it generally falls with decreasing XH_2O (i.e., H_2O_{melt}) and increases with increasing temperature from 850°C to 900°C (Fig. 13b).

Orthopyroxene

The wollastonite component of the orthopyroxenes (Electronic Appendix 3c) ranges from 3 to 6 %. It tends to increase with decreasing XH_2O and pressure (Fig. 13c). At fO_2 = FMQ, the FeO*/MgO ratio is higher for those orthopyroxenes produced at 850°C (~1.4-2.6) than at 900°C (~1.1-2.0) and, at 900°C, the FeO*/MgO ratio is higher at P = 2 kbar than at P = 4 kbar. There is not significant effect of pressure at 850°C (Fig. 13d). Finally, the NNO+1

experiment produced the orthopyroxene with the lowest FeO*/MgO (= 0.66) at H_2O-saturation (Fig. 13d).

Amphibole

As in the Minoan and Cape Riva compositions, LP2 experimental amphibole (Electronic Appendix 3e) crystallizes only at 850°C, and is stable down to $XH_2O = 0.8$ (i.e., H_2O_{melt} = 6.3 wt%) at 4 kbar-FMQ (Table 3). At H_2O-saturation, the Mg# of the amphibole is significantly higher at NNO+1 (Mg# = 71-74) than at FMQ (Mg# = 53-60; Fig. 13f). The effect of decreasing H_2O_{melt} content in lowering the Mg# can be seen at 4 kbar-FMQ (Fig. 13f).

Fe-Ti oxides

Fe–Ti oxides were produced in all our LP2 experiments (Electronic Appendix 3f). Ilmenite and magnetite have X Ilm (0.94-0.97) and X Usp (0.18-0.20), similar to those of the Fe–Ti oxides of the Minoan rhyodacite and Cape Riva dacite (Fig. 13e).

Lower Pumice 1 rhyodacite

Interstitial glass

The compositions of the LP1 experimental glasses are reported in Electronic Appendix 4a. They are rhyodacitic to rhyolitic (SiO_2 = 69.7-73.5 wt%), depending on T-P-fO_2-XH_2O conditions (Fig. 10). The glass water content decreases with decreasing pressure: at H_2O-saturation, it is estimated to be in the range 8-10 wt% at 4 kbar-FMQ and 850-900°C, and close to 7 wt% at 2 kbar and 850-900°C (both at FMQ and NNO+1), and it decreases to 3.2 wt % at 1 kbar – 850°C – NNO+1 (Table 3).

Plagioclase

The LP1 experimental plagioclases (Electronic Appendix 4b) display significantly lower anorthite contents (An_{14-26}) in comparison with those produced with the other three magmas under the same experimental conditions (An_{22-44}). The anorthite content generally decreases with falling XH_2O (i.e., H_2O_{melt}) and increases with increasing temperature from 850°C to 900°C (Fig. 14b).

Pigeonite

Low-Ca pyroxene was rare among the LP1 experimental products and difficult to analyse. The average compositions are given in Electronic Appendix 4c. Pigeonite compositions were found at 2 and 4 kbar-850°C-FMQ. The wollastonite contents range between 11 and 25 % and tend to increase with decreasing XH_2O (Fig. 14c). At fixed XH_2O, pyroxenes formed at 2 kbar show higher wollastonite content (Wo_{14-23}) and lower FeO*/MgO ratio (2.4-2.6) than those formed at 4 kbar (Wo_{11-15}; FeO*/MgO = 2.7-2.9; Figs. 14c and 14d).

Clinopyroxene

Clinopyroxene ($Wo_{31-46}En_{30-40}Fs_{15-38}$) is a ubiquitous phase in the experimental products of LP1 rhyodacite (Table 3, Electronic Appendix 4d). As observed for the other three magmas, clinopyroxene crystallizing at the lowest temperature and pressure has lower wollastonite contents (Wo < 39%) and higher FeO*/MgO ratios (= 1.2-2.1; Figs. 14e and 14f). Clinopyroxenes from the NNO+1 runs present the highest Wo content (45-46 %) at H_2O-saturation (Fig. 14e). The Wo content is positively correlated with XH_2O, except at 850°C – 4 kbar.

Fe-Ti oxides

Fe–Ti oxides are also ubiquitous phases in all experiments with the LP1 rhyodacite (Electronic Appendix 4f). X Ilm of ilmenite (0.95-0.97; FMQ runs) and X Usp of the magnetite (0.17-0.19; NNO+1 runs; Fig. 14g) are similar to those of the oxides produced with the other rhyodacites.

PHASE COMPOSITIONS IN THE NATURAL PRODUCTS

Mineral compositions

Both plagioclase and pyroxene phenocrysts in pyroclasts from the four eruptions display complex zoning patterns. For the purpose of this study, we focused our attention on the rim compositions of the phenocrysts as they are assumed to be in equilibrium with the pre-eruption melt. Plagioclase rims have an average composition ranging from An_{35} to An_{42} (Minoan: $An_{39\pm1}$, Cape Riva: $An_{38\pm1}$, Lower Pumice 2: $An_{35\pm4}$, Lower Pumice 1: $An_{42\pm3}$; Electronic appendix 5b) in agreement with the values reported by Druitt *et al.* (1999). A bytownite rim (An_{87}) belonging to a sieve-textured euhedral xenocryst was analysed in the LP1 rhyodacite (Electronic appendix 5b). The four eruptions also have similar orthopyroxene and clinopyroxene rim compositions: $Wo_3En_{50-57}Fs_{41-47}$ and $Wo_{40-43}En_{36-39}Fs_{19-23}$, respectively. The same observations can be made for ilmenite-magnetite compositions (X Ilm ~0.9 and X Usp = 0.4-0.5; Electronic appendix 5b).

Compositions of melts inclusions and interstitial glasses

Interstitial glasses and phenocrysts-hosted melt inclusions (in plagioclase, ortho- and clinopyroxene) have very similar compositions in terms of major and volatile elements (Electronic appendix 5a, Table 4). The glass compositions are rhyodacitic for the Cape Riva dacite and the Lower Pumices 1 and 2 (SiO_2 = 69.3-71.0 wt% for interstitial glasses and 70.0-71.4 wt% for melt inclusions), and rhyolitic for the Minoan (SiO_2 = 73.8 wt% for interstitial

glasses and 72.1 wt% for melt inclusions). Both interstitial glasses and melt inclusions are chlorine rich: ~ 2700 ppm and 2800 ppm in average, respectively, for Cape Riva, Lower Pumice 2 and Lower Pumice 1, and 2900 ppm (interstitial glass) up to 3500 ppm (melt inclusions) in average for the Minoan. Fluorine and sulphur are minor species, with contents in the range 500-800 ppm and 50-100 ppm, respectively. These values are comparable to the earlier data of Devine *et al.* (1984), Sigurdsson *et al.* (1990), Cottrell *et al.* (1999) and Michaud *et al.* (2000) for the Minoan eruption, and are also close to the values reported by Gertisser *et al.* (2009) for Lower Pumice 2, except for S contents, for which they report higher values, notably in MI (140 ± 50 ppm). It is to note that the S contents of the MI that we measured both by EMP (41 ± 12 ppm; Electronic Appendix 5a) and SIMS (50 ± 2 ppm; Table 4) are in agreement. Thus, LP2 melt inclusions are probably heterogeneous with respect to sulphur.

For the four eruptions, water contents of melt inclusions are mostly in the range 3-6 wt%. There is no significant difference of water content according to their location within a single crystal, nor between plagioclases and pyroxenes (Table 4). The few melt inclusions with water contents lower than 3 wt% most probably leaked (e.g., Lowenstern, 1995).

DISCUSSION ABOUT PHASE EQUILIBRIA

Attainment of equilibrium conditions during the experiments

Our experimental strategy is well known for favouring crystal nucleation in alumino-silicate glasses (Clemens & Wall, 1981; 1986; Pichavant, 1987) and the attainment of crystal-liquid equilibrium on laboratory time-scales (Pichavant *et al.*, 2007). Previous work, in particular on haplogranite compositions (equivalent to high-silica rhyolites), has shown that the use of fine-grained dry glass as starting material promotes crystal nucleation, leading to the production of equant textures in crystal-bearing charges. Attainment of equilibrium in silica-rich liquids

using such a procedure has been rigorously demonstrated by performing reversals (e.g., Pichavant, 1987), which have shown that, within experimental error, such a protocol does not lead to any mislocation of liquidus curves specific to each mineral. Our compositions are significantly less silicic than haplogranite, and our study has focused primarily on near-liquidus conditions, in keeping with the crystal-poor character of the studied Santorini magmas (ca. 2 to 20 wt%). Both factors (less silicic and crystal-poor) imply that melt viscosity, and hence component diffusivities, are significantly lower than in the high-silica rhyolites for which crystal-liquid equilibrium has been demonstrated. This in turn suggests that crystal nucleation and growth should not have been a problem in our study. In support of this statement is the following additional evidence: (1) early work performed on andesite-dacite compositions (Martel *et al.*, 1999) has shown that, when not drop-quenched, such compositions end up producing abundant quench minerals. This observation shows that the activation energy for crystal nucleation in intermediate to silicic hydrous magma is surmountable; (2) the crystal abundance varies regularly and smoothly as functions of T and H_2O_{melt}, suggesting that this parameter is tightly controlled by intensive variables and not affected by crystal nucleation kinetics; (3) the phase boundary curve shapes are as expected from first-order thermodynamic considerations: in particular, the freezing-point depression effect of water on plagioclase stability is manifest in the four phase diagrams; (4) the amphibole stability curves, although differing between the four compositions studied, are similar to those from previous experimental and theoretical studies (Rutherford *et al.*, 1985; Gardner *et al.*, 1995; Ghiorso, 1997; Scaillet & Evans, 1999; Dall'Agnol *et al.*, 1999; Martel *et al.*, 1999; Bogaerts *et al.*, 2006). The stronger depression of liquidus temperature of oxide phases (ilmenite) relative to plagioclase as pressure increases has been also previously documented by Sisson and Grove (1993). The smooth variation of phase compositions with variations of intensive parameters (Figs. 8 to 15) also supports a close approximation to

equilibrium conditions. We conclude that the phase diagrams define the equilibrium topology for each magma composition immediately prior to eruption. Differences in phase relationships between the four magmas are attributed to subtle variations in bulk chemistry, as discussed further below.

Comparison with previous phase equilibria

Previously, the phase relationships of the Minoan rhyodacitic magma have been determined exclusively under water-saturated conditions (Cottrell *et al.*, 1999); this constitutes one of the main differences with our experimental approach in which we explored both water-saturated and water-undersaturated conditions. At 1 kbar-850°C-NNO+1, Cottrell *et al.* (1999) predicted amphibole occurrence along with plagioclase, pyroxene and Fe-Ti oxides, which is in agreement with our findings except for the occurrence of clinopyroxene (Fig. 3c, Table 3). Differences between the two data sets appear at 2 kbar-850°C-NNO+1 and include orthopyroxene and plagioclase, which are not found at H_2O-saturation in our study (Table 3). As extensively discussed by Pichavant *et al.* (2007), these features may be related to the different experimental procedures employed in each study: use of gently crushed pumice (Cottrell *et al.*, 1999) versus use of dry glass material (this study), the former allowing metastable persistence of pre-existing crystals (especially if large phenocrysts, and/or phases having slow melting kinetics, such as tectosilicates, are initially present). Apart from the Cottrell *et al.* (1999) work, there is no other experimental study available on rhyodacite compositions *sensu stricto*.

For the dacitic magma of Cape Riva, which is the least silicic of the four Santorini compositions, a comparison can be made with that of the Pinatubo dacite, which has 65.5 wt% SiO_2 (Scaillet & Evans, 1999). Such a comparison reveals the same general topological arrangement between amphibole, orthopyroxene and plagioclase, the latter being displaced

down-temperature by more than 50°C (at comparable H_2O_{melt}) in Cape Riva, a result of the lower bulk CaO content relative to Pinatubo dacite (3.00 vs. 4.82 wt%). Despite the higher CaO content of the Pinatubo magma, clinopyroxene is restricted to very dry conditions in this composition at 2 kbar, while it appears on the liquidus in Cape Riva. Gardner *et al.* (1995) reported similar findings on the Wn dacite from Mt. St Helens, which has a composition very close to that of Cape Riva, except for a lower Fe/Mg ratio. Although the experimental coverage of Gardner *et al.* (1995) does not allow a detailed comparison with our 2-4 kbar phase relationships, the main feature of interest is the lack of clinopyroxene in the Wn dacite, despite the bulk rock having a higher CaO content compared to Cape Riva (3.8 vs. 3.0 wt%). The latter fact illustrates that, although clearly an essential component for clinopyroxene crystallization in magmas, the absolute abundance of CaO does not simply correlate with the stability field of clinopyroxene (i.e., the more CaO, the larger the stability field of clinopyroxene). One obvious reason is that clinopyroxene is in competition with other Ca-bearing minerals, in particular plagioclase and amphibole.

One critical difference between the above rocks is their FeO/MgO content, which is lower in the Wn and Pinatubo dacites than in Cape Riva. We tentatively suggest that, in addition to CaO, such a ratio exerts a control on the stability field of pyroxenes in hydrous intermediate to silicic magmas, calcic pyroxenes being favored by higher FeO/MgO ratios, everything else being equal. This parameter is not the only one affecting pyroxene stability, however. Experiments at higher pressures on the Pinatubo dacite (Prouteau & Scaillet, 2003) have shown that, as pressure increases, clinopyroxene progressively replaces orthopyroxene as the main pyroxene on the liquidus. The same is observed on Cape Riva, in which the orthopyroxene stability field shrinks considerably when going from 2 to 4 kbar (Fig. 4), but also on the other compositions, which crystallize both pyroxenes (Minoan and LP1). Expansion of the clinopyroxene stability field (relative to orthopyroxene) at higher pressure

goes along with that of amphibole, both being accompanied by the decreased stability of plagioclase. This suggests that water complexation with melt components affects more the melt precursor species of plagioclase than those leading to amphibole/clinopyroxene crystallization. The fact that orthopyroxene stability increases with decreasing pressure in intermediate to silicic magmas is reminiscent of the expansion of the stability field of olivine (relative to clinopyroxene) documented at low pressure in basalt (e.g., Di Carlo *et al.*, 2006). In the more felsic magmas olivine is replaced by orthopyroxene by virtue of the higher prevailing silica activity. Altogether (and to a first order), provided that compositional effects have been well circumvented, this suggests that occurrence of orthopyroxene in place of clinopyroxene is an indication of low pressure magma equilibration conditions, as exemplified by the case of the Minoan (Fig. 3c).

Comparison of phase relationships between Santorini magmas

The above comparisons illustrate how subtle compositional factors may affect phase relationships of magmas of similar compositions (e.g., rhyodacites) in a rather complex way. Comparison between the four Santorini compositions serves to illustrate this sensitivity, with the advantage that the phase equilibria were determined using the same procedure and synthesis conditions. Taking into account that our P-T-fO_2-XH_2O experimental conditions were rigorously the same for all four magmas, observed differences can only be attributed to compositional differences between the starting products (Table 1).

Except for the LP2 rhyodacite in which clinopyroxene did not crystallize, the main mineral phases present in the natural rocks were reproduced experimentally for the four compositions. However, their phase relationships show marked differences (Figs. 3 to 6). Such significant topological differences were not anticipated, in particular between the Minoan and LP2 which are very similar, both petrologically and geochemically (Druitt *et al.*,

1999). This is illustrated on Figures 15A and 15B, which compare the equilibrium curves of each phase in the four compositions used in this work. Clearly, both plagioclase and amphibole liquidus curves are similar in shape and T-XH_2O coordinates, while curves for pyroxenes and ilmenite differ from each other more markedly. Differences in the location of the ilmenite stability field may be attributed primarily to variations in FeO and TiO_2 contents (see Table 1): the Minoan composition has the lowest FeO (2.85 wt%) and TiO_2 (0.45 wt%) contents and displays the smallest ilmenite stability field (Fig. 15), whereas in the Cape Riva composition, which has the highest FeO (4.35 wt%) and TiO_2 (0.68 wt%) contents, the ilmenite stability field extends over all (at 2 kbar, Fig. 15A) or almost all (at 4 kbar, Fig. 15B) the phase diagram. Plagioclase systematics can be easily correlated with the variation in bulk CaO content, higher CaO producing higher plagioclase saturation temperatures at fixed H_2O_{melt} (or XH_2O). The amphibole stability field also follows a similar rationale, its stability increasing with bulk CaO content (Figs. 15A and 15B). LP1 has the most extended clinopyroxene stability field both at 2 and 4 kbar (Figs. 15A and 15B), and this appears to be correlated with its higher FeO/MgO ratio (4.48) and lower CaO content (2.03 wt%) than those of the Minoan and Cape Riva, the clinopyroxene fields of which are smaller. The lack of clinopyroxene in LP2 is a case in point. The fact that this mineral has not been identified in both 2 and 4 kbar runs makes it difficult to propose phase overlooking as a possible explanation and strongly suggests instead that this is an intrinsic feature of LP2 phase equilibria (leaving aside nucleation problems as discussed previously). LP2 has the second highest FeO/MgO (4.24) after LP1 (FeO/MgO = 4.48), and a slightly higher CaO content (2.30 wt%, comparable to the Minoan; Table 1), which could favor clinopyroxene crystallization. The fact that this is not observed suggests that another compositional factor plays a role. Indeed, the stability fields of pyroxenes cannot be related in any simple way to the variation of a given major oxide. Instead, pyroxene stabilities result from the complex

interplay of several elements in particular Ca, Fe, Mg, Na and H_2O, or parameters such as pressure or fO_2, the individual and additive effects of which remain to be unraveled. It is remarkable that LP1, despite having the lowest CaO content of all of the four magmas, is the one in which clinopyroxene displays the largest stability field at either 2 or 4 kbar. This goes along with the smallest inferred stability field for amphibole (and plagioclase), both features indicating that amphibole and clinopyroxene are fundamentally in a reaction relationship as previously observed in silicic magmas (e.g., Dall'Agnol *et al.*, 1999).

In summary, the systematics revealed by the four phase diagrams show that the variations of stability fields of alumino-silicate minerals (plagioclase and amphibole) in broadly chemically similar magmas can be reasonably explained with the use of simple melt "descriptors", such as bulk CaO content in the present case. Conversely, it appears that silicate phases lacking aluminium as an essential component (pyroxenes) have stability fields that vary in a complex, and so far unpredictable, way, underlining the need for a more detailed knowledge of the atomic structures of hydrous natural multicomponent silicate melts.

CONSTRAINTS ON PRE-ERUPTIVE CONDITIONS

Phase equilibrium constraints

The phase relationships discussed above can be now used to set constraints on pre-eruption conditions, using the fact that the mineral assemblage Plg-Opx-Cpx-Fe-Ti oxide is common to the four compositions. First order constraints on temperature are provided by the fact that clinopyroxene reacts out generally below 850°C regardless of pressure and water content (Figs. 3-4), except in LP1 in which it is stable down to 800°C (Fig. 6). Clinopyroxene is replaced below 850-800°C by either amphibole (in water-rich conditions) or plagioclase (water-poor conditions). Orthopyroxene is generally not stable at H_2O-saturation in the pressure range 2-4 kbar: hence its occurrence indicates water-undersaturated conditions with

$XH_2O < 0.9$, corresponding to H_2O_{melt} generally lower than 6 wt% (Figs. 3-6), except for LP2 where water-saturation cannot be excluded using this sole criteria. Similarly, the lack of amphibole in the phenocryst assemblage of the four compositions points either to a pre-eruptive temperature higher than ca. 875°C or to H_2O_{melt} lower than 6 wt% (Figs. 3-6). The use of topological arguments alone provides no basis for a pressure estimate, which is equivalent to saying that there is no particular problem in reproducing the canonical phase assemblage at either 2 or 4 kbar.

Further insight can be gained by combining phase relationships with temperature constraints obtained from Fe-Ti oxides (Table 2), the different estimates of each rock being represented on Figs. 3-6 as grey bands. In all cases, upper and lower bounds on H_2O_{melt} are provided by plagioclase precipitation and its coexistence with pyroxenes, respectively. We first carry out such an analysis at 2 kbar, a possible long standing reservoir pressure for felsic eruptions as shown by Cottrell *et al.* (1999). For the Minoan magma, the H_2O_{melt} is in the range 5.2-6.3 wt% for a pre-eruptive temperature of 850°C (Fig. 3a), which fits well with melt inclusion analyses of this study (H_2O_{melt} = 4.0-5.8 wt%; Table 4) and those of Cottrell *et al.* (1999) (H_2O_{melt} = 3.5-6.5 wt%). The Cape Riva magma has a higher Fe-Ti oxide temperature, a slightly larger Plg stability field, and a restricted Cpx-Opx coexistence domain, which all combine to set an H_2O_{melt} value centered at 6.1 wt% (Fig. 4a). For the LP2 magma, the H_2O_{melt} cannot be higher than approximately 6 wt% at 865°C, which also agrees both with our SIMS measurements (H_2O_{melt} = 3.2-5.3 wt%; Table 4) and the FTIR measurements of Gertisser *et al.* (2009) (H_2O_{melt} = 4.5 wt%). The occurrence of clinopyroxene in LP2 pumices may be, to a first approximation, explained as resulting from admixing of crystals from invading mafic magmas, which also provided calcic plagioclase and olivine (Gertisser *et al.*, 2009). Finally, LP1 requires an H_2O_{melt} of about 5 wt% at 865°C, which is best constrained by the stability field of orthopyroxene. Increasing pressure to 4 kbar does not significantly

change the above figures except for Cape Riva, which would require somewhat drier conditions, around 2.6 wt% H_2O_{melt} (Fig. 4b). Therefore, if stored at 2 kbar, Santorini silicic magmas seem to achieve dissolved water contents in the range 4-6 wt% prior to eruption, pre-eruptive temperatures falling in a rather small temperature interval, 850-900°C.

While the natural mineral assemblages are broadly reproduced in the conditions explored, the absence of magnetite (which co-exists with ilmenite in the natural rocks) in the FMQ run products indicates that experiments were more reduced than the natural system. Conversely, the absence of ilmenite in the NNO+1 charges illustrates that the natural system is less oxidizing. It is concluded that the pre-eruptive redox states of the magmas lay between around FMQ and NNO+1, in agreement with Fe-Ti oxide constraints discussed earlier (Fig. 2, Table 2).

Melt inclusion constraints

The water contents measured in the melt inclusions (Table 4) indicate minimum trapping pressures (calculated from Newman & Lowenstern, 2002) ranging from 1.0 to 2.4 kbar for the four eruptions (considering the average and the highest H_2O for each eruption; Table 5): 1.3-2.0 kbar for the Minoan, 1.6-2.4 kbar for the Cape Riva, 1.0-1.7 kbar for the LP2 and, 1.3-2.2 kbar for the LP1. As some of the melt inclusions may have lost water, the highest values are probably the most meaningful (e.g., Lowenstern, 1995; Wallace, 2005). Chlorine contents, mostly between 2300 and 3500 ppm, are among the highest contents reported in the literature for silicic arc magmas (e.g., Lowenstern, 1995, Webster, 1997a; Wallace, 2005). It is noteworthy that such contents are similar to those found for Cl saturation (i.e., brine saturation) in many experimental investigations of silicic liquids at 2 kbar (i.e., 2600-3000 ppm; Webster & Holloway, 1988; Malinin *et al.*, 1989; Metrich & Rutherford, 1992; Webster, 1992a, 1992b, 1997b). On a diagram of chlorine (ppm) versus H_2O (wt%) (Fig. 16), the

Santorini data show that whatever the amount of dissolved water in the trapped melt, chlorine remains approximately constant, illustrating the contrasted behavior between chlorine and water (e.g., Webster, 1997a; Lowenstern, 2000). Melt inclusion data mainly fall on or above the H_2O-Cl (brine) saturation curve of the haplogranitic melts at 2 kbar (Webster, 1997a, 1997b), the offset being likely due to slightly higher Cl solubility of the Fe-natural melts as opposed to those Fe-free synthetics used in most experiments. This supports our assumption of considering the highest H_2O values as representative, i.e., the maximum H_2O-saturation pressure estimates of 1.7-2.4 kbar rather than 1.0-1.6 kbar (Table 5). Such a Cl-H_2O pattern suggests that magmas could have been saturated with both a hydrosaline liquid (brine) and a H_2O-Cl vapor prior to eruption (Fig. 16). In contrast to Cl, fluorine contents (~500-800 ppm) are comparable to those found in other silicic arc magmas (e.g., Lowenstern, 1995). Our unpublished data indicate that fluorine strongly partitions into apatite ($D_F^{apatite/melt}$ = 35-44, while $D_{Cl}^{apatite/melt}$ = 2.8-3.6; A. Cadoux *et al.*, in preparation) which agrees very well with experimental results for felsic melts at 2 kbar and 900-924°C, saturated in brine ($D_F^{apatite/melt}$ = 11-44 and $D_{Cl}^{apatite/melt}$ = 1.0-4.5; Webster *et al.*, 2009).

The low sulphur contents are common in silicic magmas in general. Because of strong temperature dependence of S solubility (e.g., Carroll & Webster, 1994; Scaillet *et al.*, 2003), low temperature magmas like dacite and rhyolite have very low dissolved S (< 200 ppm and often < 60 ppm; Lowenstern, 1995). However, Santorini melts appear particularly depleted in sulphur when compared to the compositionally similar Krakatau dacite and rhyodacite magmas (Fig. 17a). The S contents of Santorini melts are comparable to silica-richer melts such as Pinatubo (SiO_2 ~76 wt%) or Katmai (SiO_2 ~77 wt%; Fig. 17a). It has been demonstrated that the maximum amount of S that can be dissolved in a silicate melt is controlled by saturation of the melt with a sulfide and/or a sulfate phase (e.g., Carroll and Rutherford, 1987; Luhr, 1990; Scaillet *et al.*, 1998; Clemente *et al.*, 2004), which is the case

for our Santorini silicic magmas, in which pyrrhotite globules are found in inclusions in pyroxenes and/or Fe-Ti oxides. The presence of this sulfide phase also provides additional evidence for the moderately reduced state of the system (e.g., Scaillet *et al.*, 1998; Clemente *et al.*, 2004). This reduced character may be at least partly at the origin of the very low sulphur contents in Santorini dacite and rhyodacites (Fig. 17c). It is unclear, however, if the low content of sulphur results from its degassing prior to melt inclusion entrapment, from sulphide disposal (i.e., settling) at early stages of magma fractionation, or from an intrinsically sulphur-poor system (i.e., sulphur-poor source), or from a combination of any of these mechanisms.

Comparison between natural and experimental phases compositions

Minoan rhyodacite

The natural bulk crystallinity and the composition of the interstitial glass are similar to those produced in the rhyodacite at a temperature of 850°C and a H_2O_{melt} of about 5-6 wt% ($0.7 < XH_2O < 1$; Figs. 7 and 11a) at either 2 kbar (FMQ and NNO+1) or 4 kbar - FMQ. The natural clinopyroxene composition is also reproduced in these three experiments for XH_2O = 0.9-1.0 (Figs. 11e and 11f). The composition of the orthopyroxene is clearly not reproduced at a pressure of 4 kbar (Figs. 5c and 5d). Significantly, the compositions of the dominant phases in the natural product, plagioclase and orthopyroxene, are best reproduced at 850°C - 2 kbar – FMQ and H_2O_{melt} = 6.3 wt% (XH_2O = 0.9; Figs. 11b to 11d). These temperature and water values are consistent with the temperature estimated from natural Fe-Ti oxides (Fig. 2; Table 2) and H_2O content measured in the melt inclusions (both in pyroxene and plagioclase, Table 4), respectively. The bulk crystallinity and phase proportions of the corresponding charge (9.7 wt%, Gl = 90.3, Plg = 6.9, Opx = 1.9, Cpx = 0.4, Ilm = 0.5 wt%; Table 3) are in close agreement with the natural product (10-15 wt%, Gl = 85.4, Plg = 11.2, Opx = 1.9, Cpx = 0.8,

Ilm = 0.4 wt%; Electronic Appendix 6). The mineral assemblage in the FMQ and NNO+1.8 runs (either ilmenite or magnetite, respectively), confirms that the fO_2 of the natural system lies between the two fO_2 explored, as also inferred from natural co-existing ilmenite and magnetite pairs (NNO-0.1; Fig. 2). Thus, combining natural and experimental constraints, we conclude that the pre-eruptive storage conditions of the Minoan rhyodacitic magma are: $P \geq 2$ kbar, T = 853 ± 7°C, H_2O_{melt} = 5-6 wt%, Cl ~ 3500 ppm, F ~ 800 ppm, S ~100 ppm and $fO_2 = 10^{-12.82 \pm 0.19}$ (NNO-0.1).

Cape Riva dacite

Bulk crystallinity and interstitial glass compositions can be reproduced at 850°C, FMQ, 2 and 4 kbar and XH_2O ~0.9, as well as at 900°C, 2 kbar, FMQ for XH_2O = 0.7-0.8 (Figs. 8 and 12a). The run products of the 900°C - 4 kbar experiment reached neither the crystallinity nor the glass compositions of the natural pyroclast. The fact that clinopyroxene did not crystallize in any of the runs performed at T = 850°C (Table 3) indicates that the pre-eruptive temperature was > 850°C, which is in agreement with the temperature estimates from natural sample (879-909°C; Table 2). The natural clinopyroxene composition was reproduced in the runs performed at 900°C, 2 kbar, FMQ, XH_2O ~0.9 (Figs. 12e and 12f). Similarly, plagioclase composition is best reproduced at 900°C, 2 kbar, FMQ for XH_2O ~0.8 (H_2O_{melt} = 6.1 wt%). The same observation can be made for orthopyroxene in terms of FeO*/MgO ratio, although it does not match in terms of wollastonite content (Figs. 12c and 12d). Although there is no exact match, ilmenite composition is close to the natural one at 900°C, 2 kbar, FMQ at XH_2O = 0.8-0.9. As at XH_2O = 0.9, plagioclase and orthopyroxene are lacking in the mineral assemblage: hence XH_2O conditions were lower than 0.9 and higher than 0.7 (no Cpx at XH_2O = 0.7), which corresponds to H_2O_{melt} comprised between 6.7 and 4.4 wt% (Table 3). This is consistent with melt inclusions data, as the majority has H_2O_{melt} varying between 4.1

and 6.6 wt% (total average of ~5 wt%; Table 4). The absence of magnetite, which co-exists with ilmenite in the natural sample, reflects slightly more oxidizing conditions in the natural system as determined with ilmenite-magnetite pairs (log fO_2 =-12.92 ± 0.35; i.e., NNO-0.7). Both natural and experimental products indicate that pre-eruptive storage conditions of the Cape Riva dacite magma are: P ≥ 2 kbar, T = 879 ± 15°C, H_2O_{melt} =5-6 wt%, Cl ~ 2800 ppm, F ~ 800 ppm, S ~100 ppm and $fO_2 = 10^{-12.92 \pm 0.35}$ (NNO-0.7).

Lower Pumice 2 rhyodacite

Bulk crystallinity and interstitial glass compositions can be both reproduced over most of the P-T-XH_2O explored, except in the NNO+1 runs. The composition of the main phase in the natural assemblage, plagioclase, is reproduced at 850°C both at 2 and 4 kbar for XH_2O ~ 0.7-0.8 (i.e., ~ 5.5 wt% H_2O_{melt} at 2 kbar and 4.6-5.1 wt% at 4 kbar; Table 3) but also at 900°C both at 2 and 4 kbar for lower XH_2O ~ 0.6-0.7 (i.e., ~ 3.5 wt% H_2O_{melt} at 2 kbar and 3.0 wt% at 4 kbar). However, at 900°C-2 kbar and XH_2O ~ 0.6-0.7, the crystallinity is too high in comparison with the natural one (respectively 14-18 wt% and 6-8 wt%; Table 3, Electronic appendix 6) excluding these as pre-eruptive conditions. The orthopyroxene composition is better reproduced in the 850°C (at 2 kbar and 4 kbar) runs at H_2O saturation (XH_2O = 1), than in the 900°C - 4 kbar run. The ilmenite composition is close to the natural one at 850°C, FMQ, at 2 and 4 kbar. These observations agree with a pre-eruptive temperature of about 850°C, which is consistent with the 856 ± 16°C temperature estimated from the natural Fe-Ti oxides pairs (Table 2). Both 2 kbar and 4 kbar can be considered as potential pre-eruptive pressures. However, in the considered XH_2O range (= 0.8-1.0) the main mineral assemblage and crystallinity at 4 kbar do not match: at XH_2O = 0.8, the assemblage has 2.7 wt% amphibole whereas it occurs rarely in the natural rock. At 2 kbar and XH_2O = 0.8, the bulk crystallinity (22.4 wt%) is significantly higher than the natural sample (6-8 wt%) while, at

H_2O saturation, the assemblage (3.3 wt% crystals) comprises 1.6 wt% amphibole, unlike the natural assemblage. In spite of lack of data at $XH_2O = 0.9$ (leakage of capsule), we can infer by extrapolation that the natural assemblage is produced at 850°C - 2 kbar - FMQ and XH_2O ~ 0.9 which corresponds to $5.5 < H_2O_{melt} < 8.0$ wt%. This is broadly consistent with the highest measured H_2O content of 5.34 ± 0.54 wt% in melt inclusions (Table 4) which leads to a minimum pressure of 1.7 kbar (Table 5). Together with H_2O-Cl solubility constraints (Fig. 16), these data strongly support a 2 kbar, rather than 4 kbar, storage pressure. Thus, one may consider that the melt inclusions with H_2O < ~4.5 wt% (considering the error of the by-difference method of ±1 wt%) most likely underwent post-entrapment leakage. Although phase equilibrium experiments did not yield an exact natural mineral assemblage (absence of Cpx, discussed before), the composition of the main phases (glass, Plg and Opx) has been reproduced. Combining natural and experimental constraints, we thus conclude that the pre-eruptive storage conditions of the LP2 rhyodacitic magma are: $P \geq 2$ kbar, T = 856 ± 16°C, H_2O_{melt} ~5-6 wt%, Cl ~ 2800 ppm, F ~ 800 ppm, S ~50 ppm and fO_2 = FMQ ($10^{-13.45 \pm 0.37}$; i.e., NNO-0.8).

Lower Pumice 1 rhyodacite

Both bulk crystallinity and interstitial glass compositions for LP1 are generally best reproduced in the products from experiments performed at T = 900°C in the XH_2O range = 0.8-1.0, at either 2 or 4 kbar. However, plagioclase did not crystallize at 4 kbar. It formed at 2 kbar but for lower $XH_2O < 0.8$ and overall, the composition of the experimental plagioclase is significantly less calcic (An < 28%) than the natural one in LP1 (An = 42%; Fig. 14b), and also less than the experimental plagioclases produced in the three other compositions (Figs. 11b, 12b, 13b), reflecting the higher Na and K contents of the starting bulk rock (Table 1). Orthopyroxene, the second most important phase of the natural rock, was not formed either;

instead, pigeonite crystallized in the 850°C - FMQ runs. This demonstrates that the orthopyroxene and the An_{42} plagioclase cannot be in equilibrium with the LP1 rhyodacite. This is also supported by mass balance calculations which suggest that orthopyroxene and plagioclase are xenocrysts (Electronic Appendix 6). These latter have been most probably included in a LP1 clinopyroxene- and oxides-bearing silicic magma during a mixing event with a less evolved plagioclase- and orthopyroxene-bearing magma. The mixed system was not equilibrated at the time of eruption.

Despite this event, which prevents accurate experimental reconstruction of the pre-eruptive phase equilibria, one may still consider the constraints gained from the LP1 natural rhyodacite and its comparison with the products of the three other silicic eruptions, which show broadly similar phase assemblages and compositions. The minimum pressure estimates from melt inclusions are in the range 1.3-2.2 kbar (Table 5), pre-eruptive temperature and fO_2 are estimated to be 869 ± 20°C and ~ FMQ ($10^{-13.30 \pm 0.59}$ = NNO-0.9, Table 2) and volatiles contents are very close to the Minoan, Cape Riva and Lower Pumice 2: maximum H_2O_{melt} ~ 6.3 wt% (mean H_2O_{melt} = 4.5 ± 0.4 wt%), Cl ~ 2800 ppm, F ~ 900 ppm, S ~100 ppm (Table 4).

ON AMPHIBOLE OCCURRENCE AND ITS IMPLICATIONS

Minoan rhyodacite

Phenocrystic amphibole is absent in the Minoan rhyodacite. However, Cottrell *et al.* (1999) suggested that amphibole should have crystallized on the basis of: (1) the high amount of water in the Minoan glass inclusions (up to 6.5 wt%), and (2) previous experimental works on compositions similar to the Minoan rhyodacite which produced amphibole (e.g., Mount St Helens silicic rocks; Rutherford *et al.*, 1985; Gardner *et al.*, 1995).

The working hypothesis of those authors was thus that, if amphibole had crystallized at one time, its absence in the erupted rocks was due to a major change in the storage conditions prior to eruption. Cottrell *et al.* (1999) proposed a two stage equilibration model for the Minoan rhyodacitic magma. It was first stored at pressures > 2 kbar and T~ 825°C with ca. 6 wt% H_2O_{melt}; it then moved to a shallower ~ 0.5 kbar storage region with ca. 3 wt% H_2O_{melt} and a slightly higher temperature (885°C), owing to mafic magma input, during which amphibole phenocrysts reacted out.

Our phase equilibrium results show that such a change in storage conditions is not required to explain the absence of amphibole, for the following reasons:

(1) Cottrell *et al.* (1999) based their experiments and interpretations on the assumption that the Minoan magma was water-saturated, which our new, mixed-volatile experiments do not support. Amphibole can be absent at 2 kbar and 850°C in a water-rich magma such as the Minoan if the magma is slightly water-undersaturated (XH_2O ~0.9).

(2) They analysed melt inclusions in the cores (An_{49-63}) of plagioclase phenocrysts, but none in the rims ($An_{39\pm2}$). Their model predicts that those in the rims should contain no more than 2.5-3.0 wt% H_2O (the saturation values at 0.5 kbar). However, we have analysed inclusions from both cores and rims (Table 4a) and find that both fall in the range 4-6 wt%, without any systematic difference. The rim inclusions commonly lie in deep re-entrants in the cores, where they are surrounded by thin shells of rim composition plagioclase. Water contents of melt inclusions in the rims (up to 4.65 wt%; Table 4a) are much higher than predicted by the model of Cottrell *et al.* (1999).

(3) They reported the occurrence of rare iron-rich hornblende inclusions hosted by orthopyroxene grains, and used this as evidence that amphibole had been

previously stable in the magma at 2 kbar, but had reacted out when the magma moved to the last 0.5 kbar storage zone. While this is possible, we note that amphibole occurs abundantly in a suite of crystal-rich pumices that were co-erupted with the main rhyodacitic magma at the start of the Minoan eruption (Druitt *et al.,* 1999). They represent parts of a highly crystalline intrusion that was partly pushed out by the ascending rhyodacite, with mingling between the two magmas (Druitt, 2014). Both the amphibole and host orthopyroxenes reported by Cottrell at al (1999) are compositionally very similar to those in the crystal-rich pumices (Fig. 18), raising the possibility that the orthopyroxene and its inclusion were introduced by syn-eruptive mingling into the rhyodacite, and have no bearing on the P-T-X evolution of the rhyodacite. It is notable that the crystal-rich magma appears to have been stored at a similar depth as the rhyodacite since the amphibole composition of the crystal-rich pumice yields pressure of 1.9 ± 0.5 kbar (Ridolfi *et al.,* 2010).

In the present paper we argue that the phenocryst rim compositions, rim-hosted melt inclusion volatile contents, and the absence of phenocrystic amphibole in the Minoan rhyodacite form a sound basis for establishing a unique set of pre-eruptive conditions.

Lower Pumice 2 rhyodacite

Gertisser *et al.* (2009) reported rare amphibole as part of the crystal cargo of the LP2 rhyodacite, occurring either as phenocrysts, groundmass microlites or as crystals within melt inclusions. The authors used Al-in-hornblende geobarometry to estimate the depth of the storage region of the LP2 magma on the basis of:

(1) The presence of rare quartz in the LP2 pumices

(2) Assuming that the amphibole phenocrysts grew in equilibrium with quartz and the other phases in the LP2 rhyodacitic magma.

Amphibole phenocrysts of the LP2 pumices are described by Gertisser *et al.* (2009) as generally unzoned, containing 10.4 ± 0.1 wt% Al_2O_3 (n=4), and yield a pressure of 4.3 ± 0.1 kbar, using the aluminium-in-hornblende geobarometer of Johnson and Rutherford (1989). This corresponds to a depth of about 16 km, assuming a crustal density of 2.7 g/cm^3. However, the LP2 magma clearly lacks the buffering assemblage needed for a proper use of the Al-in-hornblende barometer as calibrated by Johnson & Rutherford (1989). Hence this geobarometer cannot be used to infer the pre-eruptive magma storage pressure of the LP2 rhyodacite. Application of the more recent model of Ridolfi *et al.* (2010) yields a lower pressure of 2.5 ± 0.6 kbar, a temperature of 931 ± 22°C and a H_2O_{melt} content of 5.5 ± 0.8 wt%. Calculated pressure and melt H_2O content concur with our estimate of pre-eruptive conditions ($P \geq 2$ kbar, H_2Omelt ~5-6 wt%). However, the calculated crystallization temperature is high compared to our estimated value of 856 ± 16°C. This may reflect that the amphibole crystals are antecrysts derived from less evolved magmas with higher crystallization temperatures. The low Si content of the amphibole crystals (SiO_2 = 42 wt%; Gertisser *et al.*, 2009) compared to amphiboles of our experiments (SiO_2 = 44-47 wt%, Electronic Appendix 3d) is consistent with such an interpretation.

SANTORINI MAGMA PLUMBING SYSTEM AND ITS EVOLUTION

Silicic magma storage regions

Our results show that the silicic magmas discharged during four large Plinian eruptions of Santorini were stored under similar conditions immediately prior to eruption. Considering a 2 kbar storage pressure and a crustal density of 2640 kg.m^{-3} (Konstantinou, 2010), the top of the silicic magma storage regions is located at 7.7 km depth (i.e., in the

upper crust; Fig. 19). This storage pressure for silicic magmas is in agreement with recent phase equilibrium experiments on Santorini mafic and intermediate magmas, showing that andesitic magmas fractionate to dacite and rhyodacite at about 2 kbar (Andújar *et al.*, 2012; Cadoux *et al.*, 2013). Andesite comes from a deeper (~15 km) mafic storage region (Fig. 19), where basalts fractionate to basaltic andesite (55 to 58 wt% SiO_2) with 2-3 wt% H_2O at 1040-1000°C, 4 kbar and fO_2 = FMQ-0.5 (Andújar *et al.*, 2012; Cadoux *et al.*, 2013). Interestingly, even if it has to be further constrained, a similar scenario has been proposed for the earliest (~650 ka) rhyolitic magmas (early centres of Akrotiri, South of Thera Island, Fig. 1). Indeed, according to Mortazavi & Sparks (2004), Akrotiri differentiated mafic magma intruded into porphyritic silicic magma at depths of 7–10 km (water contents of the mafic magmas are estimated to have been > 4 wt% at water pressures of ≥ 1.8 kbar at temperatures of approximately 950–1000°C).

The similar P-T-volatile storage conditions, the closely spaced eruptive vents (Druitt *et al.*, 1999) along with the large volumes (up to 30-60 km^3 DRE; Pyle, 1990; Sigurdsson *et al.*, 1990; Druitt *et al.*, 1999; Sigurdsson *et al.*, 2006) of the silicic magmas discharged during the four large Plinian eruptions, suggest that they come from the same, presumably very large, reservoir. This hypothesis implies that this latter would have been sustained since at least 184 ka (the age of the Lower Pumice 1 eruption; Fig. 1), which is in agreement with recent thermal modelling (Gelman *et al.*, 2013), that shows that an upper crustal reservoir can remain above its solidus for more than 100 ka when fed by magma fluxes typical of large magmatic provinces (i.e., < 0.005-0.008 km^3/year).

This ≥ 7.7 km reservoir depth beneath the caldera is close to that inferred for the 1650 AD rhyolite reservoir of the Kolumbo seamount, 6.5 km NE of Santorini (along the NE-SW trending Santorini-Kolumbo volcano-tectonic line; Fig. 19). The latter would be located around 6.8 km depth according to petrological, tomographic and stress field constraints

(Dimitriadis *et al.*, 2010; Konstantinou & Yeh, 2012; Cantner *et al.*, 2014). P- and S-wave tomographic images suggest that the current magma storage region is a small discrete reservoir, ca. 3 km diameter (Fig. 19; Dimitriadis *et al.*, 2010; Konstantinou & Yeh, 2012).

Size and shape of the silicic magma storage region

Currently, there is no such geophysical evidence supporting the existence of a large storage region at ≥ 7.7 km beneath the Santorini caldera. However, this depth is comparable with that of emplacement of some granitoids of the Aegean Arc, such as the Miocene Tinos and Mykonos plutons emplaced at 10–12 km and at 5-10 km depth, respectively (e.g., Altherr *et al.*, 1982; Buick, 1991; Lucas, 1999; de Saint-Blanquat *et al.*, 2011) The total thicknesses of these plutons are approximately 1–2 km and 2-3 km, respectively, with volumes of 10-80 km^3 and ~ 150 km^3, respectively (Denèle *et al.*, 2011; de Saint-Blanquat *et al.*, 2011). Reconstruction of the 3D shape of plutons from various tectonic settings has shown that the majority are tabular, wedge- or funnel-shaped (Scaillet *et al.*, 1995; McCaffrey & Petford, 1997; Cruden, 1998; Vigneresse *et al.*, 1999; Petford *et al.*, 2000; Scaillet & Searle, 2006). On the basis of the positive correlation, evidenced by de Saint Blanquat *et al.* (2011), between pluton (*s. l.*) volume and the duration of its construction, we may infer that the final volume of the Santorini silicic storage region after 200 ka of growth might be in the range of 50-500 km^3, depending on the time-averaged construction rate, between ca. 0.001 and 0.01 km^3/yr, respectively (see Fig. 4 in de Saint-Blanquat *et al.*, 2011). As the estimated magma volume discharged during the last large silicic Minoan eruption is up to 60 km^3 DRE (Sigurdsson *et al.*, 2006), the storage region volume should be larger than 60 km^3. If we assume a tabular-shaped silicic storage region with an area of 65 km^2 (corresponding to the caldera area), its thickness could be comprised between 0.9 and 7.7 km (considering a volume of the storage region comprised between 60 and 500 km^3, respectively).

The volume of erupted Minoan magma could represent almost the totality (if the storage region is ≥ 60 km^3) to only 6% of the total volume of the storage region.

Pre-eruptive magma storage variations

Although magma storage conditions for the large silicic Plinian events do not appear to have changed since about 200 ka, some evidence suggests that they may have been different during the periods separating each of these Plinian eruptions. Interplinian phases at Santorini are characterized by effusive and minor explosive activity up to subplinian in intensity (Druitt *et al.*, 1999; Vespa *et al.*, 2006) and the products range from basalt to dacite in composition. Petrological studies of the post-Minoan, intra-caldera, Kameni dacitic lavas (197 BC to AD 1950) suggest that they were stored in a shallower region at a pressure of approximately 1 kbar (2-4 km in depth; Huijsmans, 1985; Barton & Hujismans, 1986; Martin, 2005). This has supported the idea that the recent inflation of the caldera ground, the source of which has been estimated to be at 4.4 km depth (Newman et al, 2012; Parks *et al.*, 2012), was due to magma intrusion. Therefore, even if pre-eruptive constraints are lacking for the oldest interplinian phases, it cannot be ruled out that variations in magma storage conditions of Santorini, such as those documented at Mt. St Helens and Vesuvius volcanoes (Gardner *et al.*, 1995; Rutherford & Devine, 2008; Scaillet *et al.*, 2008) have occurred in the past.

CONCLUSIONS

The systematic geochemical trends displayed by both experimental glass and minerals and their coherent variation with experimental variables (Figs. 7 to 14) show that conditions close to equilibrium were attained in our experiments. They were also broadly successful in reproducing the natural phase assemblages. Hence, the latter also approached equilibrium conditions prior to eruption (except Lower Pumice 1). Phase relationships show marked

differences between eruptions, in spite of their similar whole-rock compositions, due to the sensitivity of phase equilibria to small variations (< 1 wt%) in major element composition. This demonstrates how application of a phase diagram for a particular silicic magma might incorrectly predict phenocryst assemblages for another silicic magma. This point has also been made for phonolites (Scaillet *et al.*, 2008; Andújar & Scaillet, 2012a), stressing the need for a case-by-case approach, whenever a precise estimate of pre-eruptive conditions is the chief objective of the experimental study.

Our results show that storage conditions prevailing before the four silicic Plinian eruptions of Santorini were similar and can be summarized as follows:

- T = 850°C – 900°C
- Moderately reduced conditions (ΔNNO = - 0.9 to - 0.1)
- Water-rich melts (~ 5-6 wt%)
- Sulphur depleted melts (≤ 100 ppm; buffered by pyrrhotite)
- Fluorine contents ~ 800 ppm, typical of silicic arc magmas
- Chlorine-rich melts (mostly between 2300 and 3500 ppm)
- Melts slightly undersaturated with respect to H_2O, but most probably saturated with respect to H_2O+Cl (± CO_2) and a hydrosaline liquid.
- Storage pressure of 2 kbar or slightly more, but less than 4 kbar
- Reservoir roof depth at ≥ 7.7 km.

The Minoan silicic magma slightly differs from the Cape Riva and Lower Pumices by:

- Its slightly lower pre-eruptive temperature (consistent with its higher bulk dry SiO_2; Tables 1 and 2)
- Its less reduced state (ΔNNO = - 0.1)
- Its higher chlorine content (3500 ppm in average, with maximum values > 4000 ppm)

We propose that Santorini magma plumbing system is dominated by a large, long-lived (≥ 200 ka) dominantly-silicic storage region at about 8 km depth (feeding the major Plinian eruptions; this study), which is maintained by mafic injections from a mafic reservoir at about 15 km depth (Andújar *et al.*, 2012; Fig. 19).

Finally, the fact that Santorini silicic melts may have high enough dissolved Cl to be saturated in hydrosaline liquid has significant implications for the Cl degassing budget which will be treated in a separate article.

FUNDING

The present work was carried out in the framework of the project "Storage and Mixing at Santorini", supported by the french "Agence Nationale de la Recherche" [ANR-08-BLAN-0249-01 to B.S.] and the Laboratoire d'Excellence VOLTAIRE (University of Orléans, France).

ACKNOWLEDGEMENTS

A. Cadoux acknowledges her colleagues of the Laboratoire Magmas et Volcans (Clermont-Ferrand) for their warm welcome and for sharing their skills during the year she spent among them. J.L. Devidal and J.M. Henot are thanked for their expertise, efficiency and availability during electron microprobe analyses and SEM imagery, respectively. A. Cadoux is also grateful to her colleagues of 'Magmas' team (ISTO, Orléans) for their respective help or advice during the different steps of the experimental work, especially R. Champallier and J. Andújar, as well as I. Di Carlo for her assistance in electron microprobe analysis of experimental glasses. N. Le Gall and M. Pichavant are thanked for their assistance with sample preparation and FTIR measurements of the Bishop Tuff glasses used for H_2O-CO_2 SIMS calibration. We thank O. Bachmann, J. Blundy and R. Gertisser for their constructive and helpful reviews.

REFERENCES

Albarède, F. (1995). *Introduction to Geochemical Modeling*. Cambridge University Press, 543 pp.

Altherr, R., Kreuzer, H., Wendt, I., Lenz, H., Wagner, G. A., Keller, J., Harre, W. & Hoehndorf, A. (1982). A late Oligocene/Early Miocene high temperature belt in the Attic Cycladic Crystalline Complex (Greece). *Geologisches Jahrbuch* **E23**, 97–164.

Andersen, D. J. & Lindsley, D. H. (1985). New (and final) models for the Ti-magnetite/ilmenite geothermometer and oxygen barometer (abs.). *EOS* **66**, 416.

Andersen, D. J. & Lindsley, D. H. (1988). Internally consistent solution models for Fe-Mg-Mn-Ti oxides: Fe-Ti oxides. *American Mineralogist* **73**: 714-726.

Andersen, D. J., Lindsley, D. H., Davidson, P. M. (1993). QUILF: a Pascal program to asses equilibria among Fe–Mg–Mn–Ti-oxides, pyroxenes, olivine and quartz. *Computers and Geosciences* **19**, 1333-1350.

Andújar, J. & Scaillet, B. (2012a). Experimental Constraints on Parameters Controlling the Difference in the Eruptive Dynamics of Phonolitic Magmas: the Case of Tenerife (Canary Islands). *Journal of Petrology* **53**, 1777-1806.

Andújar, J. & Scaillet, B. (2012b). Relationships between pre-eruptive conditions and eruptive styles of phonolite-trachyte magmas. *Lithos*, **152**, 122-131.

Andújar, J., Scaillet, B., Druitt, T. H., Pichavant, M. (2012). Differentiation conditions of mafic magmas as parents of andesite-rhyodacite compositions at Santorini. *14th International Conference on Experimental Mineralogy Petrology Geochemistry*. Kiel, Germany. Conference Abstracts.

Annen, C. (2011) Implications of incremental emplacement of magma bodies for magma differentiation, thermal aureole dimensions and plutonism-volcanism relationships. *Tectonophysics* **500**, 3-10.

Annen, C., Pichavant, M., Bachmann, O., Burgisser, A. (2008). Conditions for the growth of a long-lived shallow crustal magma chamber below Mount Pelee volcano (Martinique, Lesser Antilles Arc). *Journal of Geophysical Research* **113**, B07209.

Bacon, C. R. & Hirschmann, M. M. (1988). Mg/Mn partitioning as a test for equilibrium between coexisting Fe-Ti oxides. *American Mineralogist* **73**, 57-61.

Barton, M. & Huijsmans, J. P. P. (1986). Post-caldera dacites from the Santorini volcanic complex, Aegean Sea, Greece: an example of the eruption of lavas of near-constant composition over a 2200 year period. *Contributions to Mineralogy and Petrology* **94**, 472–495.

Blundy, J. & Cashman, K. (2008). Petrologic Reconstruction of Magmatic System Variables and Processes. *Reviews in Mineralogy and Geochemistry* **69**, 179-239.

Blundy, J., Cashman, K., Berlo, K. (2008). *Evolving magma storage conditions beneath Mount St. Helens inferred from chemical variations in melt inclusions from the 1980-1986 and current eruption*. In: Sherrod, D. R., Scott, W. E. & Stauffer, P. H. (eds.). *A volcano rekindled; the renewed eruption of Mount St. Helens, 2004–2006*. U.S. Geological Survey Professional Paper 1750, 755-790.

Bogaerts, M., Scaillet, B., VanderAuwera, J. (2006). Phase equilibria of the Lyngdal granodiorite (Norway): implications for the origin of metaluminous ferroan granitoids. *Journal of Petrology* **12**, 2405-2431.

Borgia, A., Tizzani, P., Solaro, G., Manzo, M., Casu, F., Luongo, G., Pepe, A., Berardino, P., Fornaro, G., Sansosti, E., Ricciardi, G. P., Fusi, N., Di Donna, G., Lanari, R. (2005). Volcanic spreading of Vesuvius, a new paradigm for interpreting its volcanic activity. *Geophysical Research Letters* **32**, L03303.

Buick, I. S. (1991). The late Alpine evolution of an extensional shear zone, Naxos, Greece. *Journal of the Geological Society, London* **148**, 93–103.

Burnham, C. W., Holloway, J. R. & Davis, N. F. (1969) Thermodynamic properties of water to 1000°C and 10000 bars. *Geological Society of America, Special Papers* **132**, 1-96.

Cadoux, A., Andújar, J., Scaillet, B., Druitt, T. H., Deloule, E. (2013). Santorini volcano magma plumbing system: constraints from a combined experimental and natural products study. *IAVCEI Scientific Assembly*, Kagoshima, Japan, 4W_1B–P9.

Cantner, K., Carey, S., Nomikou, P. (2014) Integrated volcanologic and petrologic analysis of the 1650 AD eruption of Kolumbo submarine volcano, Greece. *Journal of Volcanology and Geothermal Research* **269**, 28-43.

Carmichael, I. S. E. (1967). The iron-titanium oxides of salic volcanic rocks and their associated ferromagnesian silicates. *Contributions to Mineralogy Petrology* **14**, 36-64.

Carroll, M. R. & Rutherford, M. J. (1987). The Stability of Igneous Anhydrite: Experimental Results and Implications for Sulfur Behavior in the 1982 El Chichon Trachyandesite and Other Evolved Magmas. *Journal of Petrology* **28**, 781-801.

Carroll, M. R. & Webster, J. D. (1994). *Solubilities of sulfur, noble gases, nitrogen, chlorine, and fluorine in magmas*. In: Carroll M. R. & Holloway J. R. (eds.) *Volatiles in Magmas*. Mineralogical Society of America, 231-280.

Clemens, J. D., Holloway, J. R., White, A. J. R. (1986). Origin of A-type granite: experimental constraints. *American Mineralogist* **71**, 317–324.

Clemens, J. D., Wall, V. J. (1981). Crystallization and origin of some paraluminous (S-type) granitic magmas. *Canadian Mineralogist* **19**, 111-132.

Clemente, B., Scaillet, B., Pichavant, M. (2004). The Solubility of Sulphur in Hydrous Rhyolitic Melts. *Journal of Petrology* **45**, 2171.

Cottrell, E, Gardner, J. E., Rutherford, M. J. (1999). Petrologic and experimental evidence for the movement and heating of the pre-eruptive Minoan rhyodacite (Santorini, Greece). *Contributions to Mineralogy and Petrology* **135**, 315-331.

Costa, F., Scaillet, B. & Pichavant, M. (2004). Petrological and experimental constraints on the pre-eruption conditions of Holocene dacite from Volcan San Pedro (36°S, Chilean Andes) and the importance of sulphur in silicic subduction-related magmas. *Journal of Petrology* **45**, 855-881.

Cruden, A. R. (1998). On the emplacement of tabular granites. *Journal of the Geological Society* **155**, 853–862.

Dall'Agnol, R., Scaillet, B., Pichavant, M. (1999). An experimental study of a lower Proterozoic A-type granite from the eastern Amazonian craton, Brazil. *Journal of Petrology* **40**, 1673-1698.

De Natale, G., Troise, C., Trigila, R., Dolfi, D., Chiarabba, C. (2004). Seismicity and 3-D substructure at Somma–Vesuvius Volcano; evidence for magma quenching. *Earth Planetary Science Letters* **221**, 181–196.

Denèle, Y., Lecomte, E., Jolivet, L., Lacombe, O., Labrousse, L., Huet, B., Le Pourhiet, L. (2011). Granite intrusion in a metamorphic core complex: The example of the Mykonos laccolith (Cyclades, Greece). *Tectonophysics* **501**, 52-70.

Devine, J. D., Sigurdsson, H., Davis, A. N., Self, S. (1984). Estimates of sulfur and chlorine yield to the atmosphere from volcanic-eruptions and potential climatic effects. *Journal* of Geophysical *Research* **89**, 6309–6325.

Devine, J. D., Gardner, J. E., Brack, H. P., Layne, G. D. & Rutherford, M. J. (1995). Comparison of microanalytical methods for estimating H_2O contents of silicic volcanic glasses. *American Mineralogist* **80**, 319-328.

Di Carlo, I., Pichavant, M., Rotolo, S. G., Scaillet, B. (2006). Experimental crystallization of a high-K arc basalt: the golden pumice, Stromboli volcano (Italy). *Journal of Petrology* **47**, 1317-1343.

Di Carlo, I., Rotolo, S. G., Scaillet, B., Buccheri, V., Pichavant, M. (2010). Phase Equilibrium Constraints on Pre-eruptive Conditions of Recent Felsic Explosive Volcanism at Pantelleria Island, Italy. *Journal of Petrology* **51**, 2245-2276.

Dimitriadis, I., Papazachos, C., Panagiotopoulos, D., Hatzidimitriou, P., Bohnhoff, M., Rische, M., Meier, T. (2010). P and S velocity structures of the Santorini-Coloumbo volcanic system (Aegean Sea, Greece) obtained by non-linear inversion of travel times and its tectonic implications. *Journal of Volcanology and Geothermal Research* **195**, 13-30.

Druitt, T. H. (1983). Explosive volcanism on Santorini, Greece. PhD Thesis, University of Cambridge, United Kingdom.

Druitt, T. H. (2014). New insights into the initiation and venting of the Bronze-Age eruption of Santorini, from component analysis. *Bulletin of Volcanology* **76**, 794.

Druitt, T. H., Mellors R. A., Pyle, D. M., Sparks, R. S. J. (1989). Explosive volcanism on Santorini, Greece. *Geological Magazine* **126**, 95–126.

Druitt, T. H. & Francaviglia, V. (1992). Caldera formation on Santorini and the physiography of the islands in the late Bronze Age. *Bulletin of Volcanology* **54**, 484-493.

Druitt, T. H., Edwards, L., Mellors, R. M., Pyle, D. M., Sparks R. S. J., Lanphere, M., Davies, M., Barreirio, B. (1999). *Santorini Volcano*. Geological Society, London.

Druitt, T. H., Costa, F., Deloule, E., Dungan, M., Scaillet, B. (2012). Decadal to monthly timescales of magma transfer and reservoir growth at a caldera volcano. *Nature* **482**, 77-80.

Endrun, B., Meier, T., Lebedev, S., Bohnhoff, M., Stavrakakis, G., Harjes, H. -P. (2008). S velocity structure and radial anisotropy in the Aegean region from surface wave dispersion. *Geophysical* Journal *International* **174**, 593–616.

Fabbro, G. N., Druitt, T. H. & Scaillet S. (2013). Evolution of the crustal magma plumbing system during the build-up to the 22-ka caldera-forming eruption of Santorini (Greece). *Bulletin of Volcanology* **75**, 767.

Frost, R. B. (1991). Introduction to oxygen fugacity and its petrologic importance. *Reviews in Mineralogy and Geochemistry* **25**, 1-9.

Gardner, J. E., Rutherford, M. J., Carey, S., Sigurdsson, H. (1995). Experimental constraints on pre-eruptive water contents and changing magma storage prior to explosive eruptions of Mount St Helens volcano. *Bulletin of Volcanology* **57**, 1-17.

Gardner, J. E., Thomas, R. M. E., Jaupart, C., Tait, S. (1996). Fragmentation of magma during Plinian volcanic eruptions. *Bulletin of Volcanology* **58**, 144-162.

Gelman, S. E., Gutiérrez, F. J., Bachmann, O. (2013). On the longevity of large upper crustal silicic magma reservoirs. *Geology* **41**, 759-762.

Gerlach, T. M., Westrich, H. R., Symonds, R. B. (1996). *Preeruption vapor in magma of the climactic Mount Pinatubo eruption: source of the giant stratospheric sulfur dioxide cloud*. In: Newhall, C.G. & Punongbayan, R.S. (eds.) *Fire and Mud: Eruptions and Lahars of Mount Pinatubo, Philippines*. University of Washington Press, 415– 433.

Gertisser, R., Preece, K., Keller, J. (2009). The Plinian Lower Pumice 2 eruption, Santorini, Greece: Magma evolution and volatile behaviour. *Journal of Volcanology and Geothermal Research* **186**, 387-406.

Ghiorso, M. S. (1997). Thermodynamic Models of Igneous Processes. *Annual Review of Earth and Planetary Sciences* **25**, 221-241.

Ghiorso, M. S. & Evans, B. W. (2008). Thermodynamics of Rhombohedral Oxide Solid Solutions and a Revision of the Fe-Ti Two-oxide Geothermometer and Oxygen-barometer *American Journal of Science* **308**, 957-1039.

Hammer, J. E., Rutherford, J.M., Hildreth, W. (2002). Magma storage prior to the 1912 eruption at Novarupta, Alaska. *Contributions to Mineralalogy and Petrology* **144**, 144-162.

Harrison, T. M. & Watson, E. B. (1984). The behavior of apatite during crustal anatexis: Equilibrium and kinetic considerations. *Geochimica et Cosmochimica Acta* **48**, 1467-1477.

Hildreth, W. (1983). The compositionally zoned eruption of 1912 in the Valley of Ten Thousand Smokes, Katmai National Park, Alaska. *Journal of Volcanology and Geothermal Research* **18**, 1-56.

Huijsmans, J. P. P. (1985). *Calcalkaline lavas from the volcanic complex of Santorini, Aegean Sea, Greece: a petrological, geochemical and stratigraphic study*. Geologica Ultraiectina 41.

Huijsmans, J. P. P., Barton, M., Salters, V. J. M. (1988). Geochemistry and evolution of the calc-alkaline volcanic complex of santorini, Aegean Sea, Greece. *Journal of Volcanology and Geothermal Research* **34**, 283-306.

Jochum, K. P., Stoll, B., Herwig, K.; Willbold, M.; Hofmann, A. W.; Amini, M., Aarburg, S., Abouchami, W., Hellebrand, E., Mocek, B., Raczek, I., Stracke, A., Alard, O., Bouman, C., Becker, S., Ducking, M., Bratz, H., Klemd, R., de Bruin, D., Canil, D., Cornell, D., de Hoog, C. J., Dalpe, C., Danyushevsky, L., Eisenhauer, A., Gao, Y. J., Snow, J. E., Goschopf, N., Gunther, D., Latkoczy, C., Guillong, M., Hauri, E. H., Hofer, H. E., Lahaye, Y., Horz, K.,

Jacob, D. E., Kassemann, S. A., Kent, A. J. R., Ludwig, T., Zack, T., Mason, P. R. D., Meixner, A., Rosner, M., Misawa, K. J., Nash, B. P., Pfander, J., Premo, W. R., Sun, W. D., Tiepolo, M., Vannucci, R., Vennemann, T., Wayne, D. & Woodhead, J. D. (2006). MPI-DING reference glasses for in situ microanalysis: New reference values for element concentrations and isotope ratios. *Geochemistry, Geophysics, Geosystems* **7**, Q02008, doi: 10.1029/2005GC001060.

Johnson, M. C. & Rutherford, M. J. (1989). Experimental calibration of the aluminium-in-hornblende geobarometer with application to Long Valley caldera (California) volcanic rocks. *Geology* **17**, 837–841.

Karagianni, E. E. & Papazachos, B. C. (2007). Shear velocity structure in the Aegean area obtained by joint inversion of Rayleigh and Love waves. *Geological Society, London, Special Publications* **291**, 159-181.

Keller, J., Kraml, M., Schwarz, M. (2000). Dating major volcanic paroxysms within the deep-sea record: the example of the Thera Formation, Santorini, Greece. Abstracts, *IAVCEI General Assembly*, Bali, Indonesia, p. 16.

Klimm, K., Holtz, F., Johannes, W., King, P. L. (2003). Fractionation of metaluminous A-type granites: an experimental study of the Wangrah Suite, Lachlan Fold Belt, Australia. *Precambrian Research* **124**, 327-341.

Konstantinou, K. I. (2010). Crustal rheology of the Santorini-Amorgos zone: Implications for the nucleation depth and rupture extent of the 9 July 1956 Amorgos earthquake, southern Aegean. *Journal of Geodynamics* **50**, 400-409.

Konstantinou, K. I. & Yeh T. -Y. (2012). Stress field around the Coloumbo magma chamber, southern Aegean: Its significance for assessing volcanic and seismic hazard in Santorini. *Journal of Geodynamics* **54**, 13-20.

Lepage, L. D. (2003). ILMAT: an Excel worksheet for ilmenite–magnetite geothermometry and geobarometry. *Computers and Geosciences* **29**, 673–678.

Lowenstern, J. B. (1995). *Applications of silicate melt inclusions to the study of magmatic volatiles*. In: Thompson, J.F.H. (ed.) *Magmas, Fluids and Ore Deposits*. Mineralogical Association of Canada Short Course, 71-99.

Lowenstern, J. B. (2000). A review of the contrasting behavior of two magmatic volatiles: Chlorine and carbon dioxide. *Journal of Geochemical Exploration* **69–70**, 287–290.

Lucas, I. (1999). Le pluton de Mykonos-Delos-Rhenee (Cyclades, Grèce): Un exemple de mise en place synchrone de l'extension crustale. PhD Thesis, Université d'Orléans, France.

Luhr, J. F. (1990). Experimental phase relations of water-and sulfur-saturated arc magmas and the 1982 eruptions of El Chichón volcano. *Journal of Petrology* **31**, 1071-1114.

Malinin, S. D., Kravchuk, I. F., Delbove, F. (1989). Chloride distribution between phases in hydrated and dry chloride-aluminosilicate melt systems as a function of phase composition. *Geochemistry International* **26**, 32-38.

Mandeville, C. W., Carey, S., Sigurdsson, H. (1996). Magma mixing, fractional crystallization and volatile degassing during the 1883 eruption of Krakatau volcano, Indonesia. *Journal of Volcanology and Geothermal Research* **74**, 243.

Martel, C., Pichavant, M., Bourdier, J. -L., Traineau, H., Holtz, F., Scaillet, B. (1998). Magma storage conditions and control of eruption regime in silicic volcanoes: experimental evidence from Mt. Pelée. *Earth and Planetary Science Letters* **156**, 89-99.

Martel, C., Pichavant, M., Holtz, F., Scaillet, B., Bourdier, J. -L., Traineau, H. (1999). Effects of fO_2 and H_2O on andesite phase relations between 2 and 4 kbar. *Journal of Geophysical Research* **104**, 29453-29470.

Martin, V. M. (2005). Geochemical and Textural Analysis of Mafic Enclaves from Nea Kameni, Santorini, Greece. PhD Thesis, University of Cambridge.

Martin, V. M., Davidson, J., Morgan, D., Jerram, D. A. (2010). Using the Sr isotope compositions of feldspars and glass to distinguish magma system components and dynamics. *Geology* **38**, 539-542.

Martin, V. M., Holness, M. B., Pyle, D. M. (2006). Textural analysis of magmatic enclaves from the Kameni Islands, Santorini, Greece. *Journal of Volcanology and Geothermal Research* **154**, 89-102.

Martin, V. M., Morgan, D. J., Jerram, D. A., Caddick, M. J., Prior, D. J., Davidson, J. P. (2008). Bang! Month-Scale Eruption Triggering at Santorini Volcano. *Science, Brevia* **321**, 1178.

Mathez, E. A. & Webster, J. D. (2005). Partitioning behavior of chlorine and fluorine in the system apatite-silicate melt-fluid. *Geochimica et Cosmochimica Acta* **69**, 1275-1286.

McCaffrey, K. J. W. & Petford, N. (1997). Are granitic intrusions scale invariant? *Journal of the Geological Society, London* **154**, 1–4.

Mellors, R. (1988). Explosive volcanism on Santorini, Greece and Mt. St. Helens. PhD thesis, University of Cambridge, United Kingdom.

Metrich, N. & Rutherford, M. J. (1992). Experimental study of chlorine behavior in hydrous silicic melts. *Geochimica et Cosmochimica Acta* **56**, 607-616.

Michaud V, Clocchiatti R, Sbrana S (2000). The Minoan and post-Minoan eruptions, Santorini (Greece), in the light of melt inclusions: chlorine and sulphur behaviour. *Journal of Volcanology and Geothermal Research* **99**, 195.

Michaut, C. & Jaupart, C. (2006). Ultra-rapid formation of large volumes of evolved magma. *Earth and Planetary Science Letters* **250**, 38–52.

Michaut, C. & Jaupart, C. (2011). Two models for the formation of magma reservoirs by small increments, *Tectonophysics* **500**, 34-49.

Mortazavi, M. & Sparks, R. S. J. (2004). Origin of rhyolite and rhyodacite lavas and associated mafic inclusions of Cape Akrotiri, Santorini: the role of wet basalt in generating calcalkaline silicic magmas. *Contributions to Mineralogy and Petrology* **146**, 397–413.

Mosbah, M., Métrich, N., Massiot, P. (1991). PIGME fluorine determination using a nuclear microprobe with application to glass inclusions. *Nuclear Instruments and Methods in Physics Research* **B58**, 227-231.

Moune, S., Sigmarsson, O., Thordarson, T., Gauthier, P.- J. (2007). Recent volatile evolution in the magmatic system of Hekla volcano, Iceland. *Earth and Planetary Science Letters* **255**, 373.

Newman, A. V., Stiros, S., Feng, L., Psimoulis, P;, Moschas, F., Saltogianni, V., Jiang, Y., Papazachos, C., Panagiotopoulos, D., Karagianni, E., Vamvakaris, D. (2012). Recent geodetic unrest at Santorini Caldera, Greece. *Geophysical Research Letters* **39**, L06309.

Newman, S., Lowenstern, J. B. (2002). VolatileCalc: a silicate melt–H_2O–CO_2 solution model written in Visual Basic for excel. *Computers & Geosciences* **28**, 597–604.

Nomikou, P., Carey, S., Papanikolaou, D., Croff Bell, K., Sakellariou, D., Alexandri, M., Bejelou, K. (2012). Submarine volcanoes of the Kolumbo volcanic zone NE of Santorini Caldera, Greece. *Global and Planetary Change* **90-91**, 135-151.

Papazachos, C.B., Panagiotopoulos, D., Newman, A.V., Stiros, S., Vougioukalakis, G., Fytikas, M., Laopoulos, T., Albanakis, K., Vamvakaris, D., Karagianni, E., Feng, L., Psimoulis, P., Moschas, F. (2012). Quantifying the current unrest of the Santorini volcano: Evidence from a multiparametric dataset, involving seismological, geodetic, geochemical and other geophysical data. EGU General Assembly 2012. Vienna, Austria.

Parks, M. M., Biggs, J., England, P., Mather, T. A., Nomikou, P., Palamartchouk, K., Papanikolaou, X., Paradissis, D., Parsons, B., Pyle, D. M., Raptakis, C. & Zacharis, V. (2012). Evolution of Santorini Volcano dominated by episodic and rapid fluxes of melt from depth. *Nature Geoscience* **5**, 749-754.

Peng, G., Luhr, J. F. & McGee, J. J. (1997). Factors controlling sulfur concentrations in volcanic apatites. *American Mineralogist.* **82**, 1210–1224.

Petford, N., Cruden, A. R., McCaffrey, K. J. W., Vigneresse, J. L. (2000). Granite magma formation, transport and emplacement in the Earth's crust. *Nature* **408**, 669–673.

Pichavant, M. (1987). Effects of B and H_2O on liquidus phase relations in the haplogranite system at 1 kbar. *American Mineralogist* **72**, 1056-1070.

Pichavant, M., Costa, F., Burgisser, A., Scaillet, B., Martel, C., Poussineau, S. (2007). Equilibration scales in silicic to intermediate magmas - Implications for experimental studies. *Journal of Petrology* **48**, 1955-1972.

Pinel, V. & Jaupart, C. (2003). Magma chamber behavior beneath a volcanic edifice. *Journal of Geophysical Research* **108(B2)**, doi: 10.1029/2002JB001751.

Pinel, V., Jaupart, C., Albino, F., (2010). On the relationship between cycles of eruptive activity and growth of a volcanic edifice. *Journal of Volcanology and Geothermal Research* **194**, 150–164.

Pownceby, M. I. & O'Neill, H. S. C. (1994). Thermodynamic data from redox reactions at high temperatures. III. Activity-composition relations in Ni-Pd alloys from EMF measurements at 850-1250 K, and calibration of the NiO + Ni-Pd assemblage as a redox sensor. *Contributions to Mineralogy and Petrology* **116**, 327-339.

Prouteau, G. & Scaillet, B. (2003). Experimental constraints on the origin of the 1991 Pinatubo dacite. *Journal of Petrology* **44**, 2203-2241.

Pyle, D. M. (1990). New volume estimates for the Minoan eruption. In: Hardy D, Keller J, Galanopoulos VP, Flemming NC, and Druitt TH (Eds), *Thera and the Aegean World III*, **2**, 113–121, The Thera Foundation, London.

Pyle, D. M. & Elliott, J. R. (2006). Quantitative morphology, recent evolution, and future activity of the Kameni Islands volcano, Santorini, Greece. *Geosphere* **2**, 253-268.

Ridolfi, F., Renzulli, A., Puerini, M. (2010). Stability and chemical equilibrium of amphibole in calc-alkaline magmas: an overview, new thermobarometric formulations and application to subduction-related volcanoes. *Contributions to Mineralogy and Petrology* **160**, 45-66.

Robie, R. A., Hemingway, B. S. & Fisher, J. R. (1978). Thermodynamic properties of minerals and related substances at 298.15 K and 1 bar (10^5 Pascals) pressure and at higher temperature. *US Geological Survey Bulletin* **1452**.

Roman, D. C., Cashman, K. V., Gardner, C. A., Wallace, P. J., Donovan, J. J. (2006). Storage and interaction of compositionally heterogeneous magmas from the 1986 eruption of Augustine Volcano, Alaska. *Bulletin of Volcanology* **68**, 240-254.

Rutherford, M. J. & Devine, J. D. (2008). Magmatic Conditions and Processes in the Storage Zone of the 2004-2006 Mount St. Helens Dacite. *US Geological Survey professional paper* **1750**, 703-725.

Rutherford, M. J., Sigurdsson, H., Carey, S. (1985). The May 1, 1980 eruption of Mount St. Helens: 1, Melt composition and experimental phase equilibria. *Journal of Geophysical Research* **90**, 2929-2947.

Saint Blanquat, M. (de), Horsman, E., Habert, G., Morgan, S., Vanderhaeghe, O., Law, R., Tikoff, B. (2011). Multiscale magmatic cyclicity, duration of pluton construction, and the paradoxical relationship between tectonism and plutonism in continental arcs. *Tectonophysics*, **500**(1-4), 20-33.

Scaillet, B. & Evans, B. W. (1999). The 15 June 1991 Eruption of Mount Pinatubo. I. Phase Equilibria and Pre-eruption P-T-fO_2-fH_2O Conditions of the Dacite Magma. *Journal of Petrology* **40**, 381-411.

Scaillet, B. & Searle, M. P. (2006). Mechanisms and timescales of felsic magma segregation, ascent and emplacement in the Himalaya. *Geological Society Special Publications* **268**, 293-308.

Scaillet, B., Pichavant, M., Roux, J., Humbert, G., Lefevre, A. (1992). Improvements of the Shaw membrane technique for measurement and control of fH_2 at High-Temperatures and Pressures. *American Mineralogist* **77**, 647-655.

Scaillet, B., Pichavant, M., Roux, J. (1995). Experimental crystallization of leucogranite magmas. *Journal of Petrology* **36**, 663-705.

Scaillet, B., Clemente, B., Evans, B. W., Pichavant, M. (1998). Redox control of sulfur degassing in silicic magmas. *Journal of Geophysical Research: Solid Earth* **103**, 23937.

Scaillet, B., Luhr, J.F., Carroll, M. C. (2003). Petrological and volcanological constraints on volcanic sulfur emissions to the atmosphere. In: A Robock and C Oppenheimer (eds.) *Volcanism and the Earth's Atmosphere*. pp. 11-40. Geophysical Monograph, American Geophysical Union.

Scaillet, B., Pichavant, M., Cioni, R. (2008). Upward migration of Vesuvius magma chamber over the past 20,000 years. *Nature* **455**, 216-219.

Schmidt, B. C., Scaillet, B., Holtz, F. (1995). Accurate control of fH_2 in cold-seal Pressure-Vessels with the Shaw membrane technique. *European Journal of Mineralogy* **7**, 893-903.

Schwarz, M. (2000). Tephra korrelation im östlichen Mittelmeer (Meteor M40/4 Kerne). Diploma Thesis. Albert-Ludwigs-University of Freiburg i.Br., 257 pp.

Sigurdsson, H., Carey, S., Devine, J. D. (1990). Assessment of mass, dynamics and environmental effects of the Minoan eruption of Santorini Volcano. In: DA Hardy (ed.) *Thera and the Aegean world III*. pp. 100-112. Thera Foundation: London.

Sigurdsson, H., Carey, S., Alexandri, M., Vougioukalakis, G., Croff, K., Roman, C., Sakellariou, D., Anagnostou, C., Rousakis, G., Ioakim, C. and others (2006). New marine geological investigations of the Santorini volcanic field. *EOS Transactions, American Geophysical Union*, **87**, 337–342.

Sisson, T. W. & Grove T. L. (1993). Experimental investigations of the role of H_2O in calc-alkaline differentiation and subduction zone magmatism. *Contributions to Mineralogy and Petrology* **113**, 143–166.

Sparks, R. S. J. & Wilson, C. J. N. (1990). The Minoan deposits: a review of their characteristics and interpretation. In: D Hardy, J Keller, VP Galanopoulos, NC Flemming and TH Druitt (eds.) *Thera and the Aegean World III*. pp. 89-99. The Thera Foundation: London.

Stormer, J. C. (1983). The effects of recalculation on estimates of temperature and oxygen fugacity from analyses of multi-component iron-titanium oxides. *American Mineralogist* **68**, 586-594.

Taylor, J. R., Wall, V. J., Pownceby, M. I. (1992). The calibration and application of accurate redox sensors. *American Mineralogist* **77**, 284-295.

Vaggelli, G., Pellegrini, M., Vougioukalakis, G., Innocenti, S., Francalanci, L. (2009). Highly Sr radiogenic tholeiitic magmas in the latest inter-Plinian activity of Santorini volcano, Greece. *Journal of Geophysical Research* **114**, B06201.

Ventura, G;, Vilardo, G., Bruno, P. P. (1999). The role of flank failure in modifying the shallow plumbing system of volcanoes: An example from Somma-Vesuvius, Italy. *Geophysical Research Letters* **26**, 3681–3684.

Vespa, M., Keller, J., Gertisser, R. (2006). Interplinian explosive activity of Santorini volcano (Greece) during the past 150,000 years. *Journal of Volcanology and Geothermal Research* **153**, 262-286.

Vigneresse, J. L., Tikoff, B., Ameglio, L. (1999). Modification of the regional stress field by magma intrusion and formation of tabular granitic plutons. *Tectonophysics* **302** (3–4), 203–224.

Wallace, P. J. (2005). Volatiles in subduction zone magmas: concentrations and fluxes based on melt inclusion and volcanic gas data. *Journal of Volcanology and Geothermal Research* **140**, 217.

Webster, J. D. (1992a). Water solubility and chlorine partitioning in Cl-rich granitic systems: Effects of melt composition at 2 kbar and 800°C. *Geochimica et Cosmochimica Acta* **56**, 679-687.

Webster, J. D. (1992b). Fluid–melt interactions involving Cl-rich granites: experimental study from 2 to 8 kbar. *Geochimica et Cosmochimica Acta* **56**, 679–687.

Webster, J. D. (1997a). Chloride Solubility in Felsic Melts and the Role of Chloride in Magmatic Degassing. *Journal of Petrology* **38**, 1793-1807.

Webster, J. D. (1997b). Exsolution of magmatic volatile phases from Cl-enriched mineralizing granitic magmas and implications for ore metal transport. *Geochimica et Cosmochimica Acta* **61**, 1017-1029.

Webster, J. D. (2004). The exsolution of magmatic hydrosaline chloride liquids. *Chemical Geology* **210**, 33-48.

Webster, J. D. & Holloway, J. R. (1988). Experimental constraints on the partitioning of Cl between topaz rhyolite melt and H_2O and H_2O + CO_2 fluids: New implications for granitic differentiation and ore deposition. *Geochimica et Cosmochimica Acta* **52**, 2091-2105.

Webster, J. D., Tappen, C. M., Mandeville, C. W. (2009). Partitioning behavior of chlorine and fluorine in the system apatite-melt-fluid. II: Felsic silicate systems at 200 MPa. *Geochimica et Cosmochimica Acta* **73**, 559-581.

Westrich, H. R., Eichelberger, J. C., Hervig, R. L. (1991). Degassing of the 1912 Katmai magmas. *Geophysical Research Letters* **18**, 1561–1564.

Wulf, S., Kraml, M., Kuhn, T., Schwarz, M., Inthorn, M., Keller, J., Kuscu, I., Halbach, P. (2002). Marine tephra from the Cape Riva eruption (22 ka) of Santorini in the Sea of Marmara. *Marine Geology* **183**, 131.

Zellmer, G., Turner, S., Hawkesworth, C. (2000). Timescales of destructive plate margin magmatism: new insights from Santorini, Aegean volcanic arc. *Earth and Planetary Science Letters* **174**, 265-281.

FIGURE CAPTIONS

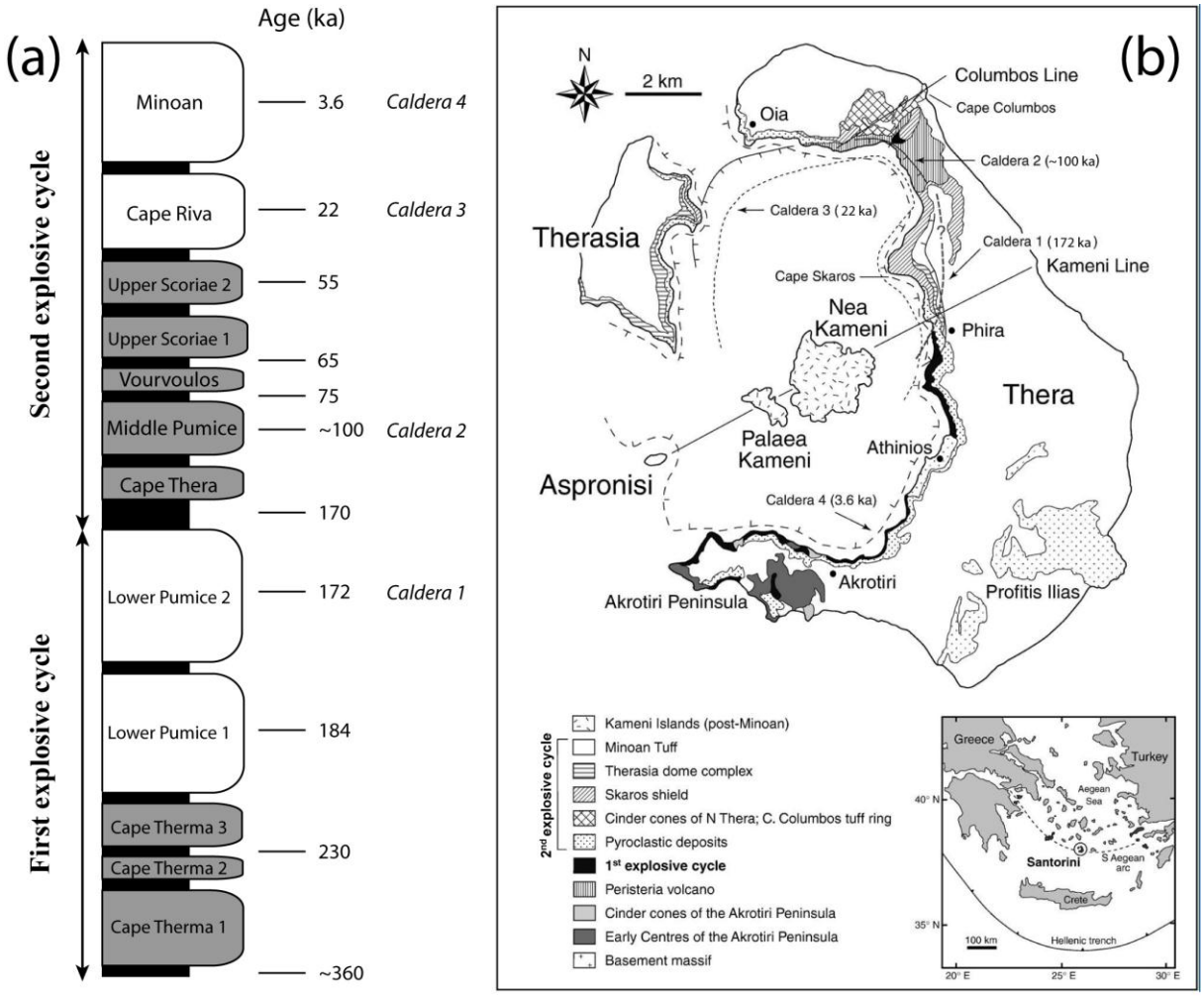

Figure 1
Cadoux et al., 2013

Figure 1. a. The sequence of the 12 major explosive eruptions of Santorini divided into two cycles (modified from Druitt *et al.*, 1999). White: dominantly silicic eruption, grey: dominantly andesitic eruption, black: interplinian eruption. **b.** Simplified geological map (slightly modified from Gertisser *et al.*, 2009).

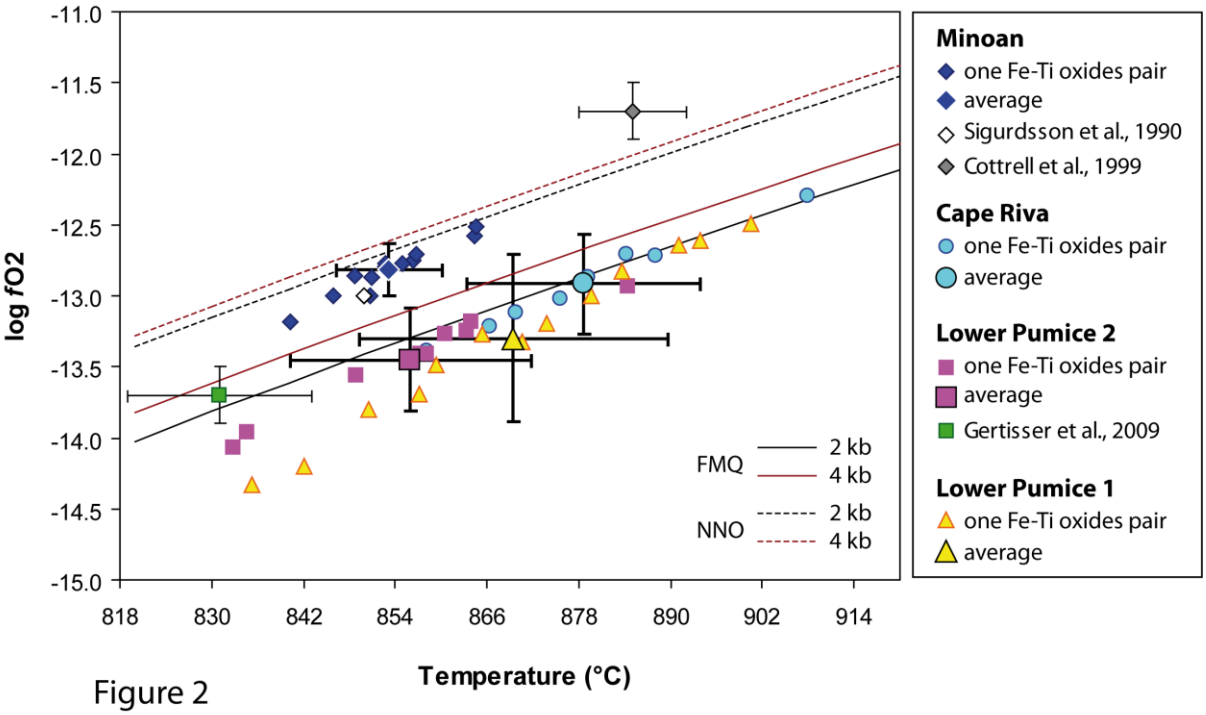

Figure 2
Cadoux et al., 2013

Figure 2. Oxygen fugacity (log fO_2) versus temperature (°C) calculated from Fe-Ti oxides from silicic pumices of the Minoan, Cape Riva, Lower Pumice 2 and Lower Pumice 1 eruptions (calculations performed with Stormer, 1983, and Andersen & Lindsley, 1985). All the ilmenite and magnetite pairs used for calculation are in equilibrium, according to their Mg/Mn ratios (Bacon & Hirschmann, 1988). They are touching and non-touching pairs included in the same pyroxene crystal or, touching pair in the groundmass. Previously published T - fO_2 estimates for the Minoan (Sigurdsson *et al.*, 1990; Cottrell *et al.*, 1999) and the LP2 (Gertisser *et al.*, 2009) eruptions are also shown. The FMQ and NNO oxygen fugacity curves were calculated for 2 and 4 kbar using Frost (1991).

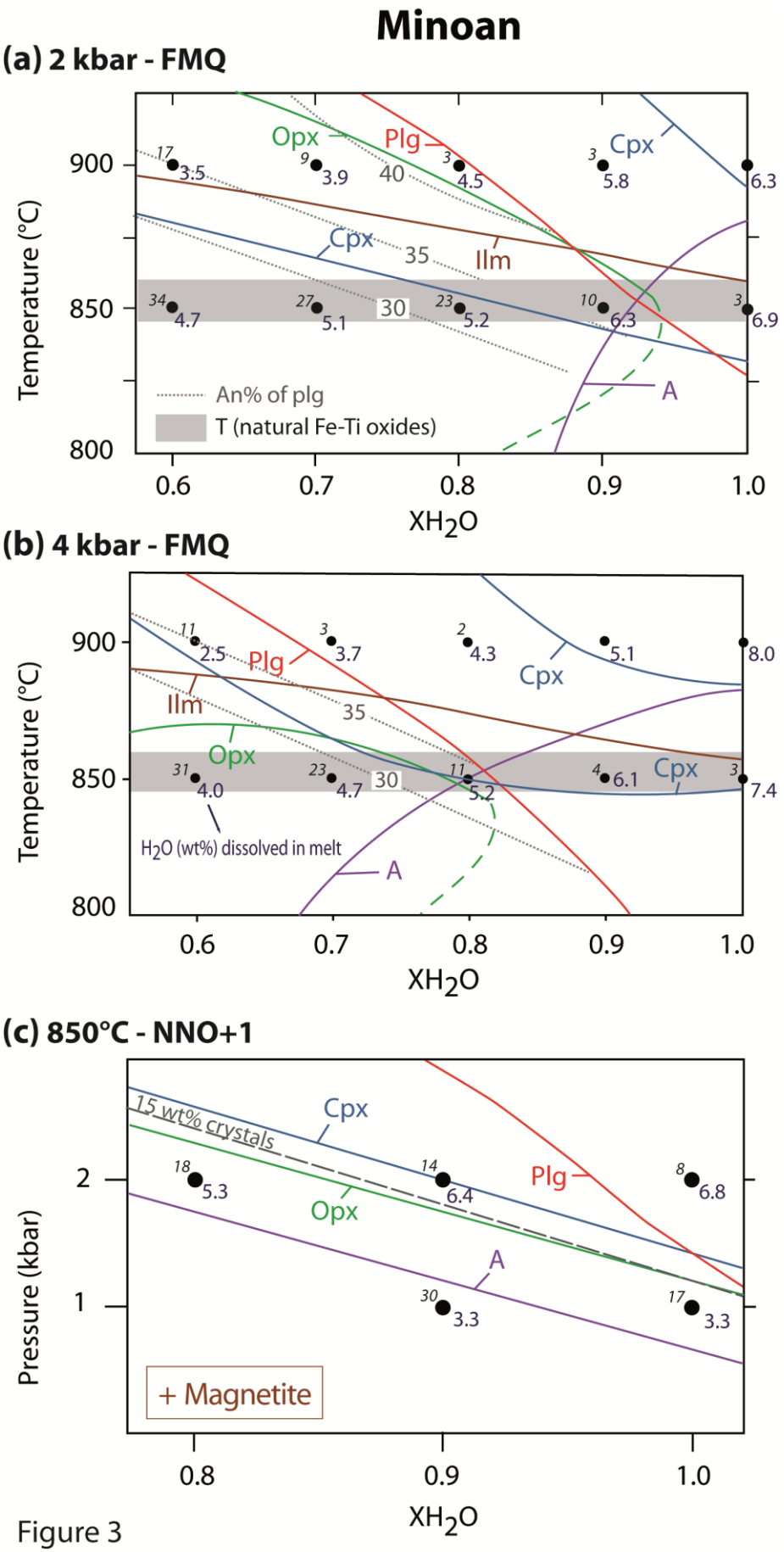

Figure 3
Cadoux et al., 2013

Figure 3. Isobaric phase relationships of the Minoan rhyodacite at (a) 2 and (b) 4 kbar and FMQ as a function of XH_2O of the coexisting fluid phase and of temperature (°C). Curves are labeled with mineral names lying inside their stability fields. Plg = plagioclase, Opx = orthopyroxene, Cpx = clinopyroxene, Pig = pigeonite, A = amphibole, Ilm = ilmenite. Each black circle represents an experimental charge. Dark blue numbers: by-difference H_2O_{melt} values in wt% (Table 3). Smaller italic black numbers are charge crystallinity in wt% (Table 3). Light grey dashed-lines indicate the anorthite content (%) of the experimental plagioclases (Electronic Appendix 1b). Grey band: pre-eruptive temperature range inferred from natural Fe-Ti oxides (Table 2). **3c.** Phase relationships at NNO+1 and 850°C as a function of XH_2O of the coexisting fluid phase and of pressure (kbar).

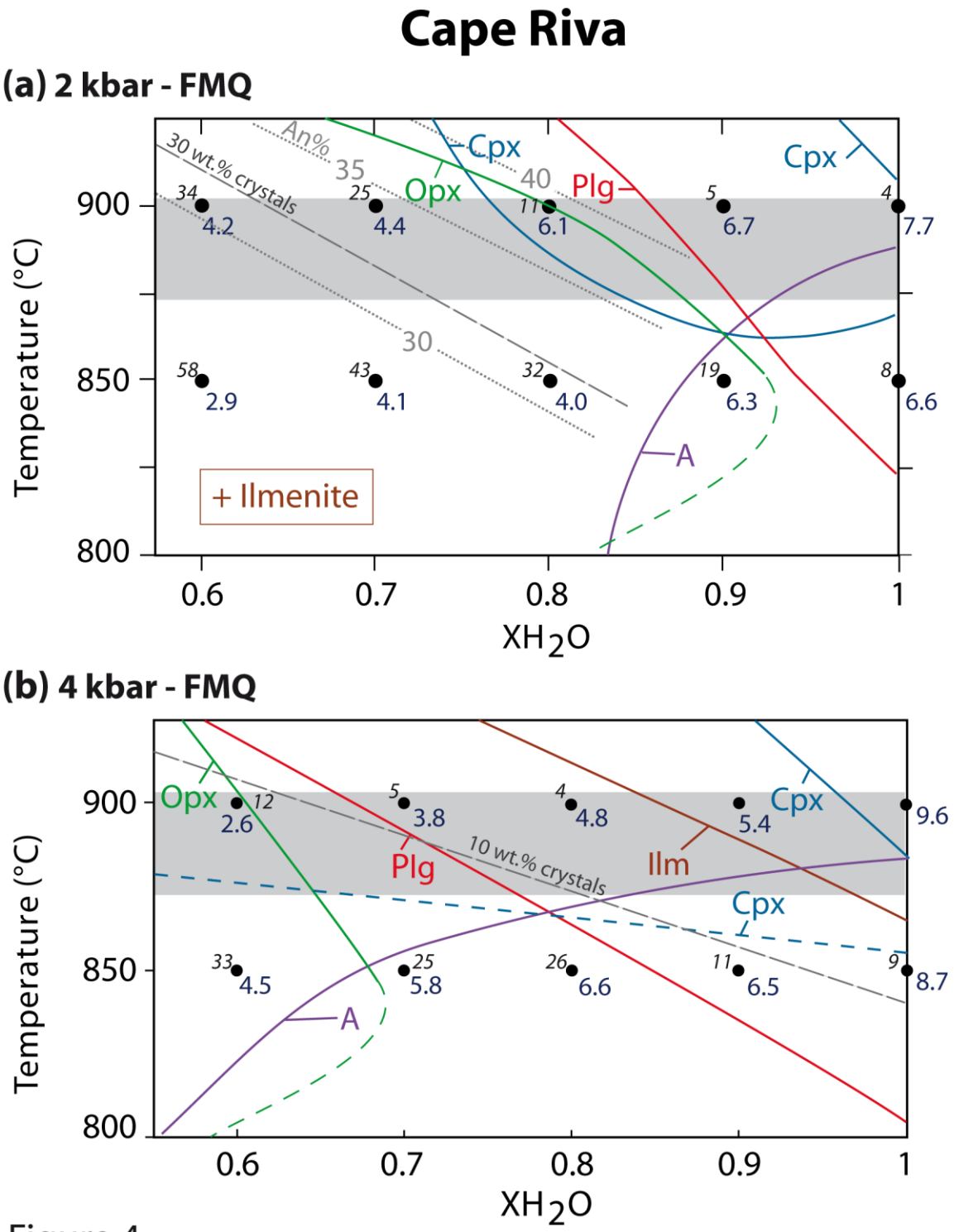

Figure 4
Cadoux et al., 2013

Figure 4. Isobaric phase relationships of the Cape Riva dacite at (a) 2 and (b) 4 kbar and FMQ as a function of XH_2O of the coexisting fluid phase and of temperature (°C). Same legend as Figure 3.

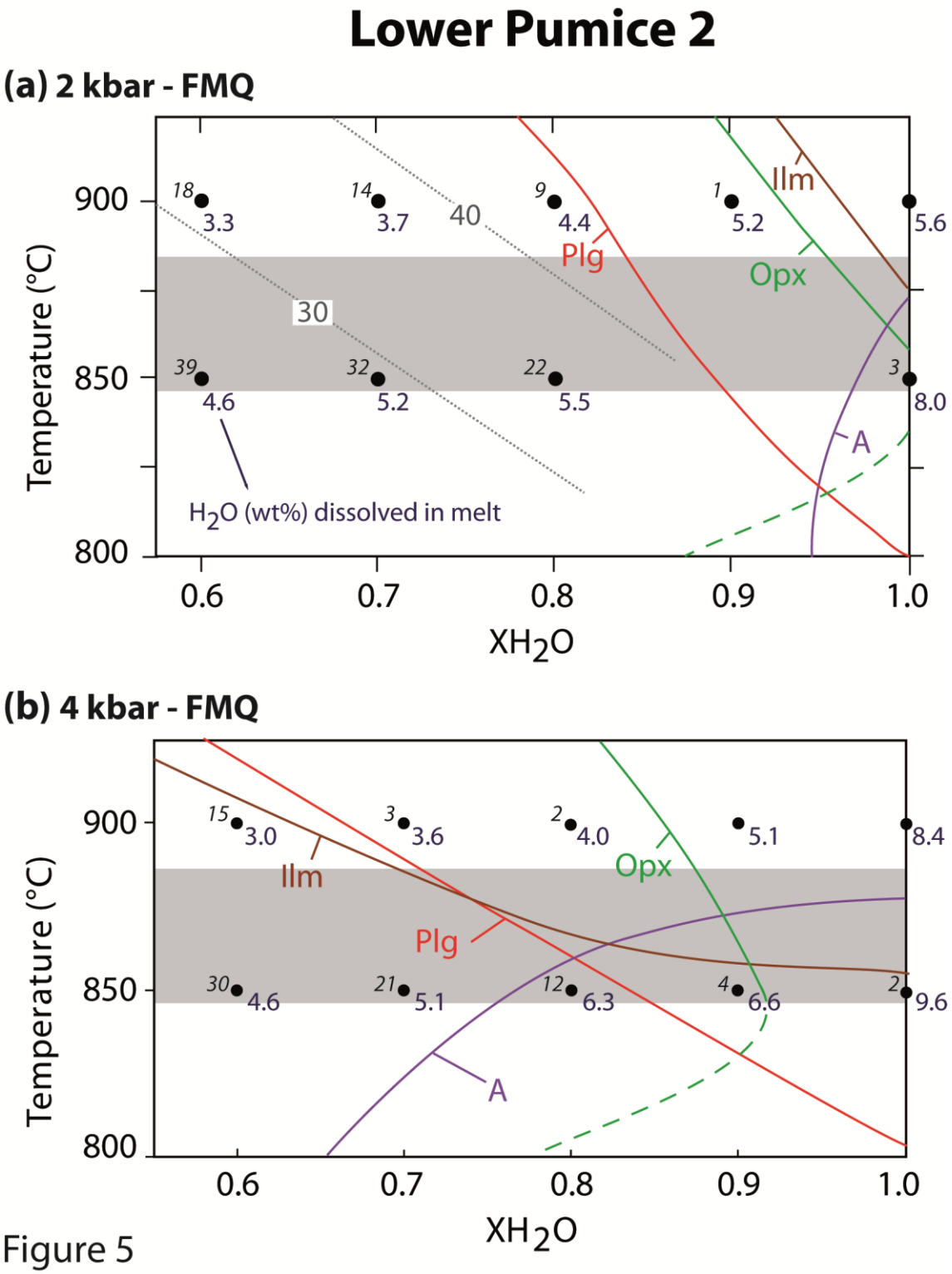

Figure 5
Cadoux et al., 2013

Figure 5. Isobaric phase relationships of the Lower Pumice 2 rhyodacite at (a) 2 and (b) 4 kbar and FMQ as a function of XH_2O of the coexisting fluid phase and of temperature (°C). Same legend as Figure 3.

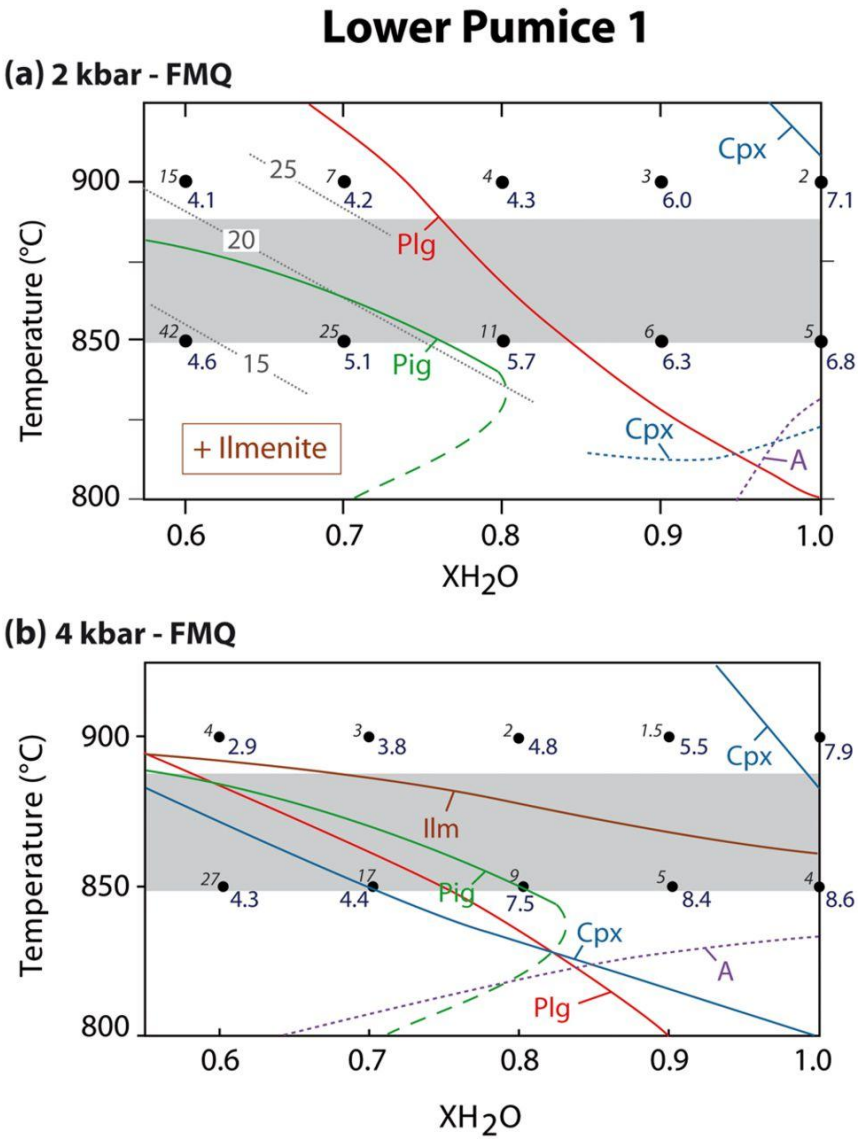

Figure 6. Isobaric phase relationships of the Lower Pumice 1 rhyodacite at (a) 2 and (b) 4 kbar and FMQ as a function of XH_2O of the coexisting fluid phase and of temperature (°C). Same legend as Figure 3.

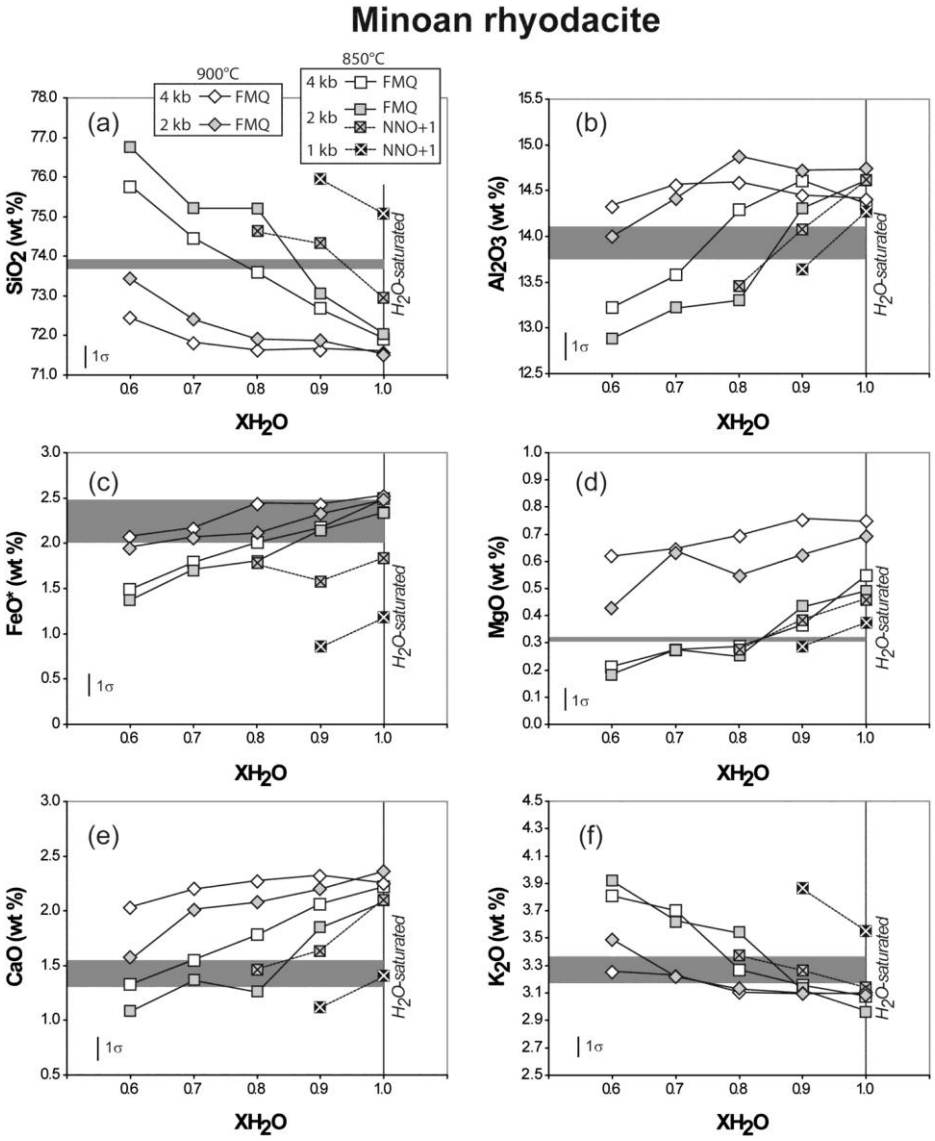

Figure 7. Experimental glass compositions of the Minoan rhyodacite as a function of XH_2O. The grey band is the composition of the natural interstitial glass and the vertical bar in the bottom left corner is the average standard deviation (wt%) for the experimental glasses. Symbols: squares and diamonds are for 850°C and 900°C runs, respectively. Fill colour: white = 4 kbar, grey = 2 kbar and black = 1 kbar. White cross within the symbol indicates NNO+1 runs, no white cross means FMQ runs.

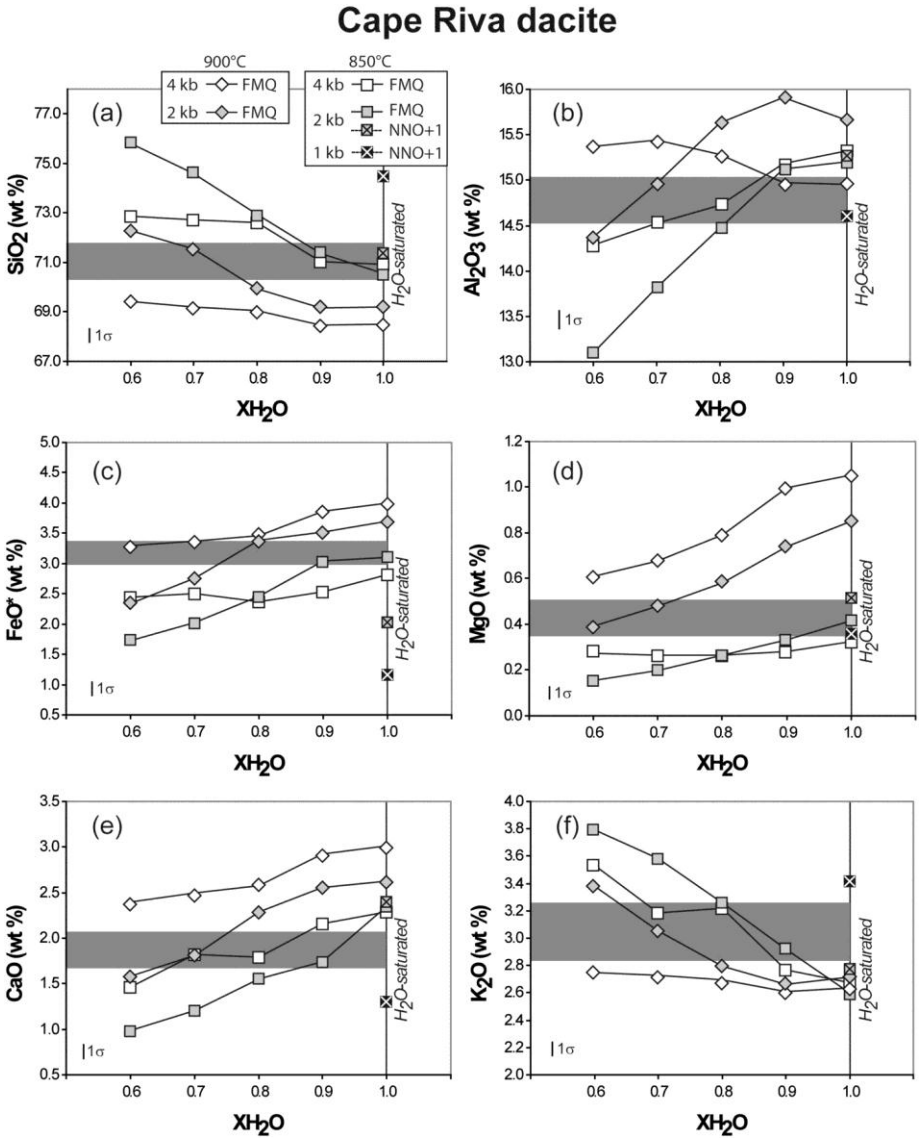

Figure 8. Experimental glasses composition of the Cape Riva dacite as a function of XH_2O. Same legend as Figure 7.

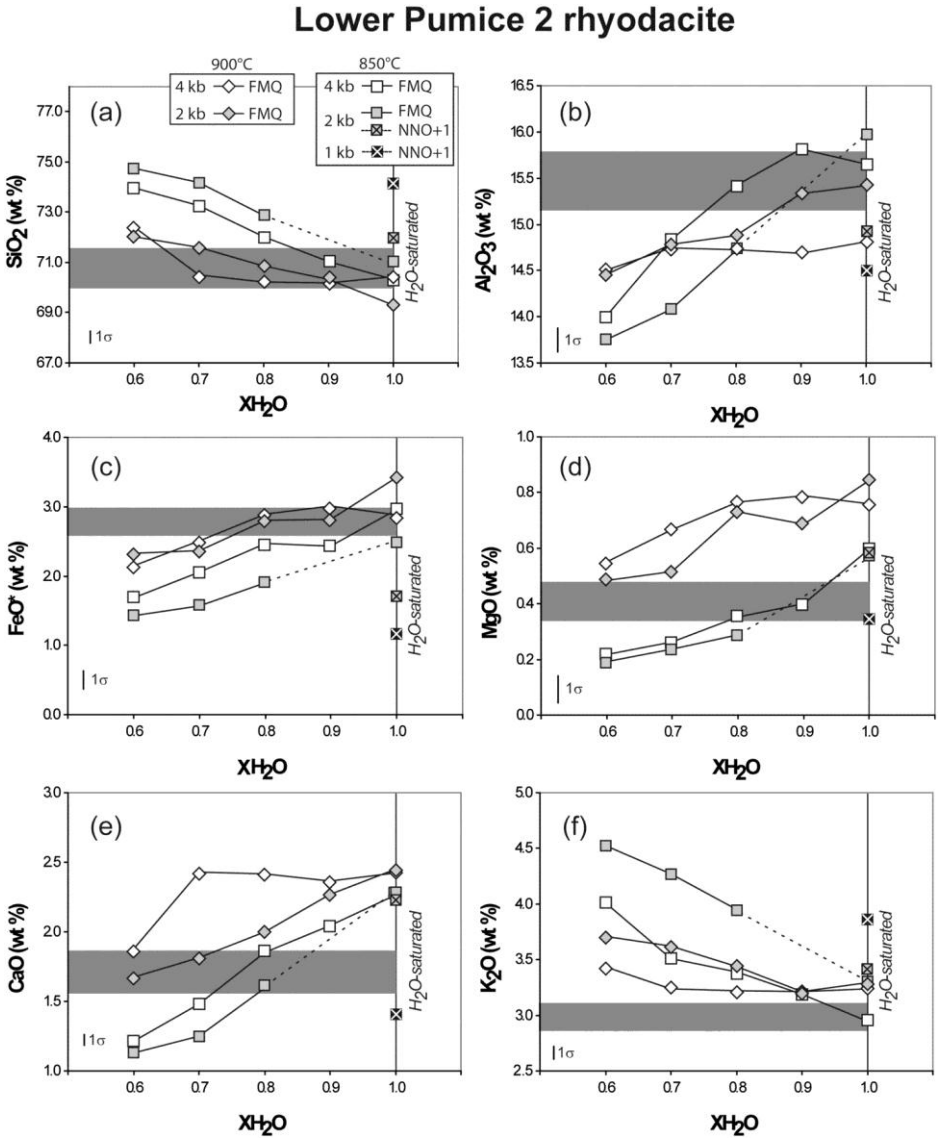

Figure 9. Experimental glasses composition of the Lower Pumice 2 rhyodacite as a function of XH_2O. Same legend as Figure 7.

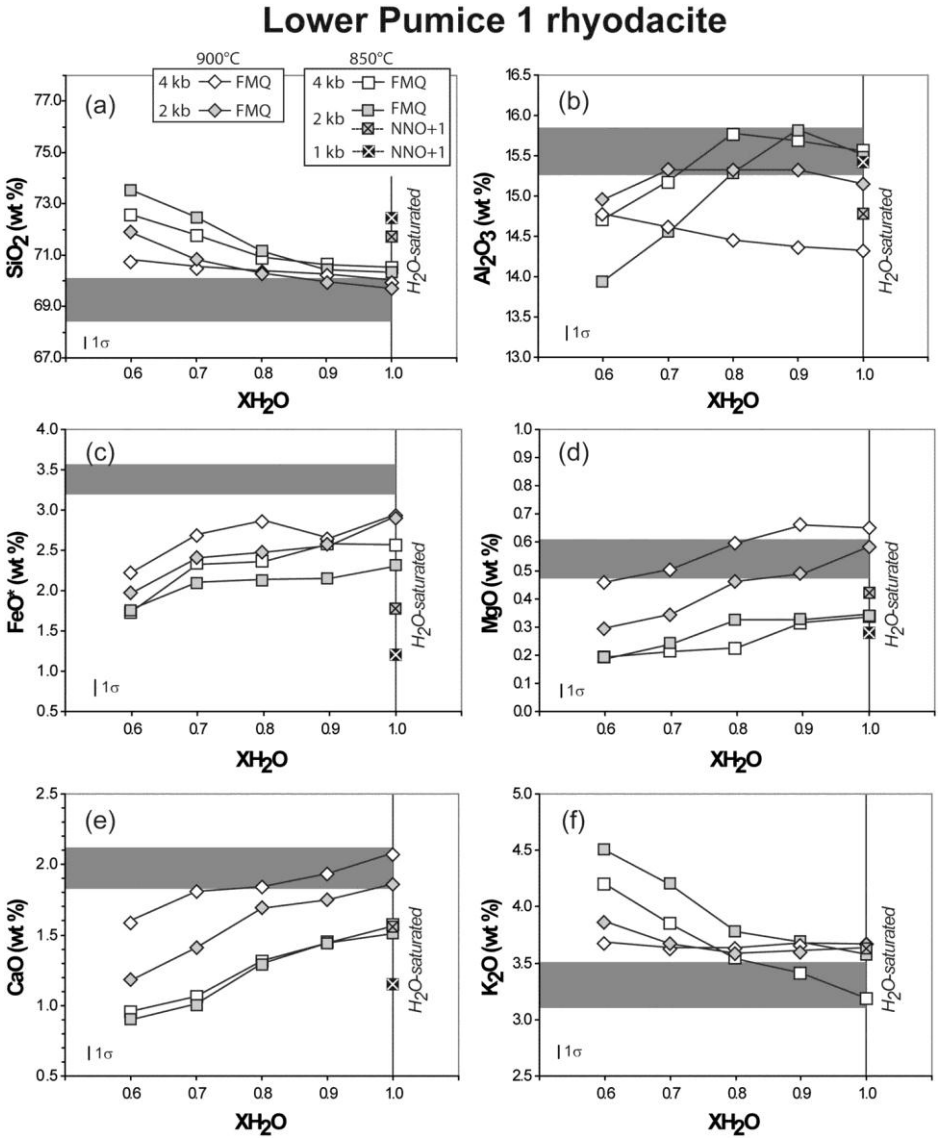

Figure 10. Experimental glasses composition of the Lower Pumice 1 rhyodacite as a function of XH_2O. Same legend as Figure 7.

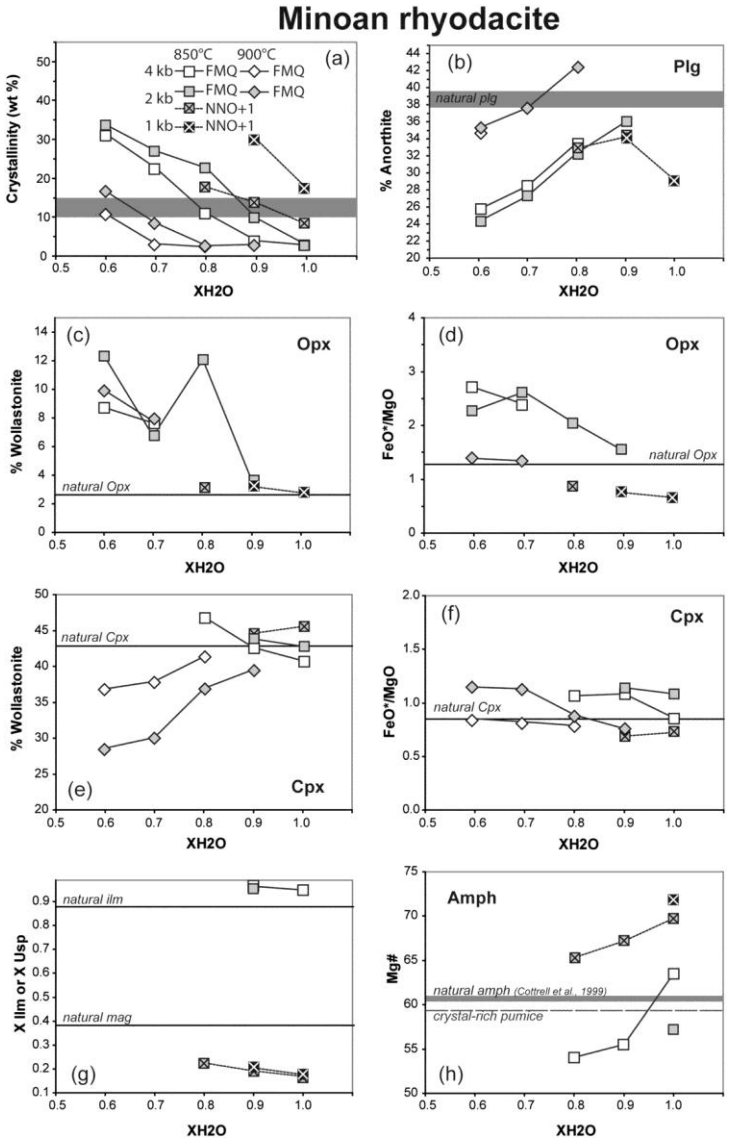

Figure 11. Crystallinity and mineral compositions of the Minoan rhyodacite as a function of XH_2O. The composition of the natural phase is reported as a grey band or a black straight line.

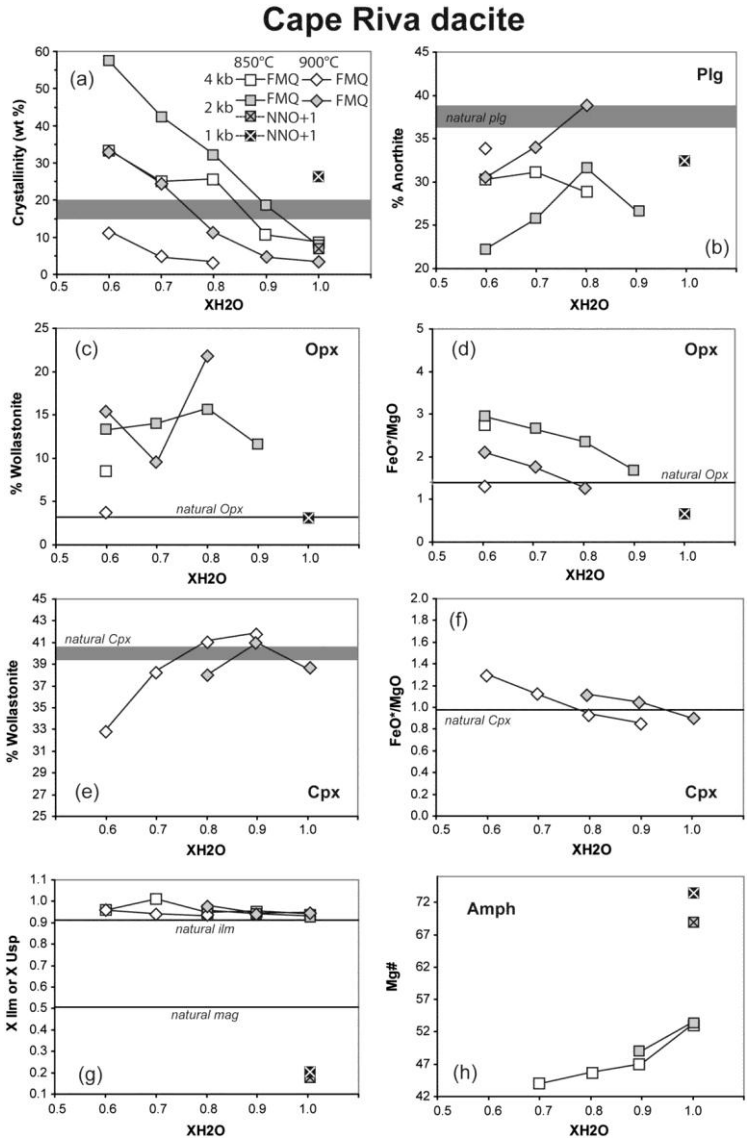

Figure 12. Crystallinity and mineral compositions of the Cape Riva dacite as a function of XH_2O. Same legend as Figure 11.

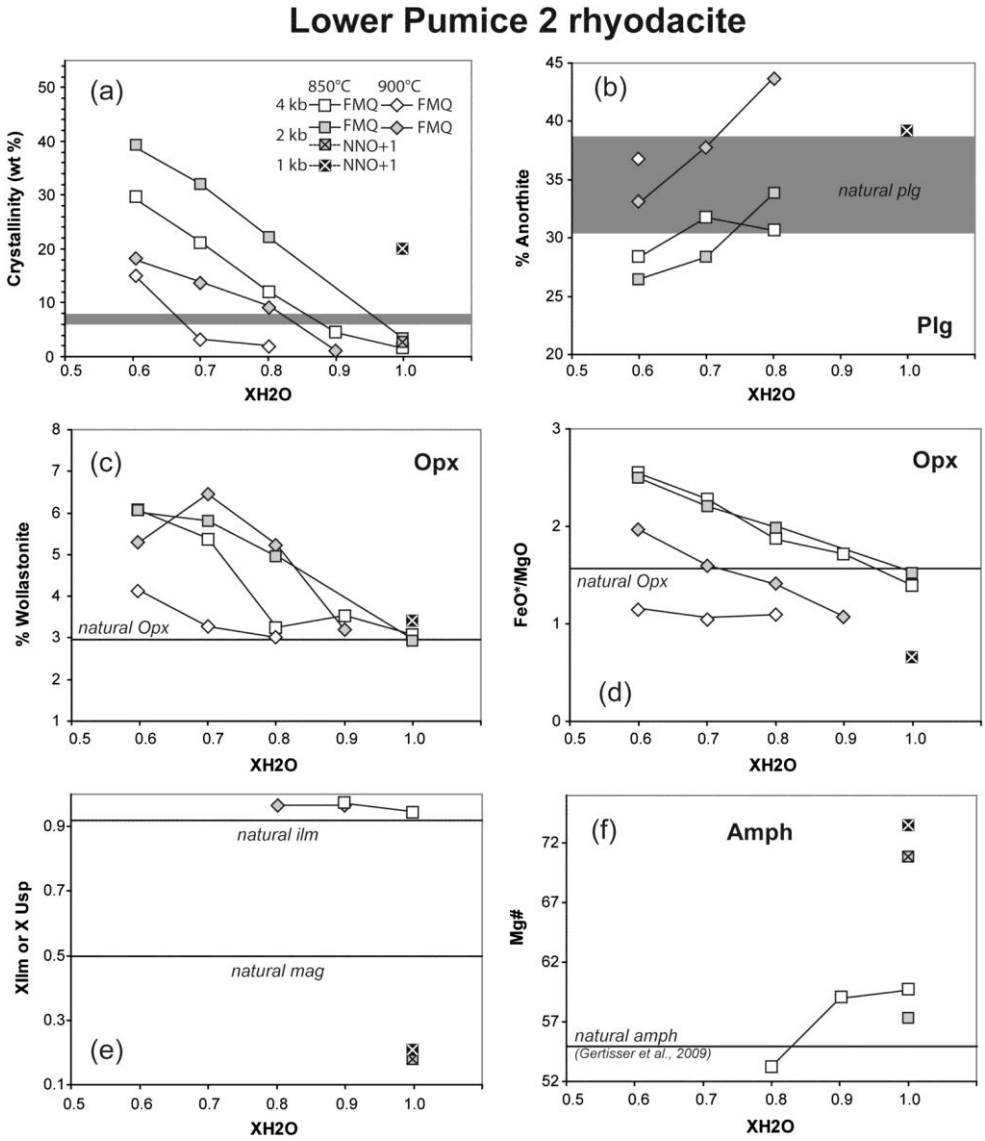

Figure 13. Crystallinity and mineral compositions of the Lower Pumice 2 rhyodacite as a function of XH_2O. Same legend as Figure 11.

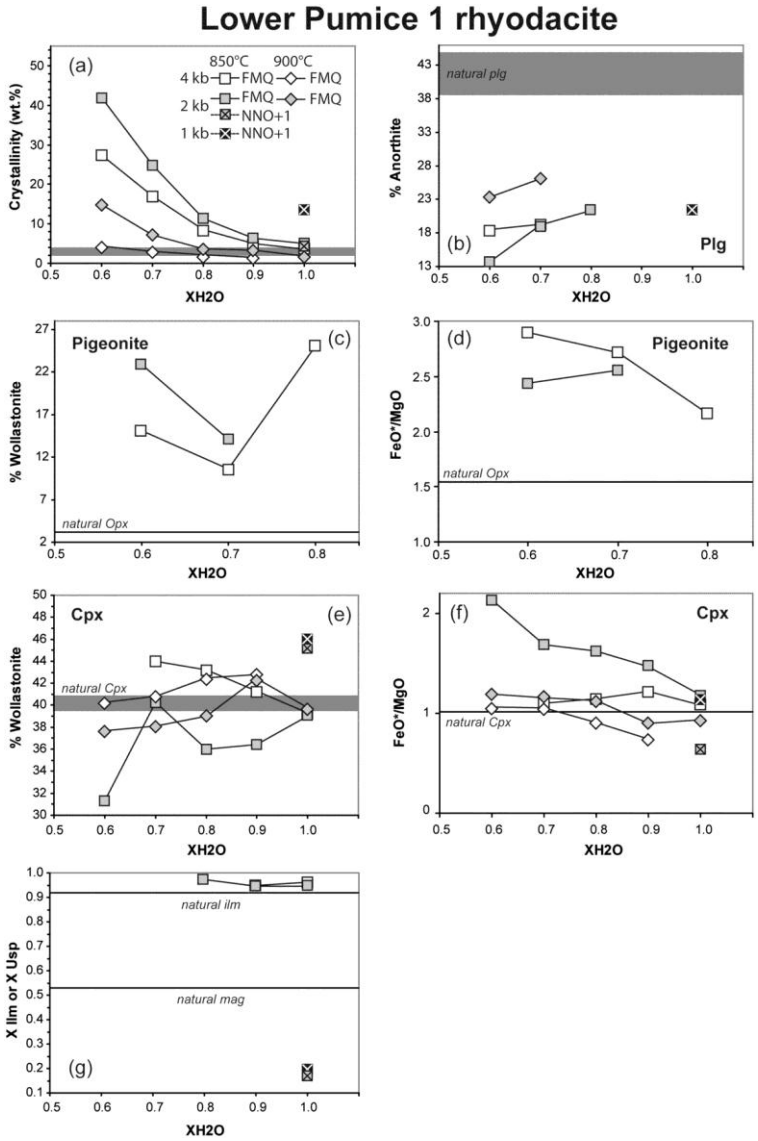

Figure 14. Crystallinity and mineral compositions of the Lower Pumice 1 rhyodacite as a function of XH_2O. Same legend as Figure 11.

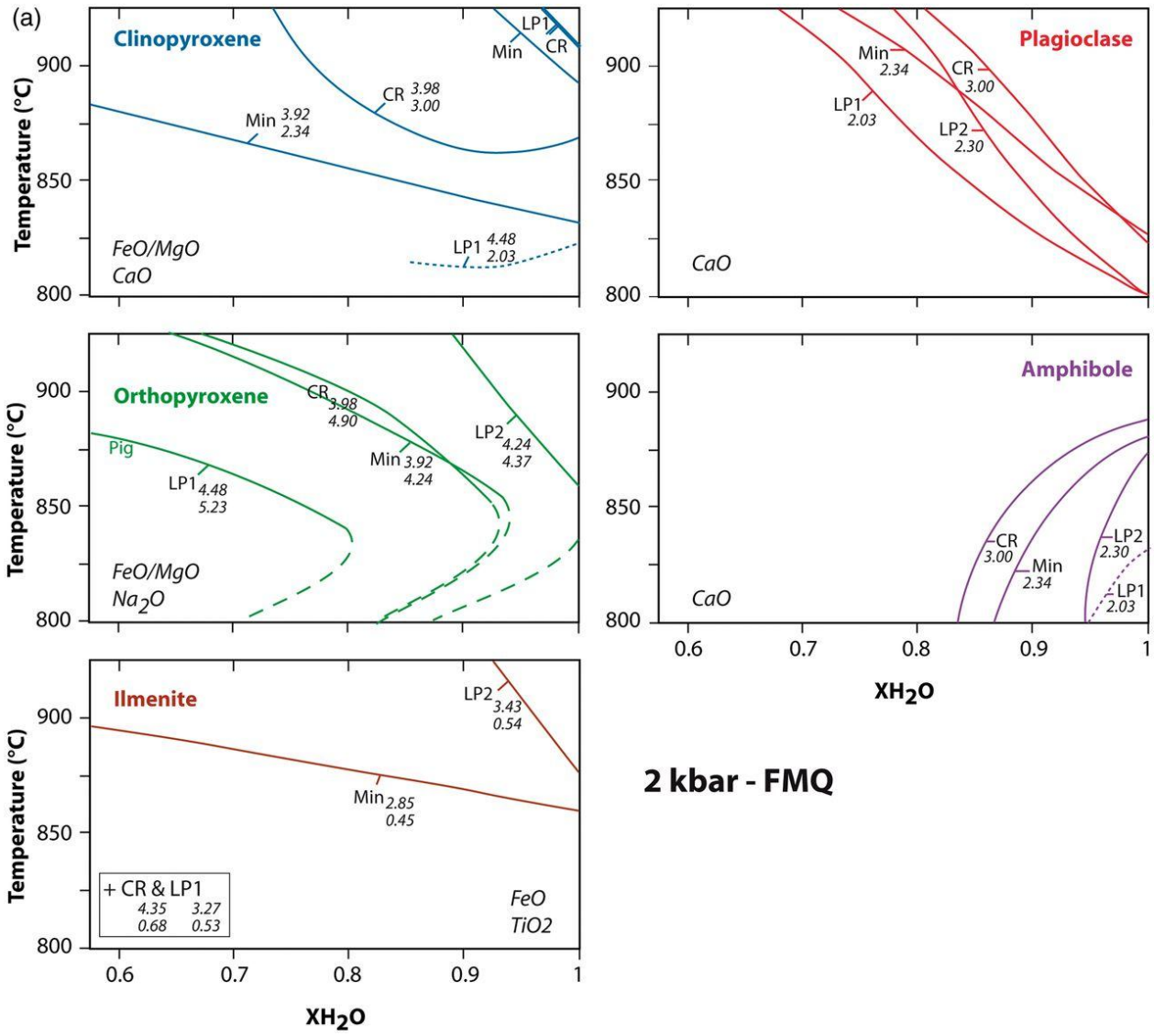

Figure 15. Comparison of each mineral phase equilibria curve for the four compositions at the same experimental conditions. **A.** at 2 kbar - FMQ, **B.** at 4 kbar - FMQ. Values of melt "descriptors" discussed in the text (FeO, TiO_2, CaO, FeO/MgO, Na_2O) are reported.

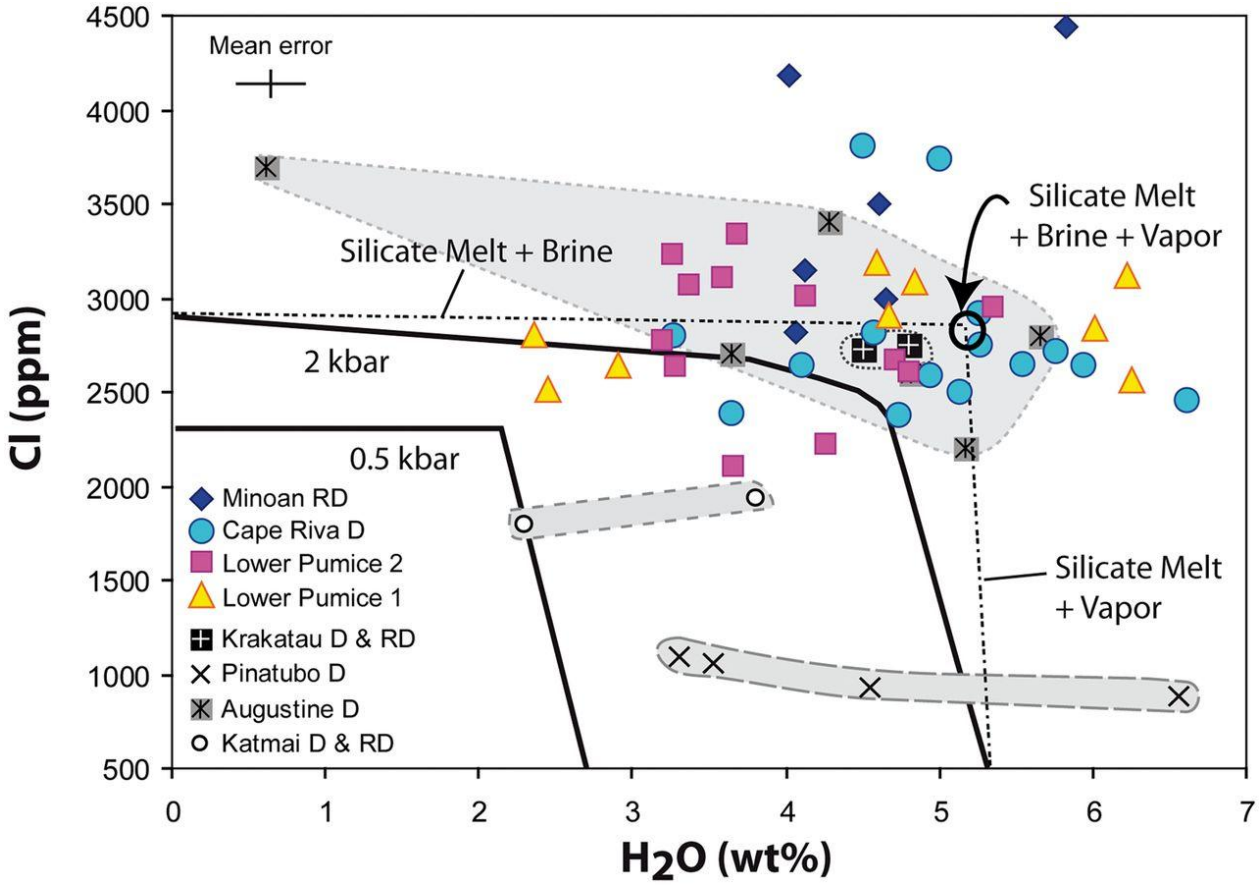

Figure 16. Chlorine (ppm) versus H_2O (wt%) contents dissolved in melt inclusions of plagioclase and pyroxene phenocrysts from the Minoan, Cape Riva, Lower Pumice 2 and Lower Pumice 1 silicic magmas. They are compared with melt inclusions of other silicic arc magmas from Augustine and Katmai volcanoes (Alaska; Hildtreth, 1983; Westrich *et al.*, 1991; Hammer *et al.*, 2002; Roman *et al.*, 2006), Krakatau (Indonesia, Mandeville *et al.*, 1996) and Pinatubo (Philippines, Gerlach *et al.*, 1996). D and RD refer to the whole-rock composition: D = dacite, RD = rhyodacite.

The Cl-H_2O solubility curves at 0.5 and 2 kbar are taken from experimental data of Webster (1997b) for haplogranite liquids at 800 to 860°C. They suggest a trapping pressure equal or higher than 2 kbar. Vapor plus hydrosaline liquid exsolve at the point of intersection, i.e., the sharp break in curves slope (e.g., Webster, 2004).

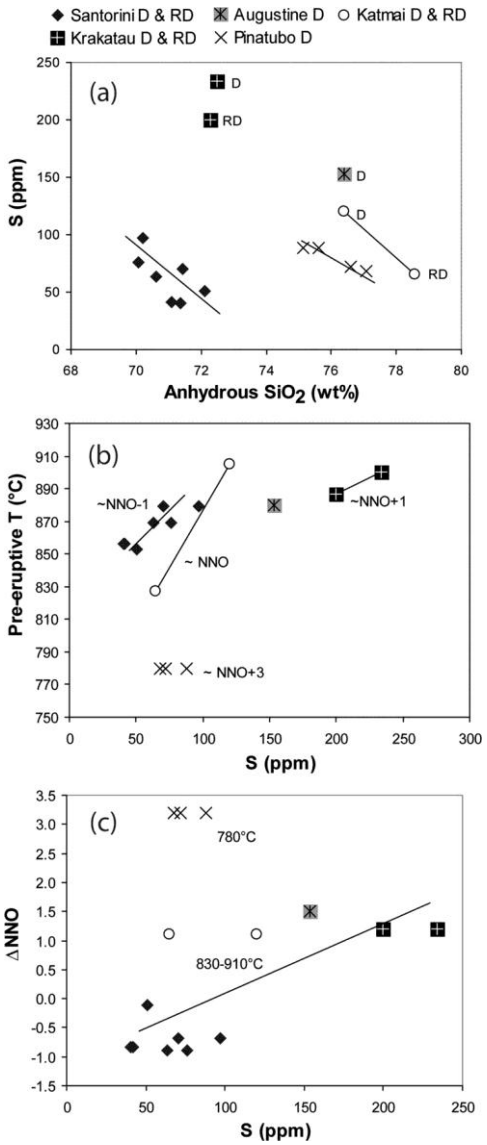

Figure 17. Sulphur contents (ppm) of melt inclusions plotted against (**a)** dry SiO_2 (wt%), **(b)** pre-eruptive temperature (°C), **(c)** ΔNNO as indicator of redox state. Data sources for Santorini in Electronic Appendix 5a, for other volcanoes: same sources as in Fig.16 plus Scaillet & Evans (1999) for ΔNNO of Pinatubo dacite.

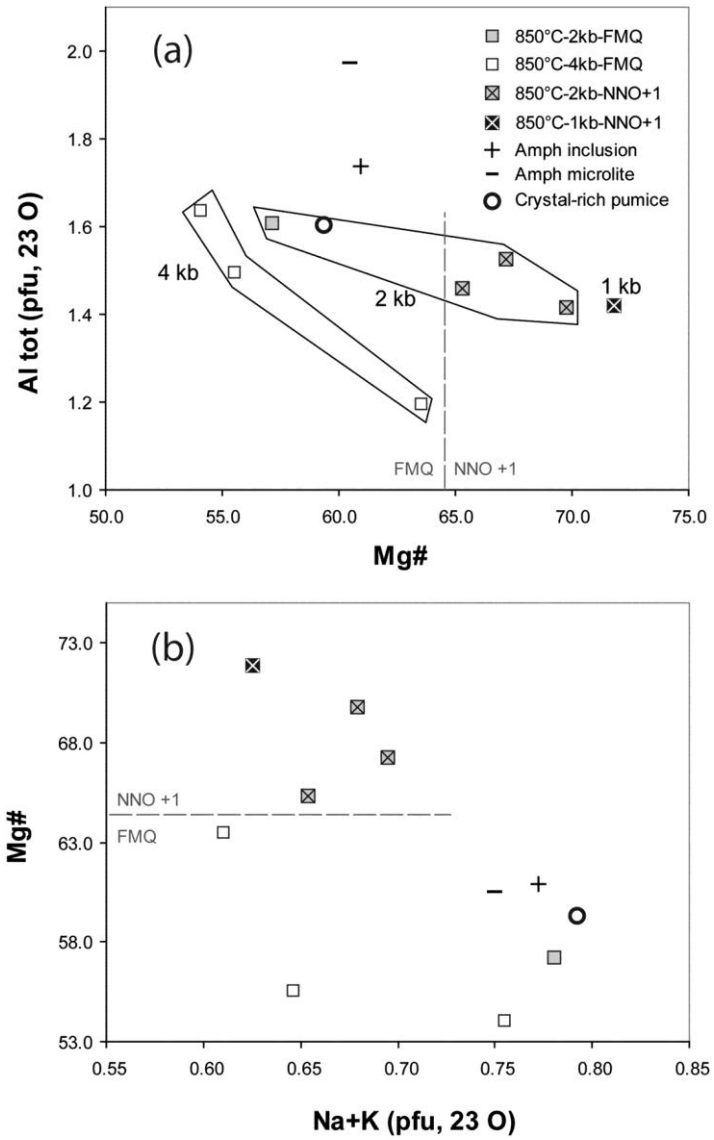

Figure 18. Amphibole compositions for the Minoan rhyodacite. **(a)** Al_{tot} versus Mg#, **(b)** Mg# versus Na+K (per formula unit, on the basis of 23 oxygen). Experimental compositions are compared with the compositions of rare amphibole crystals found in the natural rhyodacite, as well as with those found in the Minoan crystal-rich pumices (data from Cottrell *et al.*, 1999 and Druitt unpublished data, respectively).

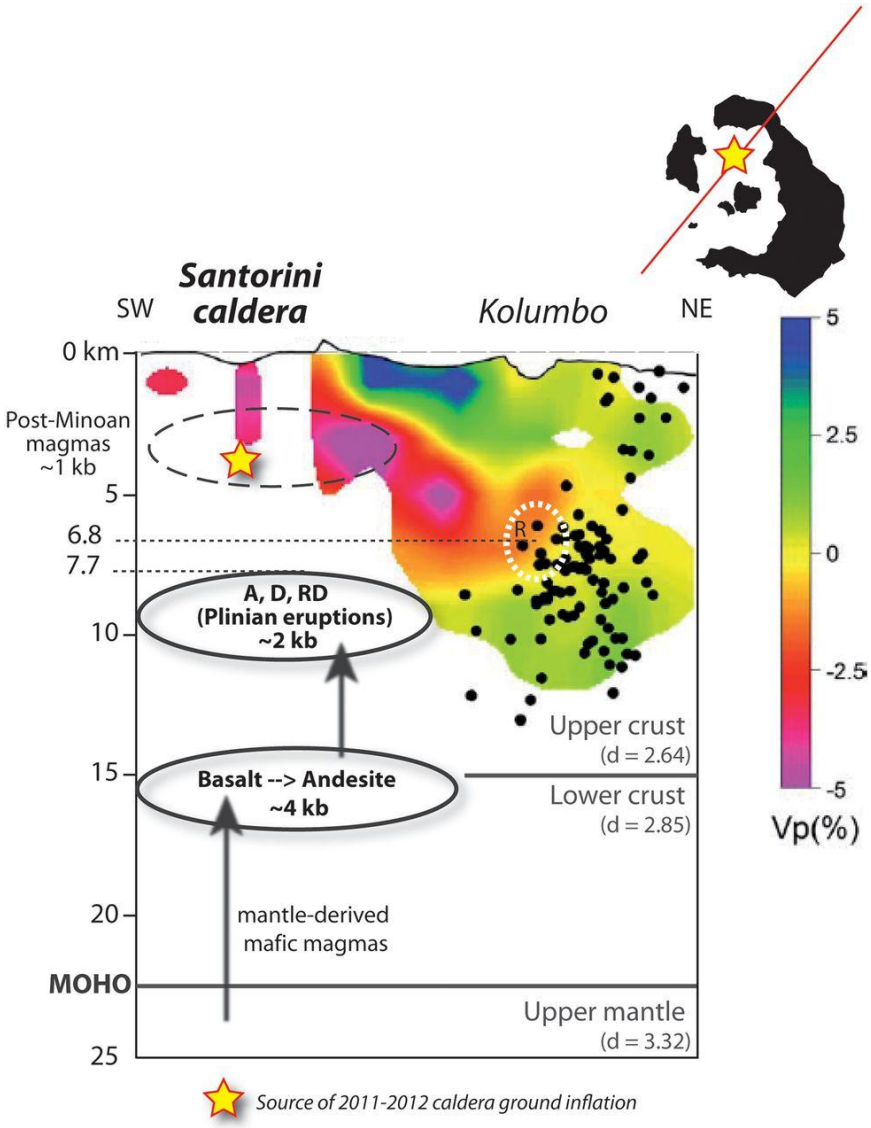

Figure 19. Schematic interpretative illustration of the Santorini-Kolumbo magma plumbing system along a SW–NE cross-section from the Santorini caldera towards the Kolumbo seamount. Illustration based on the results obtained in this work, as well as recent volcanological, petrological and geophysical studies (see text). P-waves velocity variations beneath Kolumbo along with the hypocenter distribution (2002-2005 earthquakes) used in the tomography procedure of Dimitriadis *et al.* (2010) is shown. The seismicity is anti-correlated with the presence of the low-velocity areas, similar to what has been observed in other volcanic systems (e.g., De Natale *et al.*, 2004). Sources for rheological limits and properties: Karagianni & Papazachos (2007), Endrun *et al.* (2008), Konstantinou (2010). White dashed

ellipse represents the location of the negative velocity perturbation according to S-waves, which are believed to be more consistent than the location inferred from P-waves with petrological constraints (Konstantinou & Yeh, 2012).

There are at least four main magma storage regions beneath the Santorini-Kolumbo volcanic system: a mafic reservoir at 15 km depth (at the boundary between upper- and lower-crust; Andújar *et al.*, 2012; Cadoux *et al.*, 2013), a large dominantly-silicic reservoir at 8 km depth, a discrete smaller rhyolitic reservoir at ca. 7 km depth beneath Kolumbo (Dimitriadis *et al.*, 2010; Cantner *et al.*, 2014) and a shallower one at 2-4 km depth beneath the caldera (Parks *et al.*, 2012 and references therein).

B = basalt, BA = basaltic andesite, A = Andesite, D = dacite, RD = rhyodacite, R = rhyolite.

TABLE CAPTIONS

Table 1. Whole rock and average double-fusion dry glass compositions of the four samples used as sta

	MINOAN			CAPE RIVA	
Sample S82-30	Whole Rock	Dry Glass (double fusion)	Sample S09-62	Whole Rock	Dry Glass (double fusion)
n		*22*	*n*		*25*
wt. %			wt. %		
SiO_2	70.58	71.24 (26)	SiO_2	66.88	67.58 (31)
TiO_2	0.46	0.45 (4)	TiO_2	0.68	0.68 (4)
Al_2O_3	14.64	14.87 (15)	Al_2O_3	15.15	15.43 (16)
Fe_2O_{3tot}			Fe_2O_{3tot}	4.82	
FeO_{tot}	3.05	2.85 (18)	FeO_{tot}		4.35 (22)
FeO (Fe2+)	n.a.		FeO (Fe2+)	2.50	
MnO	0.08	0.08 (5)	MnO	0.15	0.13 (6)
MgO	0.66	0.73 (5)	MgO	1.05	1.09 (4)
CaO	2.36	2.34 (14)	CaO	3.07	3.00 (9)
Na_2O	5.08	4.24 (8)	Na_2O	5.32	4.90 (14)
K_2O	3.00	3.08 (11)	K_2O	2.51	2.61 (8)
P_2O_5	0.08	0.13 (4)	P_2O_5	0.19	0.23 (4)
H_2O^+	n.a		H_2O^+	2.84	
H_2O^-	n.a		H_2O^-	0.33	
S_{tot}	n.a		S_{tot}	0.05	
CO_{2tot}	n.a		CO_{2tot}	0.08	
L.O.I	2.12		L.O.I	3.54	
Original Sum	99.99	98.40	Original Sum	99.48	97.77
ppm			ppm		
Cl	n.a.		Cl	4380	
Li	n.a.		Li	18.6	
B	n.a.		B	15	

L.O.I.: Loss On Ignition.
n : number of dry glass analyses.
Numbers in parentheses indicate one standard deviation of *n* analyses in terms of smallest units cited
n.a.: not analysed

Table 1. Whole rock and average double-fusion dry glass compositions of the four samples used as starting materials. All compositions have been recalculated to 100 wt% on a anhydrous basis. Except for the Minoan (XRF, Nottingham, UK), whole rock major element analyses were all performed at the SARM-CRPG (Nancy, France) by ICP-OES. FeO (Fe^{2+}) content was determined by wet chemistry, H_2O^+ with Karl Fisher potentiometric titration,

H_2O^- by gravimetry, CO_{2tot} and S_{tot} were measured with a Leco SC 144DR. Chlorine content was determined by wet precipitation- ferrithiocyanate spectrophotometry. Boron was measured using a Varian Cary 50 absorptiometry Spectrophotometer and Lithium by Atomic absorption spectroscopy. Dry glasses were analysed with a Cameca SX50 electron microprobe (ISTO-BRGM, France).

Table 2. Mean pre-eruptive temperatures and oxygen fugacities

	Minoan		**Cape Riva**		**Lower Pumice**	
Fe-Ti Oxides	**T (°C) ± 1SD**	**log fO_2 ± 1SD**	**T (°C) ± 1SD**	**log fO_2 ± 1SD**	**T (°C) ± 1SD**	**log fO**
Andersen & Lindsley (1985)	853 ± 7	-12.82 ± 0.19	879 ± 15	-12.92 ± 0.35	856 ± 16	-13.4
Ghiorso & Evans (2008)	866 ± 9	-12.86 ± 0.07	891 ± 17	-12.49 ± 0.10	866 ± 17	-13.5
P solubility (apatite-melt)						
Harrison & Watson (1984)	807		909		897	

Table 2. Mean pre-eruptive temperatures and oxygen fugacities. Temperature estimates from Fe-Ti oxides and P solubility are mostly consistent, showing that the less evolved Cape Riva magma is the hotter one. The calculation scheme of Ghiorso & Evans (2008) systematically leads to higher temperatures (+9 to 13°C) and lower fO_2 (up to 0.5 log fO_2) than Andersen & Lindsley (1985) but the two techniques agree within one standard deviation.

Table 3. Phase equilibria experiments: conditions, run products and phase proportions

Charge #	Starting material	log fO_2[1]	XH_2O[2]	H_2O_{melt}[3] (wt%)	Run products and ph
Experiment # 1: P_t = 2022 ±15 bar, P_{H2} = 5.8 bar (target: FMQ buffer), T = 902 ±6°C, run duration 164.8 hours					
Sensor Co-Pd		**-12.29 (FMQ + 0.2)**			
LP2 I	dry glass	-12.29	1	5.6	Gl only
LP2 II	"	-12.38	0.9	5.2	Gl (99.0), Opx (0.8), Ilm (0.1)
LP2 III	"	-12.49	0.8	4.4	Gl (90.6), Plg (7.4), Opx (1.7), Il
LP2 IV	"	-12.60	0.7	3.7	Gl (86.2), Plg (10.1), Opx (3.3), I
LP2 V	"	-12.74	0.6	3.3	Gl (81.9), Plg (14.0), Opx (3.8), I
LP1 VI	"	-12.29	1	7.1	Gl (98.1), Cpx (1.6), Ilm (0.3)
LP1 VII	"	-12.38	0.9	6.0	Gl (96.7), Cpx (2.9), Ilm (0.4)
LP1 VIII	"	-12.49	0.8	4.3	Gl (96.3), Cpx (3.3), Ilm (0.4)
LP1 IX	"	-12.60	0.7	4.2	Gl (92.8), Cpx (4.3), Plg (2.3), Il
LP1 X	"	-12.74	0.6	4.1	Gl (85.2), Plg (8.6), Cpx (5.6), Il
Min XI	"	-12.29	1	6.3	Gl only
Min XII	"	-12.38	0.9	5.8	Gl (97), Cpx (3)
Min XIII	"	-12.49	0.8	4.5	Gl (97.3),Cpx (2.2), Plg (0.5)
Min XIV	"	-12.60	0.7	3.9	Gl (91.5), Plg (6.5), Opx (2.9), Cp
Min XV	"	-12.74	0.6	3.5	Gl (83.4), Plg (13.2), Opx (4.3), C
CR XVI	"	-12.29	1	7.7	Gl (96.5), Cpx (3.1), Ilm (0.3)
CR XVII	"	-12.38	0.9	6.7	Gl (95.3), Cpx (4.0), Ilm (0.7)
CR XVIII	"	-12.49	0.8	6.1	Gl (88.7), Plg (5.5), Cpx (2.8), Op
CR XIX	"	-12.60	0.7	4.4	Gl (75.5), Plg (16.9), Opx (6.8), I
CR XX	"	-12.74	0.6	4.2	Gl (66.4), Plg (24.5), Opx (8.2), I
Experiment # 2: P_t = 2004 ±12 bar, P_{H2} = 6 bar (target: FMQ buffer), T = 850 ±1°C, run duration 212.1 hours					
Sensor Co-Pd		**-13.30 (FMQ + 0.1)**			
LP2 I	dry glass	-13.30	1	8.0	Gl (96.7), Amph (1.6), Opx (1.2),
LP2 II	"	-13.39	0.9	no data (leaking capsule)	
LP2 III	"	-13.49	0.8	5.5	Gl (77.6), Plg (16.8), Opx (4.9), I
LP2 IV	"	-13.61	0.7	5.2	Gl (67.9), Plg (25.4), Opx (6.1), I
LP2 V	"	-13.74	0.6	4.6	Gl (60.9), Plg (31.2), Opx (7.2), I
LP1 VI	"	-13.30	1	6.8	Gl (95.0), Cpx (4.3), Ilm (0.7)
LP1 VII	"	-13.39	0.9	6.3	Gl (93.6), Cpx (5.6), Ilm (0.7)
LP1 VIII	"	-13.49	0.8	5.7	Gl (88.6), Cpx (6.2), Plg (4.5), Il
LP1 IX	"	-13.61	0.7	5.1	Gl (75.1), Plg (17.2), Cpx (1.4), P
LP1 X	"	-13.74	0.6	4.6	Gl (58.1), Plg (32.5), Pig (12.0), I
Min XI	"	-13.30	1	6.9	Gl (97.1), Amph (3.4), Ilm (0.3),
Min XII	"	-13.39	0.9	6.3	Gl (90.3), Plg (6.9), Opx (1.9), Cp
Min XIII	"	-13.49	0.8	5.2	Gl (77.4), Plg (17.9), Opx (4.1), I
Min XIV	"	-13.61	0.7	5.1	Gl (73.0), Plg (22.5), Opx (4.1), i
Min XV	"	-13.74	0.6	4.7	Gl (66.2), Plg (27.4), Opx (5.8), I
CR XVI	"	-13.30	1	6.6	Gl (92.3), Amph (7.3), Ilm (0.4)
CR XVII	"	-13.39	0.9	6.3	Gl (81.4), Amph (14.0), Plg (7.3)
CR XVIII	"	-13.49	0.8	4.0	Gl (67.7), Plg (28.0), Opx (8.3), I
CR XIX	"	-13.61	0.7	4.1	Gl (57.5), Plg (32.1), Opx (9.5), I
CR XX	"	-13.74	0.6	2.9	Gl (42.5), Plg (46.6), Opx (9.9), I
Experiment # 3: P_t = 4135 ±19 bar, P_{H2} = 6.6 bar (target: FMQ buffer), T = 901 ±1°C, run duration 126.1 hours					
Sensor Co-Pd		**-12.27 (FMQ)**			
LP2 I	dry glass	-12.27	1	8.4	Gl only

Table 3. Phase equilibria experiments: conditions, run products and phase proportions.

Table 4a. Volatile compositions of the Minoan melt inclusions (MI) from SIMS measurements

Sample-Crystal#-MI#	Host	MI location	Dry SiO_2	Touching Plg	H_2O	±	Cl	±	F	±	S	±
			wt%	An%	wt%		ppm		ppm		ppm	
S82-34B-A3 MI1/2	Plg	R	73.4	42.1	4.01	0.41	4183	130	923	57	115	11
S82-34B-A3 MI3	Plg	R	73.4	41.6	4.65	0.47	2991	244	864	53	49	1
S82-30A-B3 MI4/4	Plg	C	72.4	50.2	5.82	0.58	4437	187	1218	122	92	3
S82-30A-6 MI1/2	Plg	R	72.5	39.9	4.60	0.46	3500	112	587	38	46	1
S82-11D-A5 MI1/2	Plg	C	72.3	50.0	4.13	0.42	3144	156	641	39	111	3
S82-11D-A5 MI3	Plg	C	71.4	49.4	4.07	0.43	2817	134	555	38	184	12

Table 4b. Volatile compositions of the Cape Riva melt inclusions (MI) from SIMS measurements

Sample-Crystal#-MI#	Host	MI location	Dry SiO_2	Touching Plg/Px	H_2O	±	Cl	±	F	±	S	±
			wt%	An/Wo%	wt%		ppm		ppm		ppm	
S09-62f-10 MI1	Plg	GR-RS	71.1	n.a.	5.27	0.13	2747	109	770	22	96	2
S09-62f-10 MI2	Plg	GR-RS	71.2	n.a.	4.74	0.16	2369	25	672	21	85	0
S09-62f-10 MI3	Plg	GR-RS	71.3	n.a.	5.13	0.47	2504	233	762	74	89	8
S09-62f-10 MI5	Plg	R	71.2	n.a.	4.95	0.51	2577	81	816	50	85	2
S09-62f-9 MI1	Plg	GR-RS	71.2	41.6	5.77	0.64	2711	143	804	62	97	5
S09-62f-9 MI2	Plg	GR-RS	71.9	41.5	3.65	0.42	2385	115	793	59	76	3
S09-62f-9 MI5	Plg	GR-RS	70.9	42.1	4.57	0.51	2805	151	808	62	101	5
S09-62f-2 MI1	Plg	GR-RS	71.6	42.7	4.11	0.41	2644	259	781	49	92	3
S09-62f-2 MI3	Plg	GR-RS	71.3	41.5	5.27	0.82	2912	299	834	64	92	11
S09-62h-6 MI1	Plg	GR-RS	71.2*		6.61	0.66	2451	80	766	47	85	2
S09-62c-2 MI1	Opx	C	71.4	n.a.	3.27	0.33	2793	99	773	47	84	2
S09-62c-2 MI2	Opx	C	71.0	n.a.	5.00	0.15	3738	42	983	12	137	1
S09-62c-2 MI3	Opx	C	70.5	n.a.	4.50	0.14	3810	71	967	19	111	1
S09-62i-2 MI3	Cpx	C	70.2	n.a.	5.55	0.56	2635	80	820	50	104	2
S09-62i-2 MI4	Cpx	C	71.1	39.9	5.94	0.59	2638	166	837	51	143	7

*SiO_2 used by default for water content calculation
n.a.: not analysed

Table 4. Volatile compositions of the melt inclusions (MI) from SIMS measurements. **4a.** Minoan melt inclusions, **4b.** Cape Riva, **4c.** Lower Pumice 2, **4d.** Lower Pumice 1.

Plg: plagioclase; Opx: orthopyroxene; Cpx: clinopyroxene. C: crystal core; C border: the border of the core; R: crystal rim; GR: overgrowth rim; RS: resorption surface; Interm: between core and rim. An/Wo%: anorthite and wollastonite content in plagioclase and pyroxenes, respectively. H_2O, Cl, F and S values are the results of one or two analyses per MI, depending of the MI size. The ± symbol next to each H_2O, Cl, F and S values corresponds to the error taking into account the statistic error on the measurement and the error on the calibration.

Table 5. H_2O-saturation pressure estimates for rhyolitic melts made with VolatileCalc

	Input			**Output**		
	H_2O (wt%)	CO_2 (ppm)	T (°C)	H_2Om (wt%)	OHm (wt%)	P (bars)
Minoan	4.55*	0	853	2.824	1.726	1314
	5.82**	0	853	3.986	1.834	1952
Cape Riva	4.96*	0	879	3.193	1.767	1555
	6.61**	0	879	4.733	1.877	2402
LP2	3.94*	0	856	2.290	1.650	1035
	5.34**	0	856	3.540	1.800	1711
LP1	4.48*	0	869	2.762	1.718	1304
	6.26**	0	869	4.400	1.860	2205

* Mean H_2O (wt%) from plagioclase- and pyroxene-hosted melt inclusions

** Highest H_2O (wt%) measured in plagioclase- and pyroxene-hosted melt inclusions (Table 4)

H_2Om and OHm: molecular H_2O and OH

Table 5. H_2O-saturation pressure estimates for rhyolitic melts made using the VolatileCalc software (Newman & Lowenstern, 2002).

ELECTRONIC APPENDICES

Electronic Appendix 1. Experimental phase compositions of the Minoan rhyodacite, **1a.** Anhydrous compositions of the experimental glasses (wt%), **1b.** Experimental plagioclase, **1c.** orthopyroxene, **1d.** clinopyroxene, **1e.** amphibole, **1f.** Fe-Ti oxides.

Electronic Appendix 2. Experimental phase compositions of the Cape Riva dacite, **2a.** Anhydrous compositions of the experimental glasses (wt%), **2b.** Experimental plagioclase, **2c.** orthopyroxene, **2d.** clinopyroxene, **2e.** amphibole, **2f.** Fe-Ti oxides.

Electronic Appendix 3. Experimental phase compositions of the LP2 rhyodacite, **3a.** Anhydrous compositions of the experimental glasses (wt%), **3b.** Experimental plagioclase, **3c.** orthopyroxene, **3d.** amphibole, **3e.** Fe-Ti oxides.

Electronic Appendix 4. Experimental phase compositions of the LP1 rhyodacite, **4a.** Anhydrous compositions of the experimental glasses (wt%), **4b.** Experimental plagioclase, **4c.** orthopyroxene, **4d.** clinopyroxene**, 4e.** Fe-Ti oxides.

Electronic Appendix 5. Natural phases compositions, **5a.** Anhydrous interstitial glass and melt inclusions, **5b.** Mineral phases.

Electronic Appendix 6. Phase proportions (wt%) and crystallinities (wt%) of the natural samples, determined by mass balance calculations.